WIND-TUNNEL STUDY OF THE
WEIRTON-STEUBENVILLE
CABLE-STAYED BRIDGE

by

J.E. Cermak*, B. Bienkiewicz**
and
J.A. Peterka***

for

*Director, Fluid Dynamics and Diffusion Laboratory

**Assistant Professor, Fluid Mechanics and Wind Engineering Program,
Department of Civil Engineering

***Associate Professor, Fluid Mechanics and Wind Engineering Program
Department of Civil Engineering

August 1982

ABSTRACT

A section model of the proposed Weirton-Steubenville cable-stayed bridge was used in the wind-tunnel study. The freely oscillating section model of the bridge deck was studied to evaluate the aerodynamic stability of the bridge. Basic aerodynamic derivatives were extracted in smooth flow and were used to estimate the prototype bridge critical wind speed for the one degree-of-freedeom (torsional) flutter. The amplitude of the vortex-induced bridge oscillation was also assessed.

The bridge section model response revealed one degree-of-freedom (torsional) flutter instability occurring at a critical wind speed dependent upon the value of mechanical damping of the model. The estimated critical speed for the prototype bridge was about 190 mph for the ratio of assumed damping to critical of the order of 0.8 percent and angles of attack in the range from -6 degrees to +6 degrees. Vortex-induced oscillation of the bridge section model (both in a vertical and a torsional degree-of-freedom) occurred at substantially lower speeds. The maximum amplitude of the corresponding prototype motion (higher for vertical oscillation) was estimated not to exceed 0.5 percent of B (where B is the width of the bridge deck) for the same damping level.

The aerodynamic behavior of the bridge deck was improved by streamlining of the deck geometry.

ACKNOWLEDGMENTS

TABLE OF CONTENTS

LIST OF SYMBOLS

Symbol	Description
A (D)	cross-wind dimension of bridge deck with (without) railings
A_{oh} $(A_{o\alpha})$	initial amplitude in vertical (torsional) degree-of-freedom
A_{nh} $(A_{n\alpha})$	amplitude in vertical (torsional) degree-of-freedom after n cycles
B	width of bridge deck
C_L $(C_D)[C_M]$	lift (drag) force [pitching moment] coefficient
g, G = 32.17 ft-sec^{-2}	gravitational constant
h (α)	vertical (torsional) degree-of-freedom
h_o (α_o)	amplitude of steady-state response in vertical (torsional) degree-of-freedom associated with vortex-shedding
$\alpha_1(t)$	generalized coordinate for torsional degree-of-freedom
H_i^* (A_i^*)	aerodynamic derivative for vertical (torsional) motion (i = 1,2,3)
$K = \dfrac{B\omega}{U}$	reduced frequency
L	bridge span
ℓ	length of bridge section model
L_b (M_b)	buffeting lift force (pitching moment)
$L_{se}(M_{se})$	self-excited lift force (pitching moment)
m (I)	mass (polar mass moment of inertia) per unit span
N	frequency in Hz
N_h (N_α)	natural frequency for h (α)--motion in Hz
N_v (N_T)	natural frequency for h (α)--motion in Hz
U	mean speed

Symbol	Description
U_c	critical speed for torsional flutter
β	angle of attack
$\Upsilon_h (\Upsilon_\alpha)$	damping ratio-to-critical for h (α)-- motion at a given wind speed
$\delta_h (\delta_\alpha)$	logarithmic decrement of damping for vertical (torsional) degree-of-freedom
$\zeta_h (\zeta_\alpha)$	damping ratio-to-critical for h (α)-- motion in still air
λ_I	moment of inertia scale
λ_L	geometrical scale
λ_m	mass scale
λ_N	frequency scale
λ_V	velocity scale
λ_ρ	density scale
ν	kinematic viscosity
ρ	air density
$\Phi_1(x)$	fundamental mode for torsional degree-of-freedom
ω	circular frequency $\omega = 2\pi N$
$\omega_h (\omega_\alpha)$	circular frequency $\omega_h = 2\pi N_h$ $(\omega_\alpha = 2\pi N_\alpha)$
$()_m$	refers to bridge section model
$()_p$	refers to prototype bridge
$(\dot{\ })$	time derivative

LIST OF FIGURES

vii

Table

1. INTRODUCTION

The aerodynamics of suspended-span bridges has been recognized as
an important element in analysis and design of such structures. Related
problems are studied today mainly in wind tunnels. Two basic approaches
are used. One employs a full aeroelastic model of a given bridge and
requires a relatively large wind tunnel. The other employs a typical
section of the bridge (so called the bridge section model). The wind-
tunnel tests in this case are simplified and can be conducted in a
smaller wind tunnel. The results of these tests are then supplemented
by analytical considerations and finally assessments are made with
regard to the full-bridge aerodynamic stability.

In the wind-engineering study, reported herein, a bridge section
model has been employed for the proposed Weirton-Steubenville cable-
stayed bridge over the Ohio River linking Brooke County of West Virginia
with Jefferson County of Ohio. The main purpose of the work was to
evaluate the bridge aerodynamic stability for a given range of the
assumed bridge damping. Of particular interest was the critical wind
speed for flutter-type instability and the range of amplitudes of the
anticipated vortex-induced bridge oscillation. Only the smooth flow
conditions, believed to give conservative estimates, Scanlan [1], were
considered in the study. The aerodynamic derivatives defined by Scanlan
and Tomko [2] were obtained for different configurations and they formed
the basis for further computations related to the bridge aerodynamic
stability. Results of the measurements of the model response in the
speed region where vortex-shedding controlled the bridge motion were
used in estimating the prototype bridge response.

The present report describes the foregoing investigations. The theoretical background, experimental configurations, testing procedures, instrumentation and data acquisition are presented in the next chapters. Some supplementary material is included in the Appendix.

2. THEORETICAL BACKGROUND

2.1 Concept of the Bridge Section Model

The most common procedure in the wind-tunnel study of bridge aerodynamics is use of the bridge section model. The model represents a relatively short, typical section of the bridge span, built rigidly and to model scale. It is mounted on springs and allowed to oscillate in two degrees of freedom (vertical and torsional). The bridge deck geometry, inertia, and elastic properties are scaled for the section model according to certain similarity requirements.

2.2 Similarity Requirements

The basic requirement is the geometrical length scale (model-to-prototype) ratio λ_L to which all geometrical bridge deck details should be scaled. For a given length scale λ_L the mass per unit span of the model should be scaled according to the mass scale

$$\lambda_m = \lambda_L^2 \ . \tag{1}$$

Accordingly, the polar mass moment of inertia per unit span for the model should be modeled as follows

$$\lambda_I = \lambda_L^4 \ . \tag{2}$$

The scalings (1) and (2) are valid if the mass density of the bridge deck and the model are equal, that is when the density scale is equal to

$$\lambda_\rho = 1 \ . \tag{3}$$

Since both the prototype bridge and the model are immersed in the same medium (air) the similarity requirement for the aerodynamic forces can be simplified to the following form, Simiu and Scanlan [3]:

$$\left(\frac{U}{NB}\right)_m = \left(\frac{U}{NB}\right)_p \quad . \tag{4}$$

This condition requires that the frequency scale be given by

$$\lambda_N = \lambda_V \cdot \lambda_L^{-1} \tag{5}$$

where λ_V is the velocity scale. If the Froude number similarity

$$\left(\frac{U^2}{Bg}\right)_m = \left(\frac{U^2}{Bg}\right)_p \quad , \tag{6}$$

where g is the gravitational constant, is assumed then the velocity scale λ_V is related to the length scale

$$\lambda_V = \lambda_L^{1/2} \quad . \tag{7}$$

As a consequence of relation (5), the frequency scale λ_N is also directly associated with the length scale

$$\lambda_N = \lambda_L^{-1/2} \quad . \tag{8}$$

It can be easily checked that the Reynolds number similarity

$$\left(\frac{UB}{\nu}\right)_m = \left(\frac{UB}{\nu}\right)_p \tag{9}$$

where ν is the kinematic viscosity, cannot be attained in such a situation. However, if the model Reynolds number is sufficiently high the aerodynamic forces acting on the (usually bluff) bridge do not vary significantly with the Reynolds number and the similarity requirement (9) can be relaxed, Scanlan [1].

2.3 Bridge Aerodynamic Stability

Equations of motion for the bridge section model, assumed to be symmetrical about the vertical plane of the roadway centerline, can be written in the following form:

$$m\ddot{h} + 2\zeta_h\omega_h\dot{h} + \omega_h^2 h = L$$

$$I\ddot{\alpha} + 2\zeta_\alpha\omega_\alpha\dot{\alpha} + \omega_\alpha^2\alpha = M$$

(10)

where

m = model mass per unit span,

I = model polar mass moment of inertia per unit span,

$h(\alpha)$ = vertical (torsional) deflection of the model assumed uniform over the span,

$\zeta_h(\zeta_\alpha)$ = damping rate-to-critical for vertical (torsional) degree-of-freedom,

$\omega_h(\omega_\alpha)$ = circular natural frequency for vertical(torsional) degree-of-freedom, and

$L(M)$ = lift force (pitching moment) per unit span.

It is a common practice to assume that the right-hand sides of equations (10) can be written as the following linear combination

$$L = L_{se} + L_b$$

$$M = M_{se} + M_b$$

where

$L_b(M_b)$ = lift force (pitching moment) induced through buffeting by turbulence and

$L_{se}(M_{se})$ = self-excited lift force (pitching moment) induced by oscillation of the model.

In a smooth flow only the self-excited terms are retained and in a linearized model proposed by Scanlan and Tomko [2] they are expressed as follows:

$$L_{se} = \frac{1}{2}\rho\ U^2(2B)[KH_1^* \frac{\dot{h}}{U} + KH_2^* \frac{B\dot{\alpha}}{U} + K^2 H_3^* \alpha]$$

and   (11)

$$M_{se} = \frac{1}{2}\rho\ U^2(2B^2)[KA_1^* \frac{\dot{h}}{U} + KA_2^* \frac{B\dot{\alpha}}{U} + K^2 A_3^* \alpha],$$

where

ρ = air density,

U = oncoming wind velocity,

B = deck width of the model,

$K = \frac{B\omega}{U}$ = reduced frequency, ω being the actual oscillation circular frequency, $\omega = 2\pi N$, and

H_i^* and A_i^* = nondimensional aerodynamic derivatives, functions of K ($i=1,2,3$).

In a typical situation of unstreamlined bridge decks the self-excited oscillations occur in uncoupled modes leading in most cases to a one degree-of-freedom flutter instability. In this case only the derivatives H_1^*, A_2^* and A_3^* play an important role in equations (11). For some bridge decks (especially those with H-type geometrical shape) the magnitude of the derivative A_3^* is small in comparison with the contribution of the derivative A_2^* in equations (11). In such cases, after some rearrangements, equations (11) can be written as follows:

$$\ddot{h} + 2\zeta_h\omega_h\dot{h} + \omega_h^2 h = \frac{\rho B^2 \omega}{m}\ H_1^*\ \dot{h}$$

and   (12)

$$\ddot{\alpha} + 2\zeta_\alpha\omega_\alpha\dot{\alpha} + \alpha_\alpha^2\alpha = \frac{\rho B^4 \omega}{I}\ A_2^*\ \dot{\alpha}\ .$$

Equations (12) can be further modified to give

$$\ddot{h} + 2\gamma_h \omega_h \dot{h} + \omega_h^2 h = 0$$

and   (13)

$$\ddot{\alpha} + 2\gamma_\alpha \omega_\alpha \dot{\alpha} + \omega_\alpha^2 \alpha = 0,$$

where

$$\gamma_h = \zeta_h - \frac{\rho B^2}{2m} H_1^*$$

and   (14)

$$\gamma_\alpha = \zeta_\alpha - \frac{\rho B^4}{2I} A_2^* \quad .$$

Equations (13) describe free, damped oscillations in vertical and torsional degrees-of-freedeom, mutually uncoupled, with damping being altered by the current value of the aerodynamic derivatives, H_1^* and A_2^*, respectively. Aerodynamic derivatives H_1^* and A_2^* can be determined from relations (14) based on measurements of damping γ_i (i = h,α) of the freely oscillating model for one degree-of-freedom motion (h or α), when the mechanical damping of the model ζ_i (i = h,α) is known. More generally, they can be expressed as the functions of the reduced frequency K or, more commonly, the reduced velocity $\frac{U}{NB}$.

Unstreamlined bridge decks usually exhibit one degree-of-freedom flutter instability in torsion. The condition for this situation to occur can be stated for the bridge section model as follows:

$$\zeta_\alpha - \frac{\rho B^4}{2I} A_2^* = 0$$ (15)

or

$$A_2^* \left(\frac{U_c}{NB} \right) = \frac{2I}{\rho B^4} \zeta_\alpha \quad .$$ (16)

The quantity on the right-hand side can be computed and equation (16) can be solved for the critical flutter speed if the aerodynamic derivative (a function of the reduced velocity $\frac{U}{NB}$) is known. It can be easily

shown (see Appendix) that the same condition for the critical speed holds for the full-span of the bridge if only the fundamental mode of oscillation in torsion is taken into account and the inertial and geometrical properties of the bridge deck are uniform over the span.

2.4 Vortex-Induced Response

Vortex-induced motion of the bridge deck occurs at fairly low wind speeds. The maximum amplitude of uncoupled harmonic oscillation in the vertical or torsional degree-of-freedom is attained when the frequency of the vortex-shedding coincides with the natural frequency of the vertical or torsional motion. Usually the fundamental frequency in h-motion is lower than in α-motion. Therefore, during wind-tunnel tests as wind speed is being increased the vortex-shedding induced oscillation usually occurs first in h-motion followed by a weaker oscillation in α-motion at higher speed. Based on the data obtained from the wind-tunnel tests of the bridge section model, predictions can be made with regard to the full-span vortex-induced response.

3.   WIND-TUNNEL FACILITY AND BRIDGE SECTION MODEL

3.1 Wind-Tunnel Facility

The experiments reported herein were conducted in the structural aerodynamics wind tunnel located in the Fluid Dynamics and Diffusion Laboratory at Colorado State University.

The structural aerodynamics wind tunnel shown in Figure 1 is an open circuit facility driven by a constant-pitch propeller. The test section is nominally 3 ft square and approximately 12 ft long with flow entering through a contraction having a 4:1 contraction ratio. The mean velocity is adjustable continuously from 1 - 30 fps. The mean velocity is constant across the test section except very close to the wind-tunnel walls where the wall boundary layer extends up approximately 1 inch. The background turbulence intensity is low and does not exceed 1.5 percent.

3.2 Bridge Section Model Description and Scaling

The concept of a bridge section model has been described in Chapter 2. A typical arrangement used in the wind-tunnel tests of the model is shown in Figure 2. The section model, suspended on eight vertical, helical springs, is supplied with end plates to ensure predominantly two-dimensional flow around the deck.

A general view of the Weirton-Steubenville cable-stayed bridge investigated in the present study is shown in Figure 3. Figure 4 shows distribution of mass and mass moment of inertia for the bridge's main spans. Figure 5 presents details of the bridge deck. Basic properties of the prototype bridge are gathered in Table 1. Initial considerations indicated that a 1:140 geometrical scale bridge section model would be

optimal for the present study. The scaled geometry of the model is shown in Figure 6. All the basic physical properties of the model were scaled according to the similarity requirements discussed in Chapter 2.2 and they are collected in Table 1 as the values for the "exact" model.
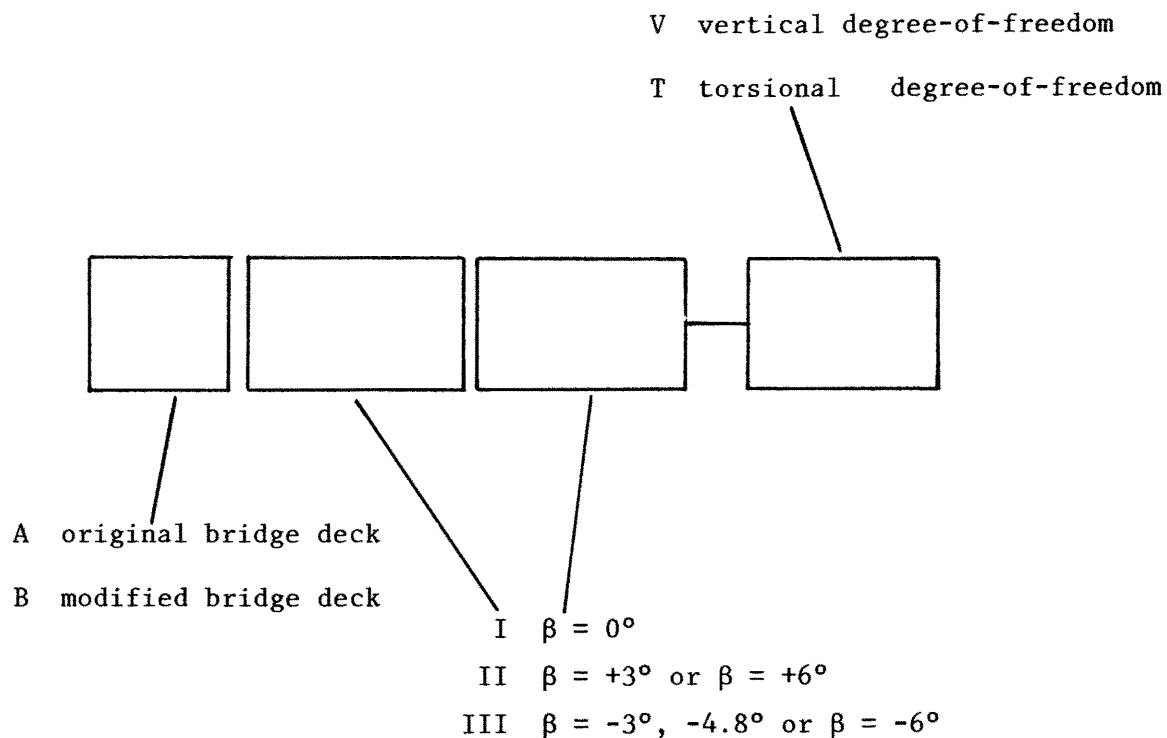
3.3 Model Construction and Details

Basically two materials were used to construct the bridge section model. The main body of the model corresponding to the concrete part of the prototype bridge deck was made of magnesium. The prototype H sections were modeled with plastic I-beams. The model was constructed in such a way that an angle of attack could be changed from -6 to +6 degrees. Elements of the model support were made of aluminum and light brass tubing. The overall length of the model was 35.5 in. An overall view of the model is shown in Figure 7 and the model placed in the wind tunnel is presented in Figure 8. Figure 9 shows elements of a viscous damper and one of four electromagnets used for simultaneous release of the model to generate uniform harmonic oscillation of the model. The main geometrical and physical properties of the model listed in Table 2 under Model are compared with the target values of the "exact" model from Table 1. The viscous damping was introduced by a series of thin vertical plates attached to both model supporting bars as shown in Figure 10. The plates submerged in a hydraulic fluid, oscillated together with the model. The amount of damping could be adjusted by changing the number of plates.

3.4 Basic Experimental Configurations

The bridge section model has been tested at different angles of attack--0°, ±3°, ±6°, and -4.8°. Most of the tests were conducted for

the original bridge deck; Configurations A in Figure 11. Additional tests were performed for the bridge deck with various modifications. Finally, a modified bridge deck was used to extract an additional series of aerodynamic derivatives; Configurations B in Figure 11. The configurations shown in Figure 11 are denoted in the following manner:

V   vertical degree-of-freedom

T   torsional   degree-of-freedom

A   original bridge deck

B   modified bridge deck

I $\beta = 0°$

II $\beta = +3°$ or $\beta = +6°$

III $\beta = -3°$, $-4.8°$ or $\beta = -6°$

Finally, Figure 12 provides a definition of the angle of attack and the degrees-of-freedom of the model. The main geometrical dimensions of the model are shown in Figure 13.

4. TESTING PROCEDURES

4.1 Overall Bridge Section Model Response

An overall response of the bridge section model was measured for different configurations and a wide range of wind speeds. For a given wind speed the model was set at rest and then released. After a sufficiently long period of time (a few minutes) measurements of vertical and torsional model oscillations were taken. The velocity was then changed and the process repeated. In this way velocity regions of the vortex-induced oscillations and flutter instability were initially established.

4.2 Aerodynamic Derivatives

The aerodynamic derivatives considered in Chapter 2.3, formulas (14), express changes in total damping of the model.

$$H_1^* = (\zeta_h - \Upsilon_h) \frac{2m}{\rho B^2}$$

and   (17)

$$A_2^* = (\zeta_\alpha - \Upsilon_\alpha) \frac{2I}{\rho B^4}$$

where

$\zeta_h(\zeta_\alpha)$ is model damping ratio-to-critical in still air for vertical (torsional) degree-of-freedom; i.e., mechanical damping of the model

$\Upsilon_h(\Upsilon_\alpha)$ is model damping ratio-to-critical at a given wind speed for vertical (torsional) degree-of-freedom; i.e., mechanical plus aerodynamic damping.

In order to measure the model damping in uncoupled vertical or torsional motion at a given wind speed, the model was given an initial displacement in one degree-of-freedom (with the other degree restrained) and then released. The model was supported at four corners and simultaneously released using four electromagnets wired in series. The

subsequent harmonic (decaying or growing) model oscillation was recorded for further analysis. A series of tests was conducted with different mechanical damping of the model in order to establish the optimal damping level for the most accurate damping measurements.

4.3 Vortex-Induced Response

The vortex-induced response for the prototype bridge was estimated based on the data obtained during evaluation of the overall bridge section model response (Section 4.1).

4.4 Mean Forces (Lift, Drag) and Pitching Moment

The bridge section model was rigidly supported for this series of tests. The overall mean lift, drag and pitching moment acting on the model (see Fig. 12) were measured at one wind speed for different angles of attack. The results were normalized and presented in the form of the lift coefficient C_L, the drag coefficient C_D and the pitching moment coefficient C_M

$$C_L = \frac{L}{\frac{1}{2}\rho U^2 B \ell} \quad,$$

$$C_D = \frac{D}{\frac{1}{2}\rho U^2 B \ell} \quad, \text{ and}$$

$$C_M = \frac{M}{\frac{1}{2}\rho U^2 B^2 \ell}$$

where

$\quad$ L(D) $\qquad$ measured lift (drag) force,

$\quad$ M $\qquad$ measured pitching moment,

$\quad$ $C_L(C_D)$ $\qquad$ lift (drag) coefficient,

C_M pitching moment coefficient,

ρ air density,

U   mean wind speed,

B   width of bridge model deck, and

ℓ length of bridge section model.

5. INSTRUMENTATION

5.1 Flow Measurement

The flow characteristics (velocity and turbulence intensity profile) were measured using a cylindrical hot film in conjunction with a TSI constant-temperature anemometer. Current values of the mean wind speed during the bridge section-model tests were measured by a Prandtl tube connected to a differential manometer with a sufficiently high resolution.

5.2 Measurement of the Bridge Section-Model Response

The bridge section-model response was measured using four strain-gage transducers shown in Figure 14. Two of the transducers monitored vertical motion (analog signals from both of them were added) and the remaining two (with signals mutually subtracted) detected torsional deflection. The transducers were connected to a signal conditioner, Figure 15. Next the two signals (proportional to a vertical and torsional deflection of the model) underwent a secondary amplification with a low-pass filtering. The voltages obtained were monitored on a dual-beam oscilloscope, recorded on a two-channel strip-chart recorder and fed to a minicomputer as is schematically shown in Figure 15. Figure 16 shows basic instruments used in the measurements.

5.3 Measurement of Mean Forces and Moment

Mean forces (lift, drag) and pitching moment acting on the bridge section model were measured using strain gage transducers.

The arrangement used for the evaluation of the bridge model response (Figure 14) was modified to allow measurement of the lift force

and pitching moment. (Soft springs were replaced by very stiff springs). Further modifications of the system were necessary to allow measurement of the drag force.

5.4 Flow Visualization

A schematic diagram of the smoke generating system, used in the present study, is shown in Figure 17. Compressed air was ducted through a jar containing a mixture of titanium tetrachloride and carbon tetrachloride. A dense white smoke (titanium dioxide) was produced as a result of a chemical reaction (due to the presence of moisture in the air). The smoke was supplied through flexible "Tygon" tubing to a brass rake located in the wind tunnel. A honeycomb was placed very close downstream from the rake in order to attenuate disturbances present in the streaklines of the generated smoke.

6. DATA ACQUISITION

6.1 Overall Bridge Section Model Response

The overall bridge section-model response data was reduced using a minicomputer (HP-1000). During experiments the time histories of the vertical and torsional model oscillations were directly fed to the mini-computer on line. The mean values and the normalized root-mean-squares of the model deflections were then plotted versus reduced wind speed $\frac{U}{N_i B}$ (i = h, α) for each configuration.

6.2 Aerodynamic Derivatives and Stability

Time series of the vertical and torsional oscillation of the bridge model, recorded on a strip-chart recorder, were used to compute the aerodynamic derivatives (17). Each record was divided into three sections. For each section the logarithmic decrement of damping

$$\delta_i = \frac{1}{n} \, \ell n \, \frac{A_{0i}}{A_{ni}} \quad (i = h, \, \alpha) \tag{18}$$

where

A_{0i} = initial amplitude of motion, and

A_{ni} = amplitude of motion after n cycles

and the damping ratio-to-critical

$$\Upsilon_i \simeq \frac{\delta_i}{2\pi} \quad (i = h, \, \alpha) \tag{19}$$

were computed. Since the damping considered was low, the appoximate formula (19) was used instead of the exact expression

$$\Upsilon_i = \frac{1}{\sqrt{1 + \left(\frac{2\pi}{\delta_i}\right)^2}} \qquad (i = h, \alpha). \qquad (20)$$

Mean values of Υ_1 (taken over three record sections) were employed in computations. The aerodynamic derivatives (17) were computed using physical properties ζ_h, ζ_α, m, I, B of the model

$$H_1^* = \zeta_{hm} - \Upsilon_{hm} \frac{2m_m}{\rho B_m^2}$$

and (21)

$$A_2^* = \zeta_{\alpha m} - \Upsilon_{\alpha m} \frac{2I_m}{\rho B_m^4}$$

where

$(\ )_m$ refers to the model.

The nondimensional derivatives (21) were plotted versus nondimensional wind speed $\frac{U}{N_i B}$ (i = h, α) where $N_h(N_\alpha)$ is the natural frequency for vertical (torsional) motion.

The one degree-of-freedom torsional flutter instability is expressed by condition (16). Estimation of the prototype bridge critical speed U_{cp} should be used on the physical properties of the prototype--

$$A_0^* \frac{U_{cp}}{N_{\alpha p} B_p} = \frac{2I_p}{\rho B_p^4} \zeta_{\alpha p} \qquad (22)$$

where

$(\ )_p$ refers to the prototype bridge.

The requirement (22) and the aerodynamic derivative A_2^* (21) were used to compute the critical speed (U_{cp}) as a function of the assumed

prototype bridge mechanical damping. The calculations were performed for the different bridge configurations.

6.3 Vortex-Induced Response

As mentioned in Chapter 4.3 the vortex-induced response for the prototype bridge was estimated from the data obtained during evaluation of the overall bridge section model response. The maximum response for vertical and torsional (model) response was rescaled for the prototype conditions.

7. RESULTS

The main purpose of the study was to determine aerodynamic characteristics (overall aerodynamic response, aerodynamic derivatives, critical wind speed for flutter, vortex-induced oscillation) of the bridge deck by means of section-model tests in a low-speed, low-turbulence wind tunnel. The secondary objective was to determine the mean lift, drag and pitching moment coefficients.

During the course of study additional efforts were made to establish desired modifications of the bridge deck which would result in reduction of the vortex-induced bridge oscillation.

7.1 Original Bridge Deck

7.1.1 Overall Bridge Section-Model Response

The overall bridge section-model response was measured for different configurations. Figures 18 and 19 show the response of the model (vertical motion--Fig. 18, torsional motion--Fig. 19) for different angles of attack $\beta = 0°$, $\pm3°$, $\pm6°$ and very low damping level ($\zeta_v = 0.06\%$, $\zeta_T = 0.13\%$, where ζ_v (ζ_T) is the damping ratio for the vertical (torsional) motion). The plots show a one degree-of-freedom torsional flutter instability and vortex-induced oscillation both in torsional and vertical motion. The critical velocity for flutter (in torsion) and the magnitude of the vortex-induced oscillation (for both vertical and torsional motion) depends on the angle of attack β. Generally, the bridge deck is the most unstable at the angle of attack $\beta = -6°$. The overall response of the model with a relatively higher damping level ($\zeta_v \cong 0.81\%$, $\zeta_T \cong 0.84\%$), shown in Figures 20 and 21, exhibits similar features. However, the torsional flutter occurs at relatively

higher reduced speed and the vortex-induced oscillation (both for the vertical and the torsional motion) is reduced approximately by a factor of two.

The model proved to be torsionally unstable at the reduced wind speed $U/N_T B \geq 4.0$. The critical velocity for the one degree-of-freedom torsional flutter depended on the angle of attack β, being the lowest for $\beta = -6°$. The vortex-induced oscillation was observed for both the vertical and torsional motion. The magnitude of this oscillation reached the maximum at the angle of attack $\beta = -6°$.

7.1.2 Aerodynamic Derivatives and Stability

The aerodynamic derivatives $-H_1^*$ and A_2^* extracted for the angle of attack $\beta = -6°$, $-4.8°$, $-3°$, $0°$, $3°$, $6°$ are shown in Figures 22 to 33. The test configurations are defined in Figure 11. The prototype critical speed for the torsional flutter was computed for the different values of the mechanical damping according to the procedure described in Chapter 2.3. Only the most unstable configurations were considered, $\beta = -4.8$ and $\beta = -6°$. The results are shown in Figure 34. In addition, the critical speed, obtained from measurement of the model overall response (Figure 21, $\beta = -6°$), was rescaled for the prototype conditions. The resulting value is marked in Figure 34 for a comparison. The agreement between the computed and the calculated value of the critical wind speed is good. Figure 34 indicates that the prototype critical wind speed for the torsional flutter should exceed 190 mph for the damping ratio in the torsional motion higher than $\zeta_T = 0.8\%$.

7.1.3 Vortex-Induced Response

It follows from Figure 20 that the maximum RMS normalized vortex-induced oscillation for vertical motion equals

$$\frac{h_{RMS}}{B} \cong 0.0032$$

and it occurs (for the angle of attack β = -6°) at the reduced wind speed

$$\frac{U}{N_v B} \cong 1.5 \quad .$$

Based on this data the prototype values can be computed

$$h_{op} \cong \frac{0.0032*103.5}{0.707} \cong 0.47 \text{ ft and}$$

$$U_p = 1.5*0.3*103.5* \frac{3600}{5280} \cong 32 \text{ mph}$$

where

h_{op} = amplitude of vortex-induced oscillation (harmonic motion) for the prototype bridge,

U_p = prototype speed at which the vortex-induced oscillation (vertical motion) reaches maximum,

B = 103.5 ft (from Table 1), and

N_v = 0.30 Hz (from Table 1).

The corresponding maximum acceleration can be estimated to be

$$a_o = h_o \omega^2 = 0.47 *(2\pi * 0.3)^2 \cong 1.67 \text{ ft/sec}^2$$

$$\cong 0.052 \text{ g}$$

where

$g \cong 32.17$ ft/sec^2 is gravitational acceleration.

The vortex-induced oscillation of the prototype bridge deck was estimated in the same way for the remaining angles of attack. The results are summarized in Table 3. It can be seen that the maximum deflection (and the corresponding acceleration) at the angle of attack β = -6° drops by approximately 40% as the angle is changed to be β = -4.8°.

7.1.4 Mean Forces (Lift, Drag) and Pitching Moment

The coefficient of the mean lift force C_L, drag force C_D and pitching moment C_M were defined in Chapter 4.4. The values of these coefficients measured for the bridge deck are gathered in Figures 35 to 37.

7.2 Modified Bridge Decks

Various modifications of the bridge deck were considered during the next stage of the study. The primary objective was to determine necessary modifications (of the original bridge deck) which should result in improved aerodynamic performance of the deck. Figure 38 summarizes configurations discussed in this part.

7.2.1 Overall Response and Flow Visualization

The overall bridge model response and flow visualization results for each configuration are presented in Figures 39 to 50. Visualization of flow patterns around a bridge deck is very helpful in identifying bridge aerodynamic characteristics. The flow pattern around the bridge deck 4, Figure 38, is shown in Figure 50. It exhibits rather narrow and steady wake, compared to the other configurations (Figures 41, 44 and 47). As a result of streamlining of the deck geometry, the deck is aerodynamically more stable than the other configurations (compare Figures 39, 42, 45, 48 for vertical motion and Figures 40, 43, 46, 49 for torsional motion). If the overall response of the modified bridge deck is compared to the original bridge deck (Figures 48, 49 and 39, 40, also 20, 21) it is concluded that the maximum vortex-induced oscillation (for the vertical motion) is reduced by a factor of 3 for the modified bridge deck. Also the modified bridge deck is more stable at higher reduced wind speeds.

In summary, the modified bridge deck (bridge deck number 4 in Figure 38), shown in detail in Figure 51, appears to be most desirable as far as the bridge aerodynamic stability is considered.

7.2.2 Aerodynamic Derivatives for the Optimal Bridge Deck

The aerodynamic derivatives for the optimal bridge deck, shown in Figure 51, are presented in Figures 52 to 57. They include the derivatives $-H_1^*$ and A_2^* extracted at the angle of attack $\beta = 0°, \pm 6°$. For the definition of the test configurations see Figure 11.

8. CONCLUSIONS

A. The bridge section-model of the original bridge deck exhibited (for the range of angles of attack $-6° \leq \beta \leq 6°$) one degree-of-freedom torsional flutter. The critical wind speed depended upon mechanical damping of the model and upon the angle of attack.

B. The vortex-induced response for vertical and torsional degree-of-freedom ($-6° \leq \beta \leq 6°$) occurred at speeds much lower than the critical wind speed. The amplitude of oscillation depended on the damping level of the model and the angle of attack.

C. The lowest critical wind speed for the prototype bridge at the bridge damping ratio (in torsion) $\zeta_T = 0.8\%$ was estimated to be 190 mph. For higher damping levels this value is expected to increase.

D. The vortex-induced oscillation for the vertical degree-of-freedom was estimated to occur for the prototype bridge at a wind speed of approximately 32 mph.

E. The maximum vortex-induced amplitudes of oscillation and acceleration occurred at the angle of attack $\beta = -6°$.

F. The highest amplitudes of vertical oscillation (estimated for the prototype bridge) did not exceed 0.5 percent of the width of the bridge deck B for the damping ratio $\zeta_T \cong 0.84$ percent.

G. The corresponding amplitude of acceleration was approximately equal to 5 percent of g (g = 32.17 ft/sec^2).

H. As the angle of attack β was changed from $-6°$ to $4.8°$ the vortex-induced vertical oscillation was reduced by approximately 40 percent.

I.   Modifications   of   the   original   bridge   deck,   leading   to   a
     streamlined (optimal) bridge deck, resulted in a substantial
     improvement of the bridge deck aerodynamic behavior.

J.   The results presented are a somewhat conservative estimate   of
     the bridge aerodynamic response due to the assumption of a
     rather broad range of the angle of attack $-6° \leq \beta \leq 6°$.

9. REFERENCES

[1] Scanlan, R.H., "Recent Methods in the Application of Test Results to the Wind Design of Long, Suspended-Span Bridges," Report No. FHWA-RD75-115, October 1975.

[2] Scanlan, R.H. and Tomko, J.J., "Airfoil and Bridge Deck Flutter Derivatives, " Jnl. Eng. Mech. Div., ASCE, Vol. 97, EM6, December 1971, pp. 1717-1737.

[3] Simiu, E. and Scanlan, R.H., Wind Effects on Structures: An Introduction to Wind Engineering, John Wiley and Sons, Inc., 1978.

10. FIGURES

RIGID FRAME AND SUSP.
SYSTEM FOR BRIDGE
SECTION MODEL

6'

4'-6"

3'

WIND

8'

2'-4"

(4) 3' SECTIONS

37'
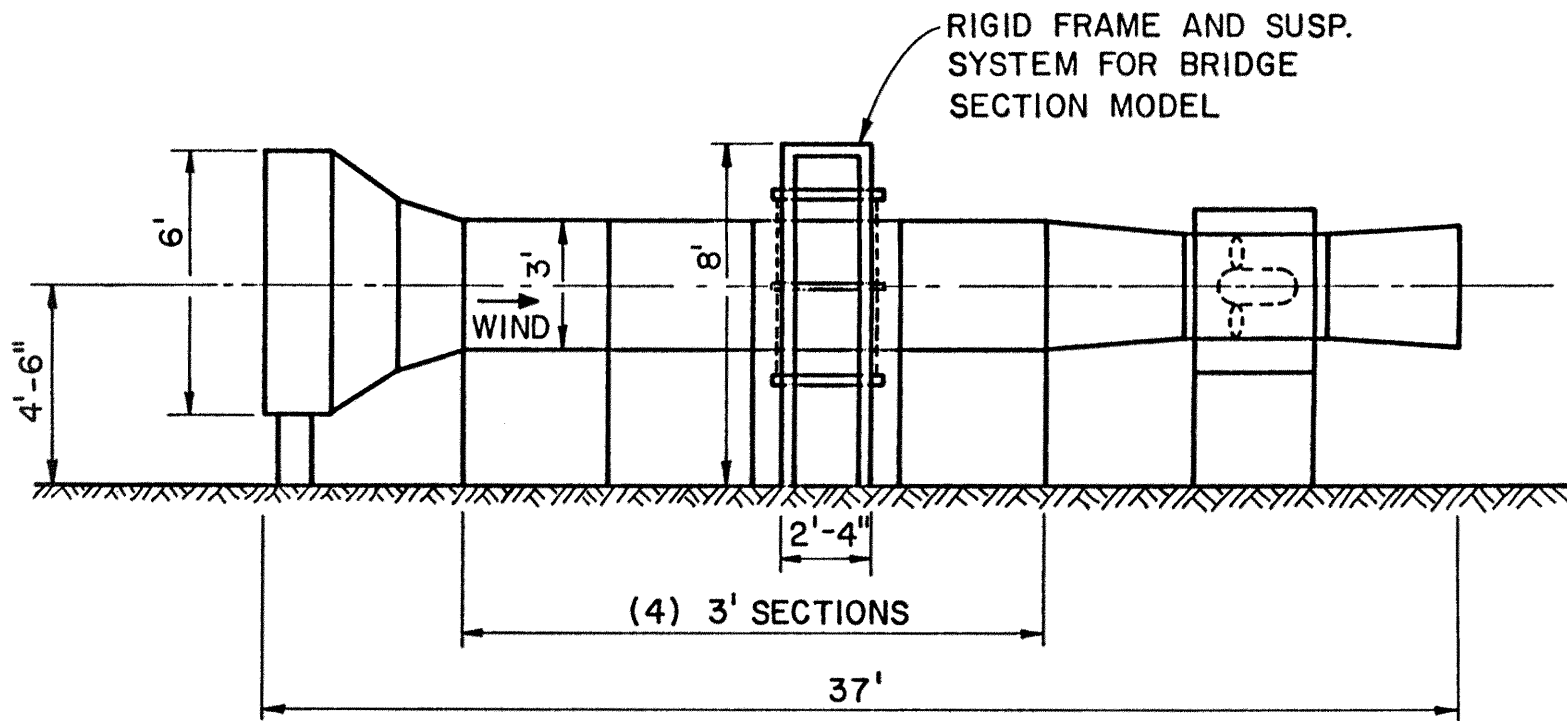
Figure 1. Structural Aerodynamics Wind Tunnel

Wind
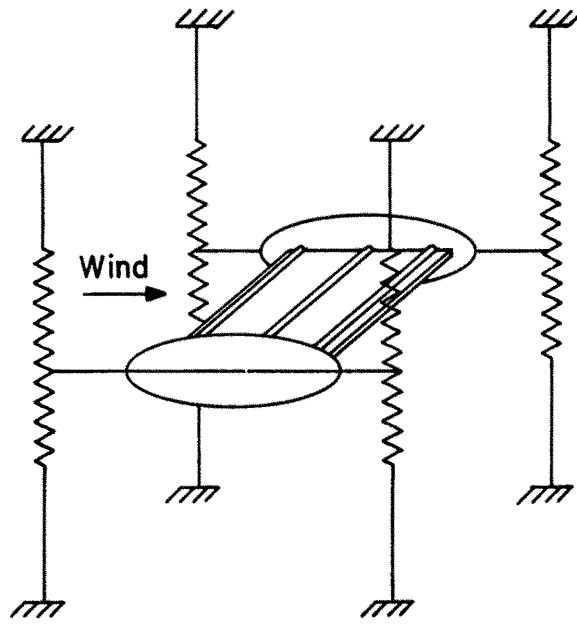
Figure 2. Bridge Section Model

Flow

Ohio River

PLAN

El. 1060.0

Normal Pool El. 645.0

820' 687'

ELEVATION
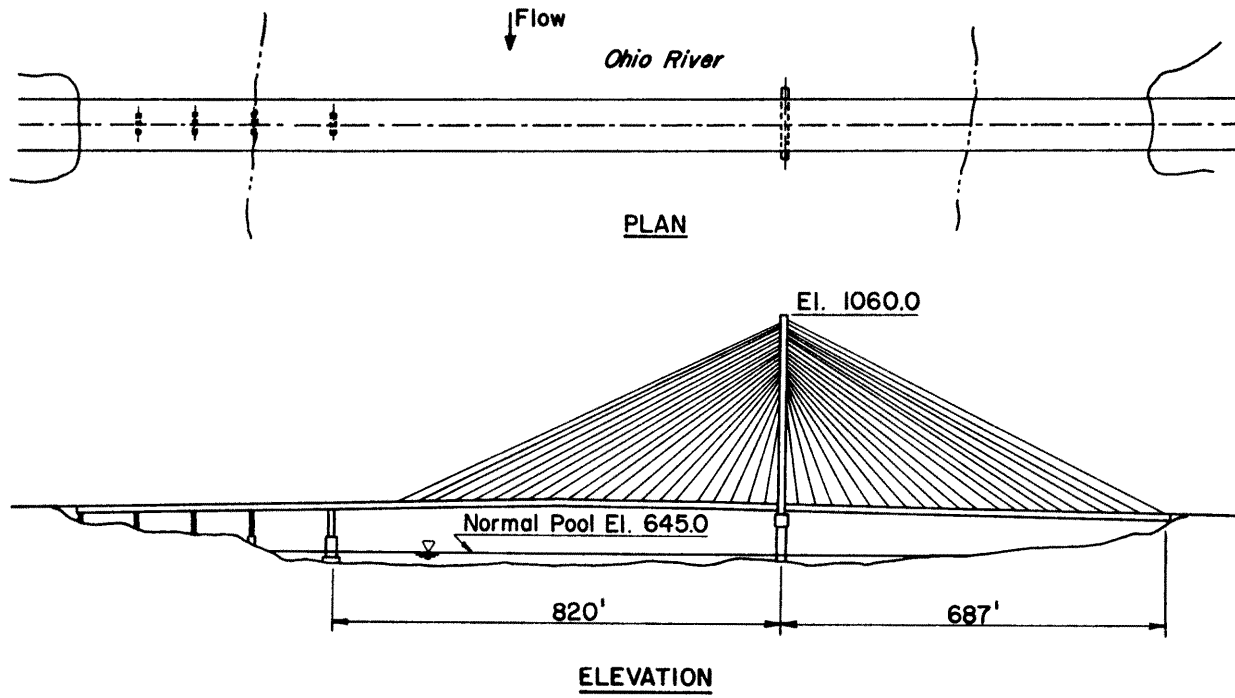
Figure 3. Main Spans of Weirton-Steubenville Cable-Stayed Bridge
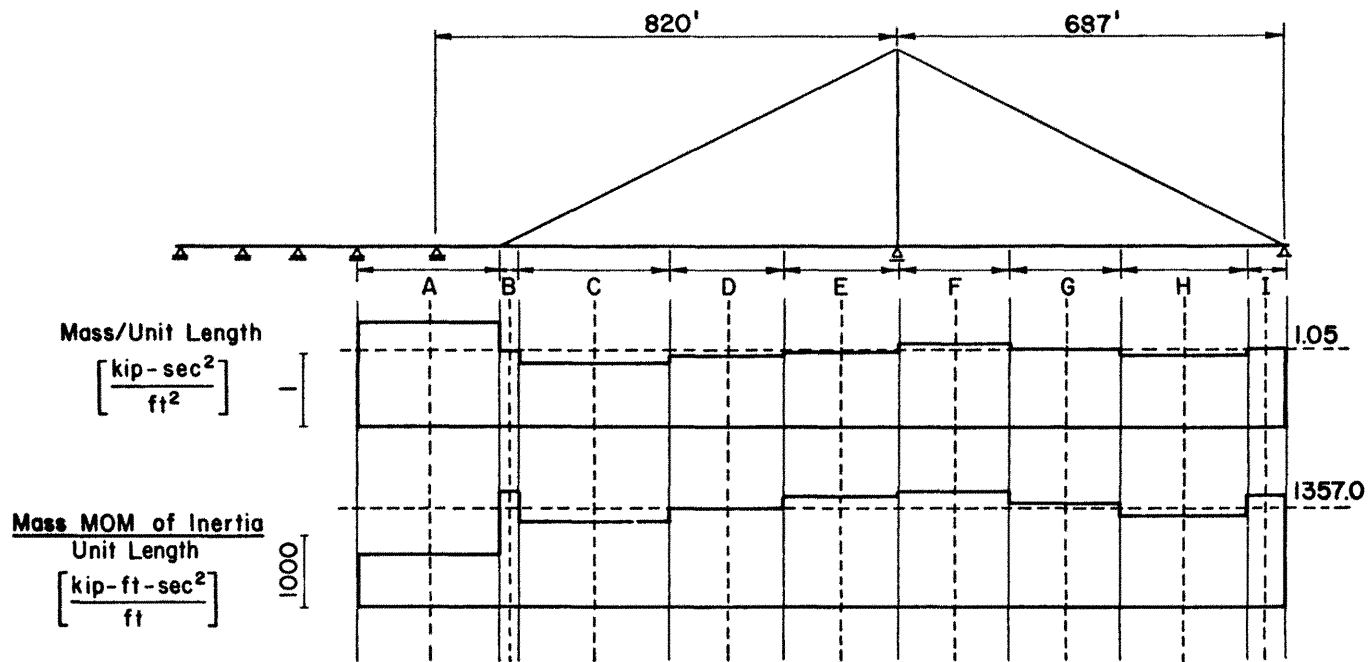
Figure 4. Mass and Mass Moment of Inertia of Bridge Deck
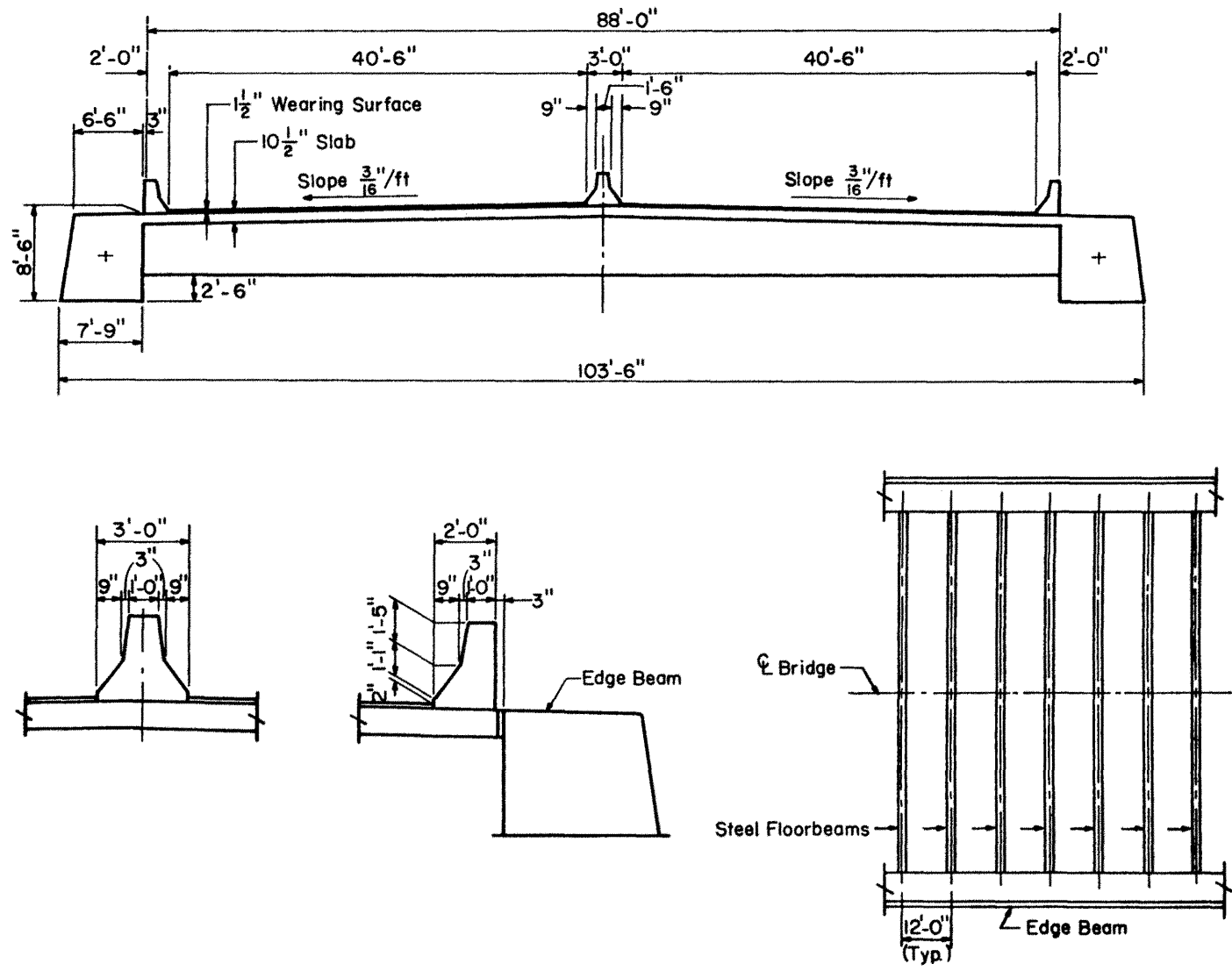
Figure 5. Prototype Bridge Deck
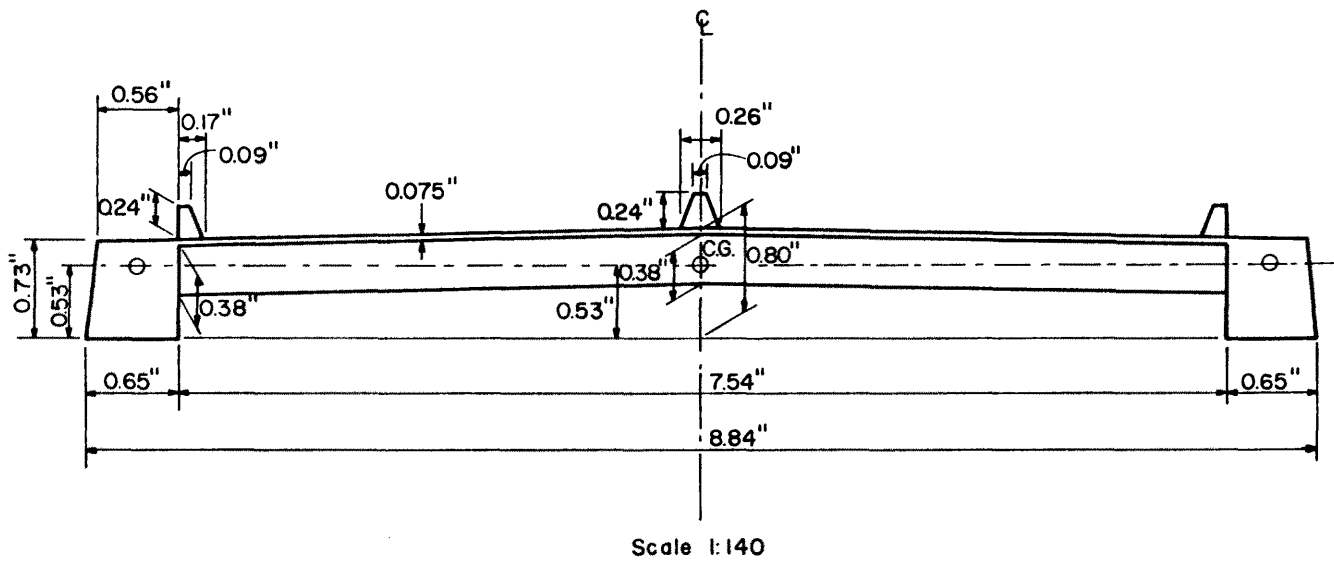
Figure 6. Model Bridge Deck
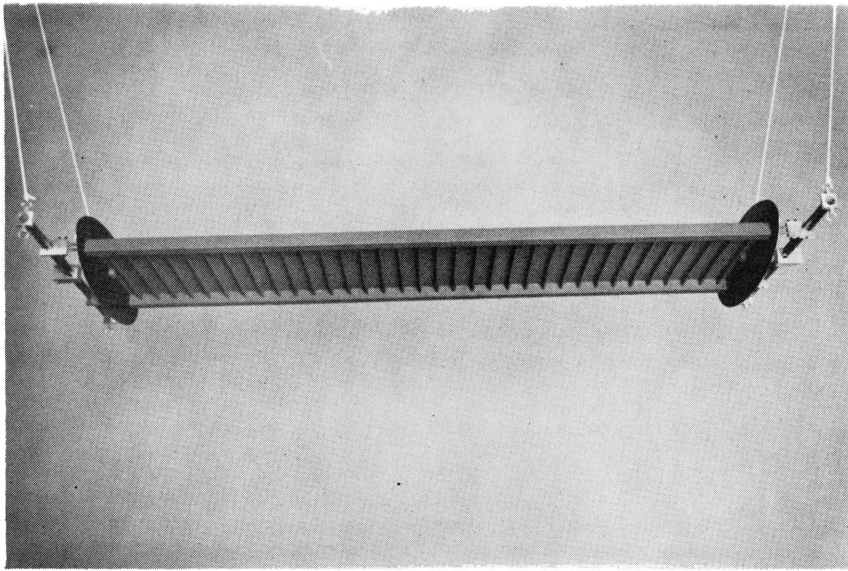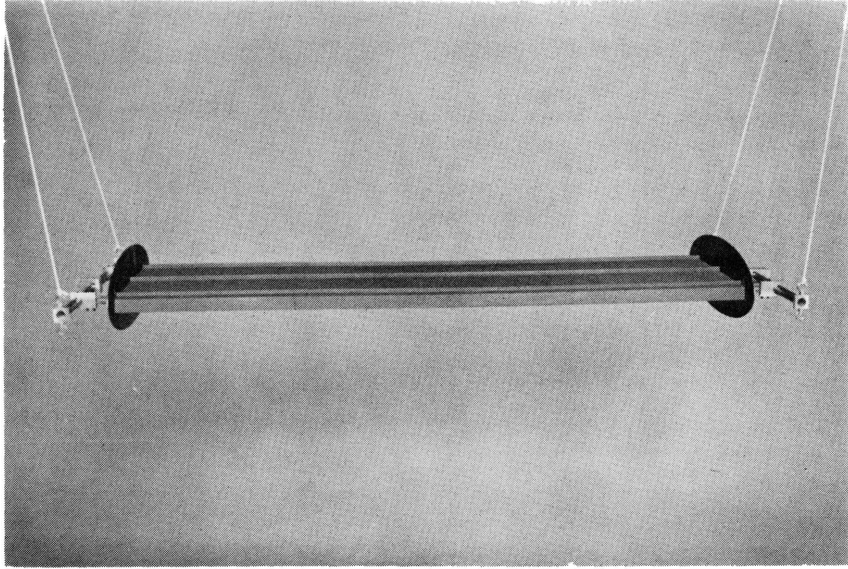
Figure 7. Section Model of Bridge
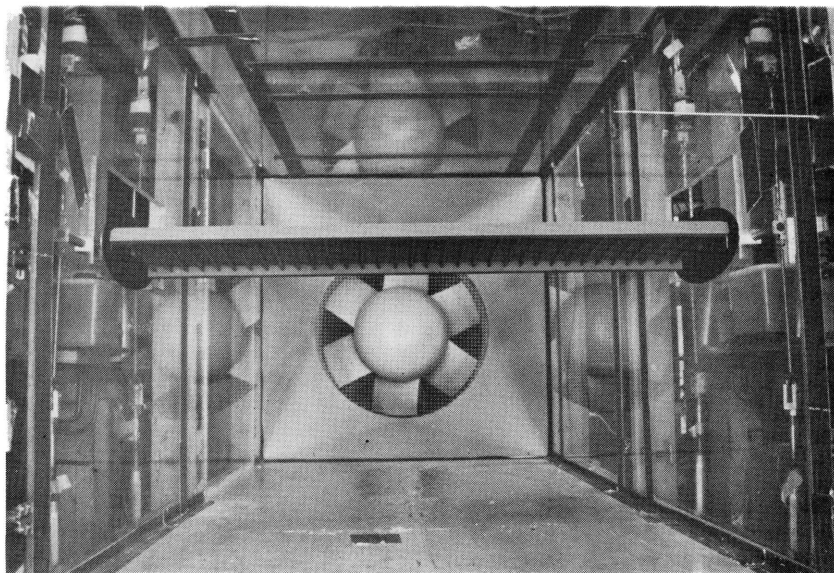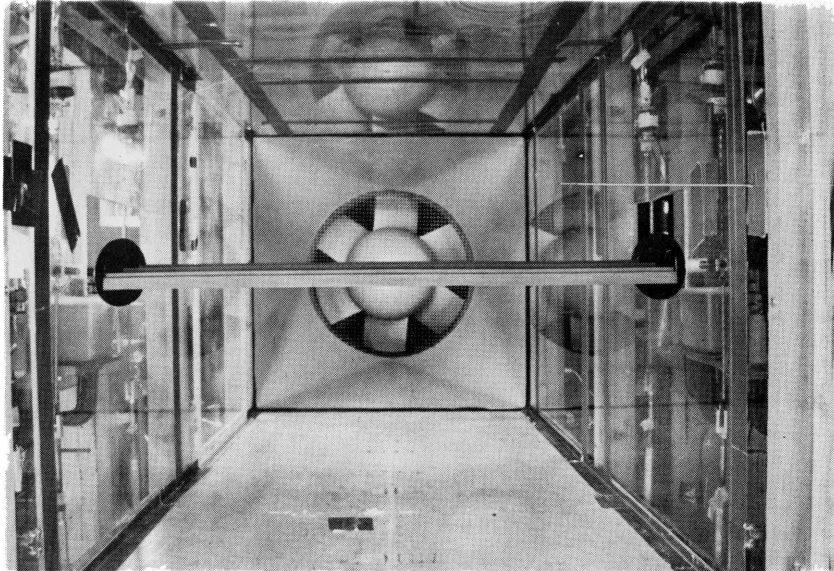
Figure 8.   Bridge Section Model in Wind Tunnel
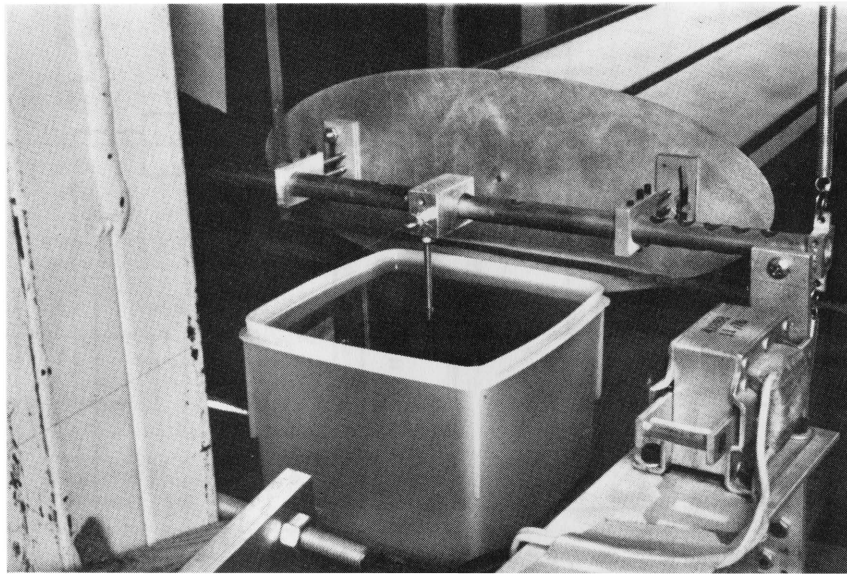
Figure 9. Viscous Damper and Element of Model Support
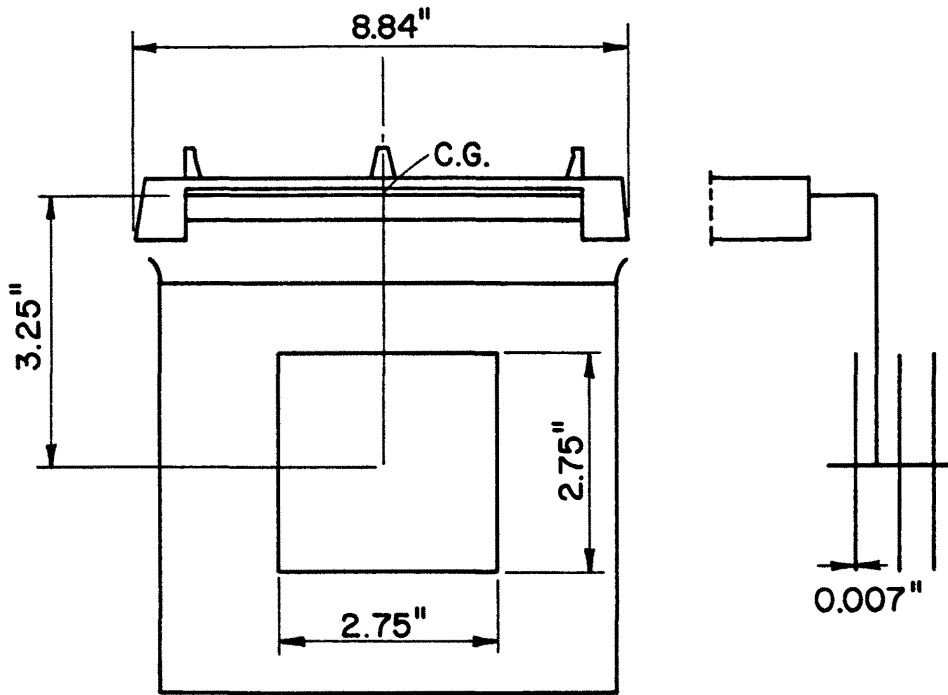
Figure 10. Viscous Damper - Details
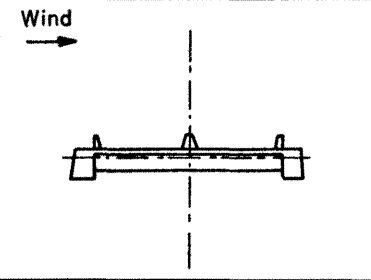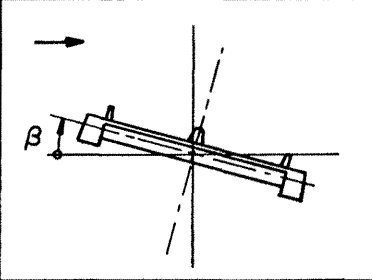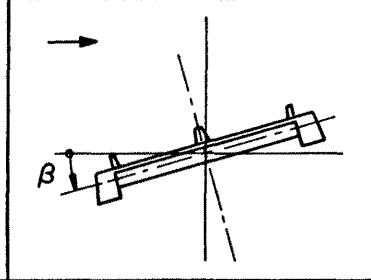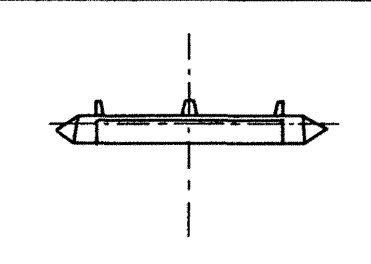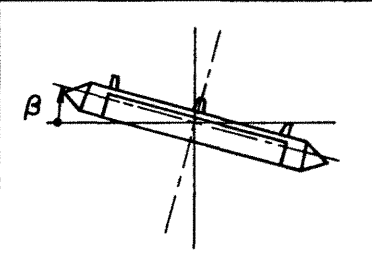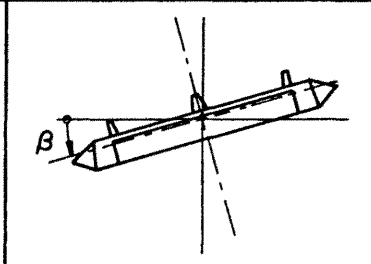
	I	II	III
A	Wind →	→	→
	Vertical AIO-V	Vertical $\beta = 3°$ A II 3-V $\beta = 6°$ A II 6-V	Vertical $\beta = -3°$ A III 3-V $\beta = -4.8°$ A III 48-V $\beta = -6°$ A III 6-V
	Torsional AIO-T	Torsional $\beta = 3°$ A II 3-T $\beta = 6°$ A II 6-T	Torsional $\beta = -3°$ A III 3-T $\beta = -4.8°$ A III 48-T $\beta = -6°$ A III 6-T
B			
	Vertical BIO-V	Vertical $\beta = 6°$ B II 6-V	Vertical $\beta = -6°$ B III 6-V
	Torsional BIO-T	Torsional $\beta = 6°$ B II 6-T	Torsional $\beta = -6°$ B III 6-T

Figure 11. Experimental Configurations
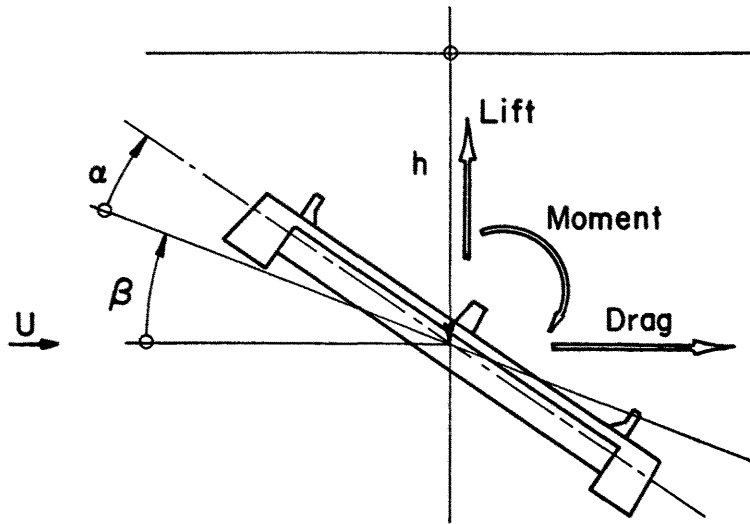
Figure 12. Basic Definitions
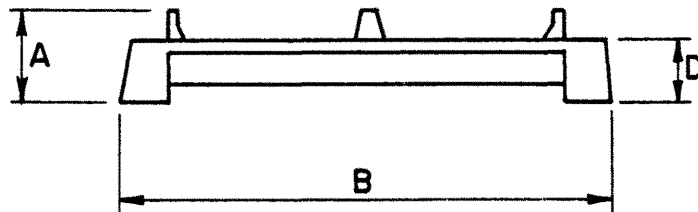
Figure 13. Basic Geometrical Dimensions
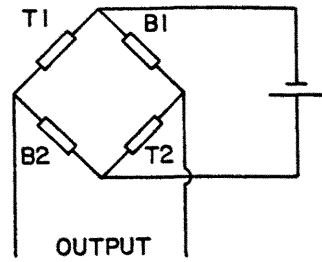
Figure 14. Arrangement for Aerodynamic Measurements

VERTICAL MOTION   TORSIONAL MOTION

SIGNAL CONDITIONER
(HONEYWELL)

AMPLIFIER & DC FILTER
(DANA)

DUAL BEAM
OSCILLOSCOPE
(TEKTRONIX)

TWO-CHANNEL
STRIP CHART
RECORDER
(BRUSH)

MINICOMPUTER
(HP-1000)
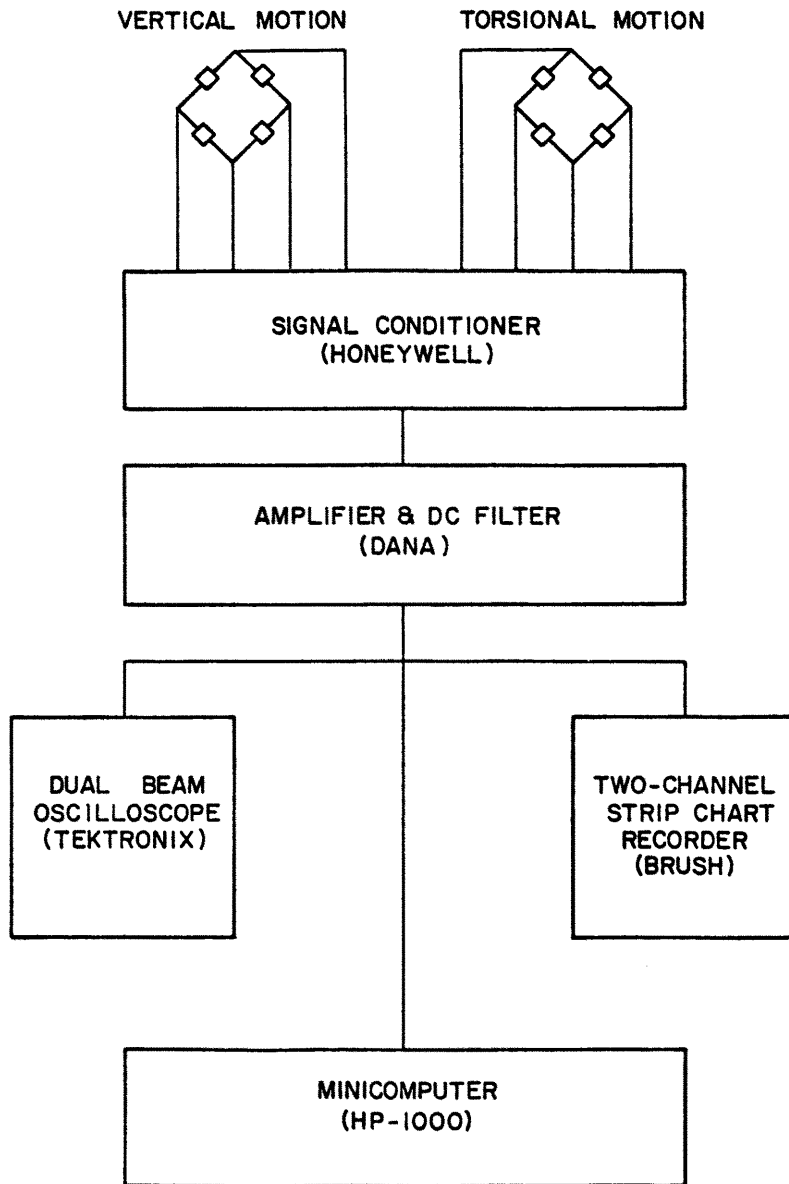
Figure 15.   Instrumentation
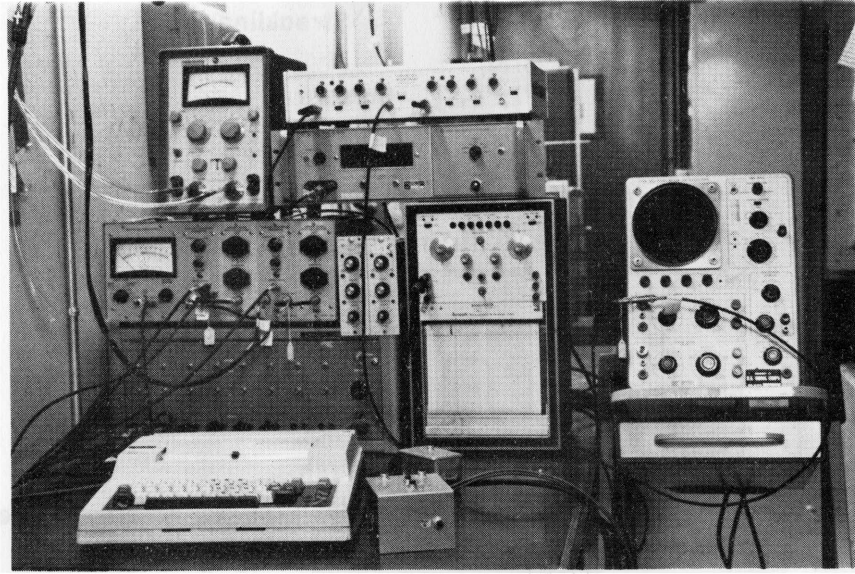
Figure 16.   General View of Some of the Instruments Used
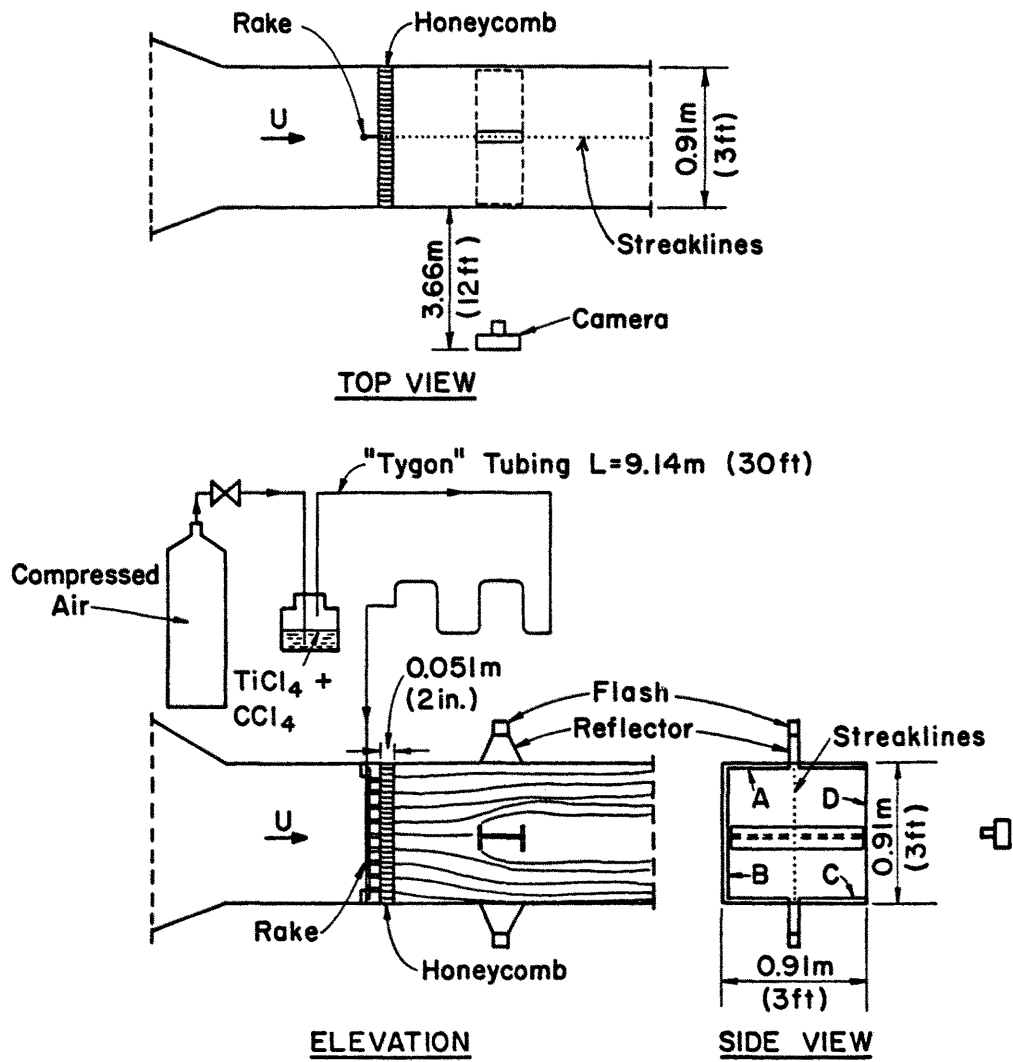
Figure 17. Flow Visualization Arrangement
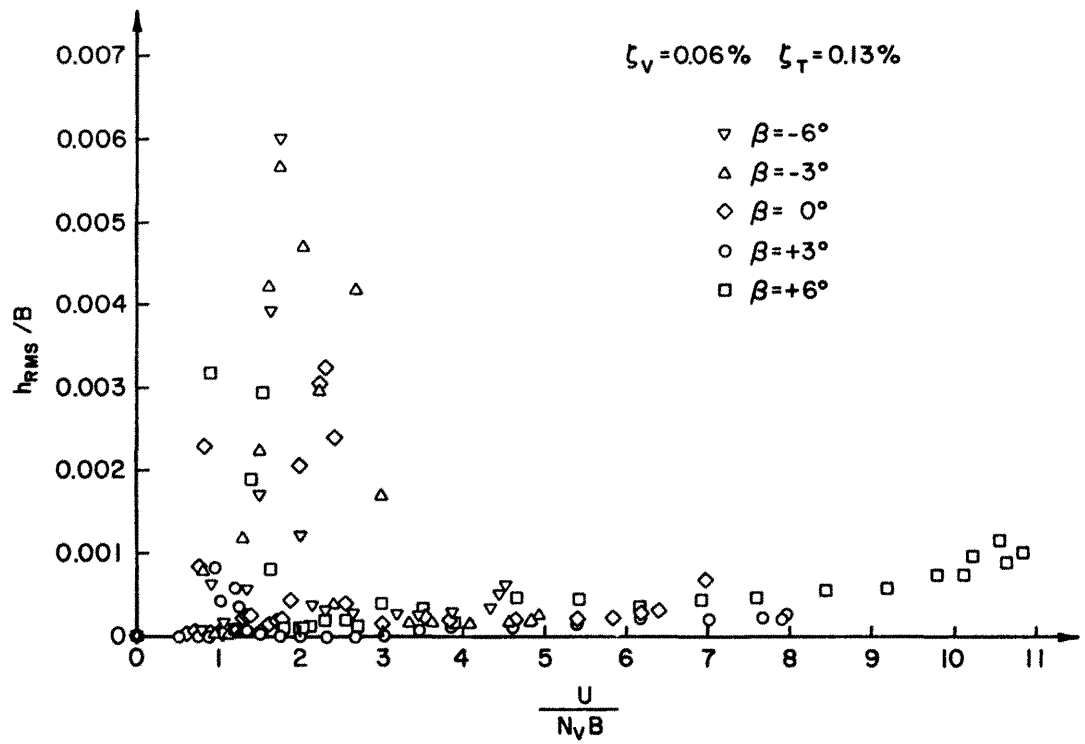
Figure 18. Vertical Response of Section Model with Very Low Damping at Different Angles of Attack
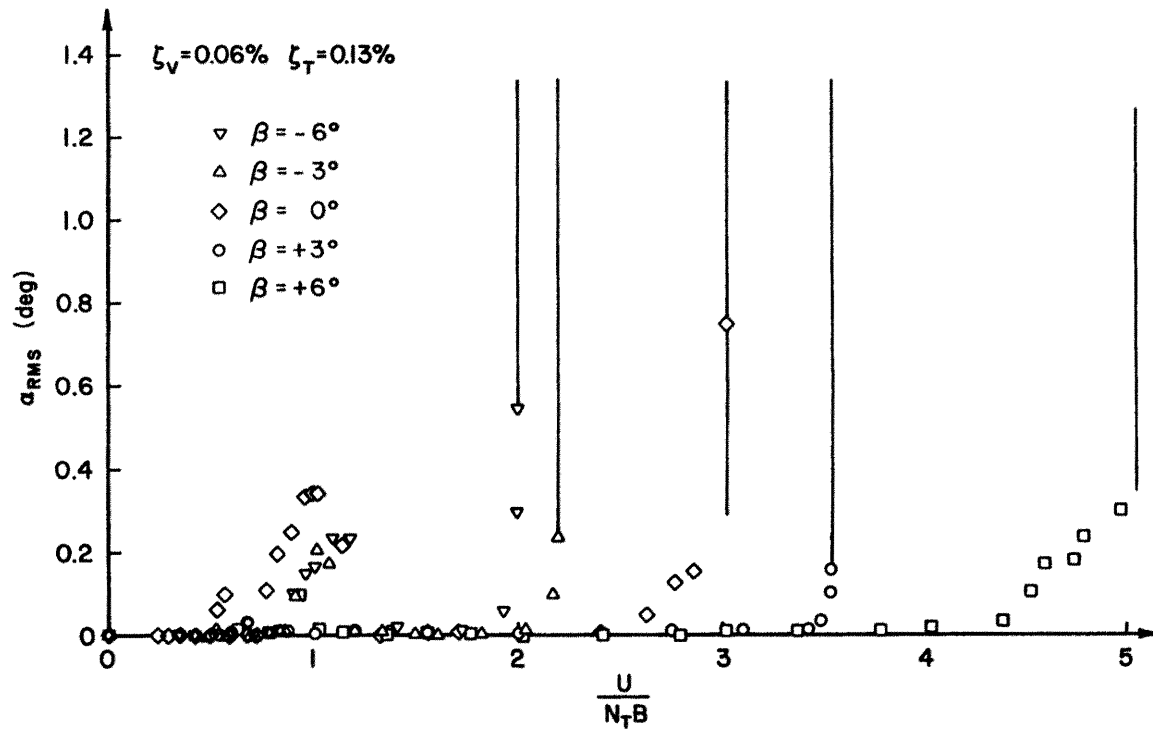
Figure 19.   Torsional Response of Section Model with Very Low Damping
at Different Angles of Attack
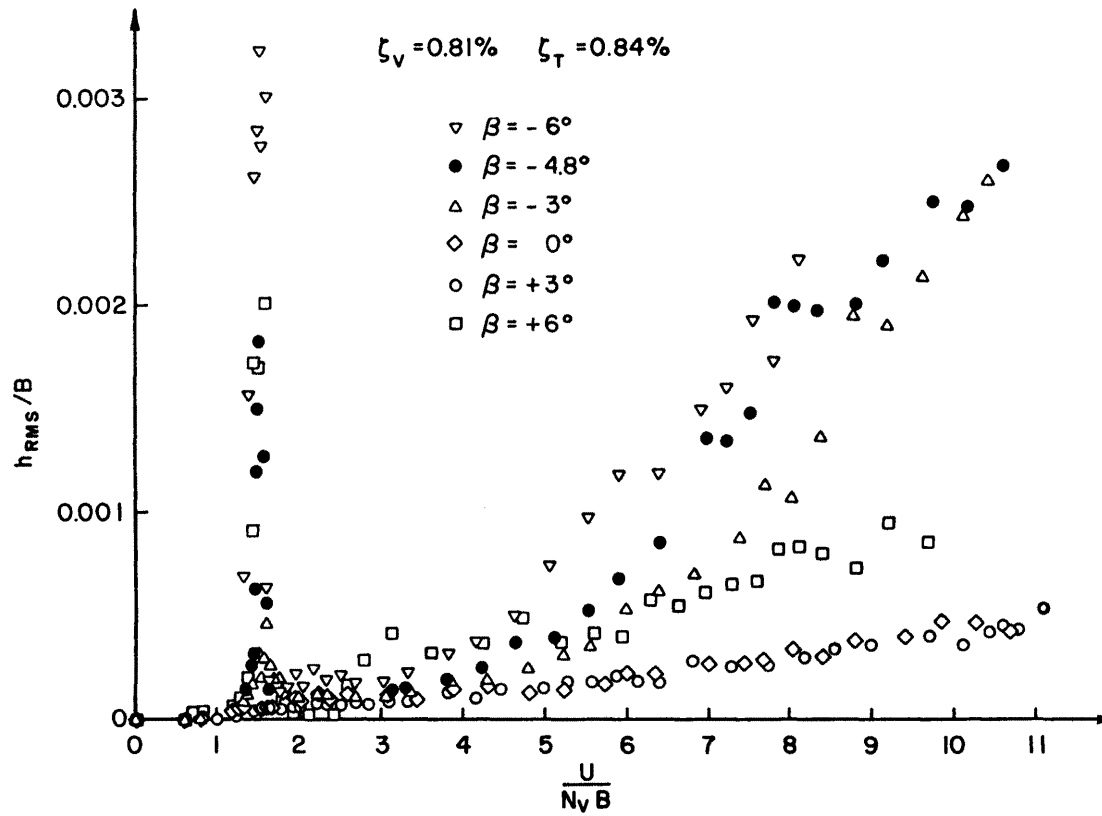
Figure 20. Vertical Response of Section Model with Moderate Damping at Different Angles of Attack

47
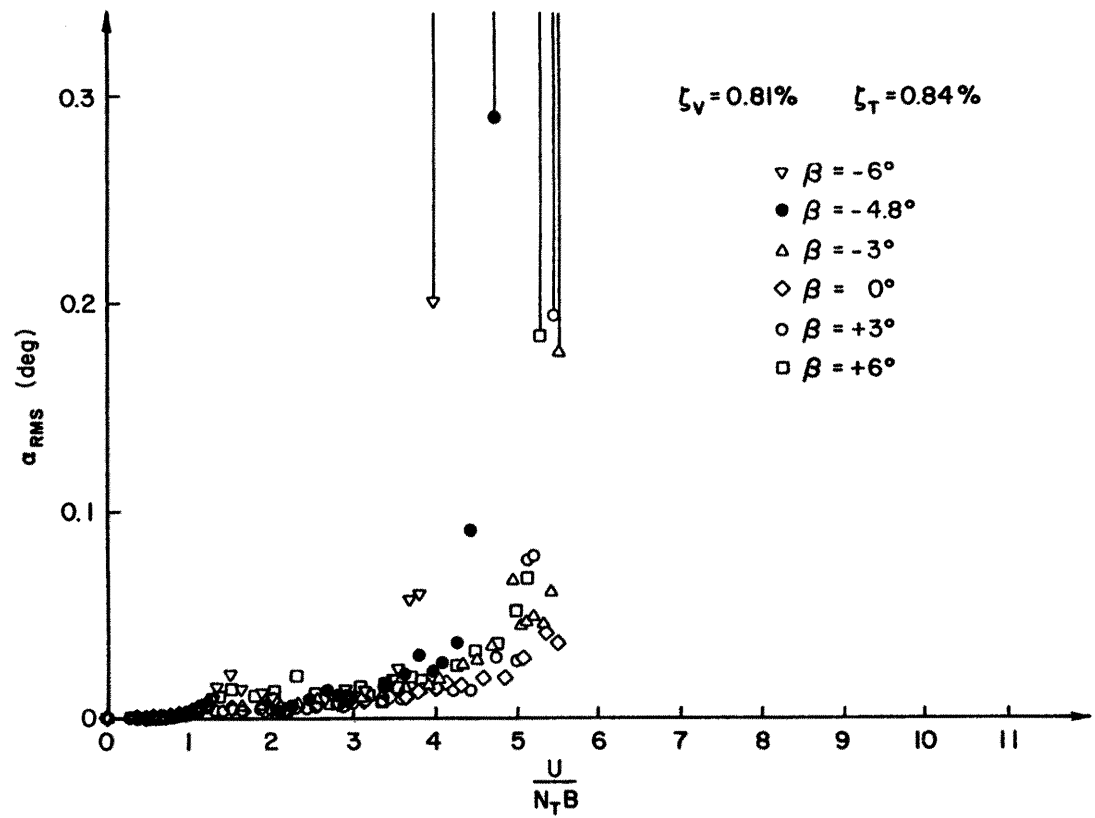
Figure 21.   Torsional Response of Section Model with Moderate Damping
at Different Angles of Attack
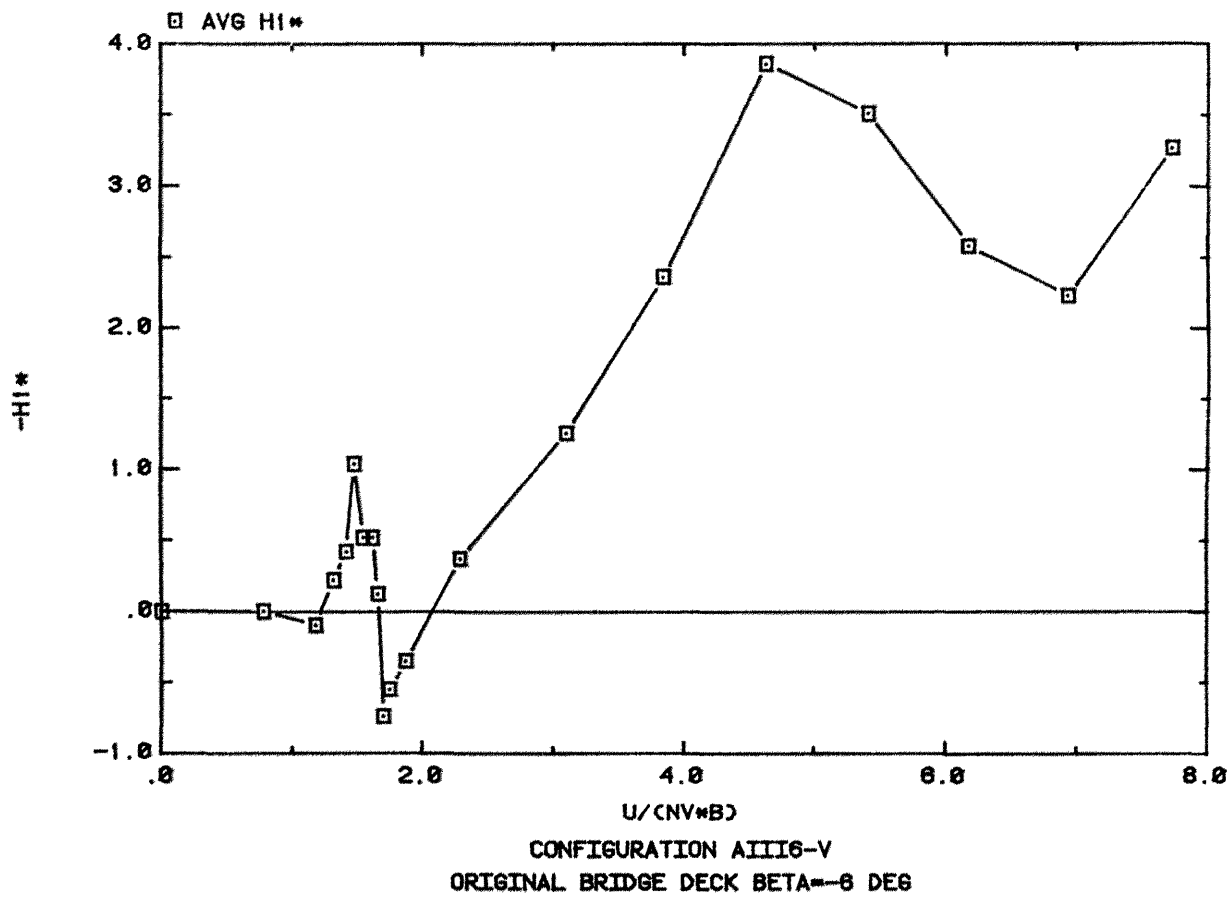
Figure 22.   Aerodynamic Derivative $-H_1^*$, Angle of Attack $\beta = -6°$
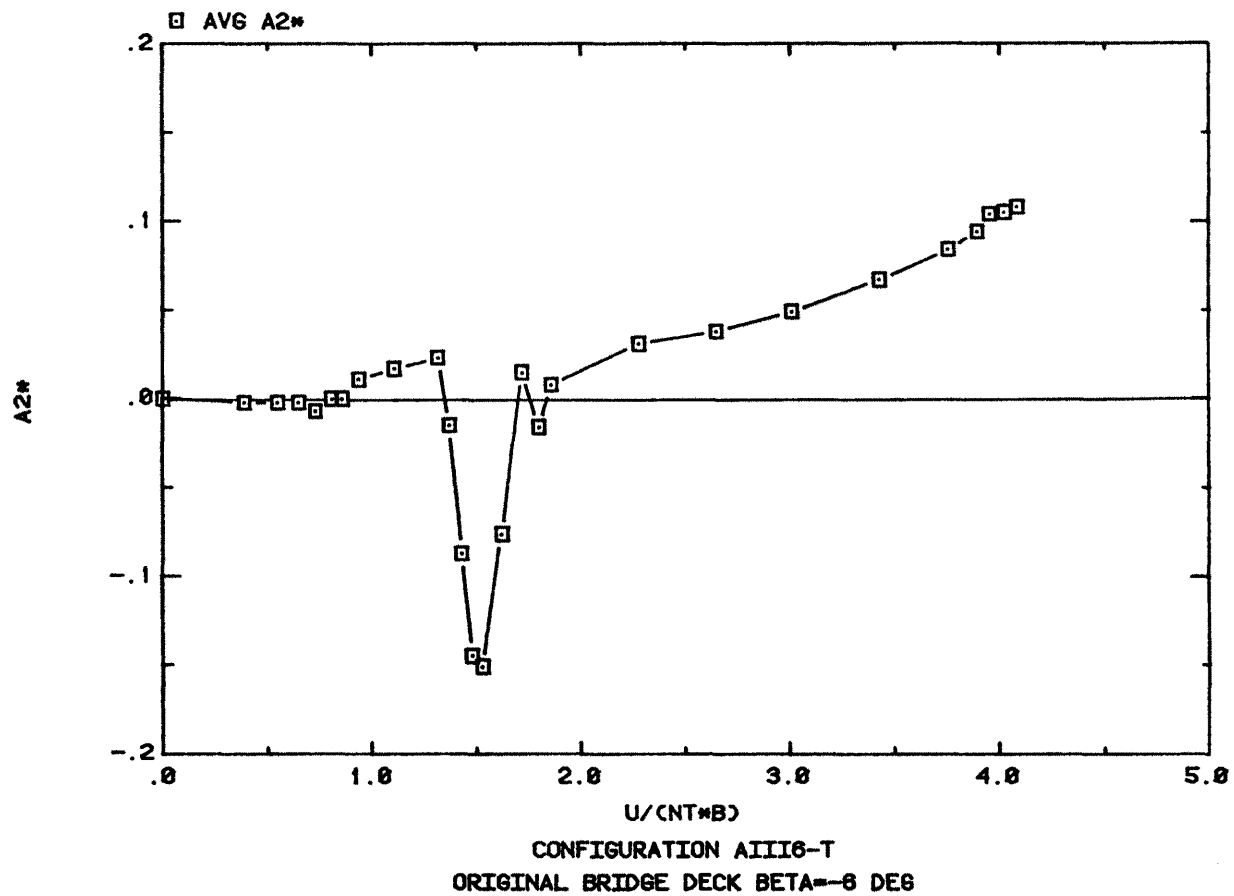
Figure 23. Aerodynamic Derivative A_2^*, Angle of Attack $\beta = -6°$
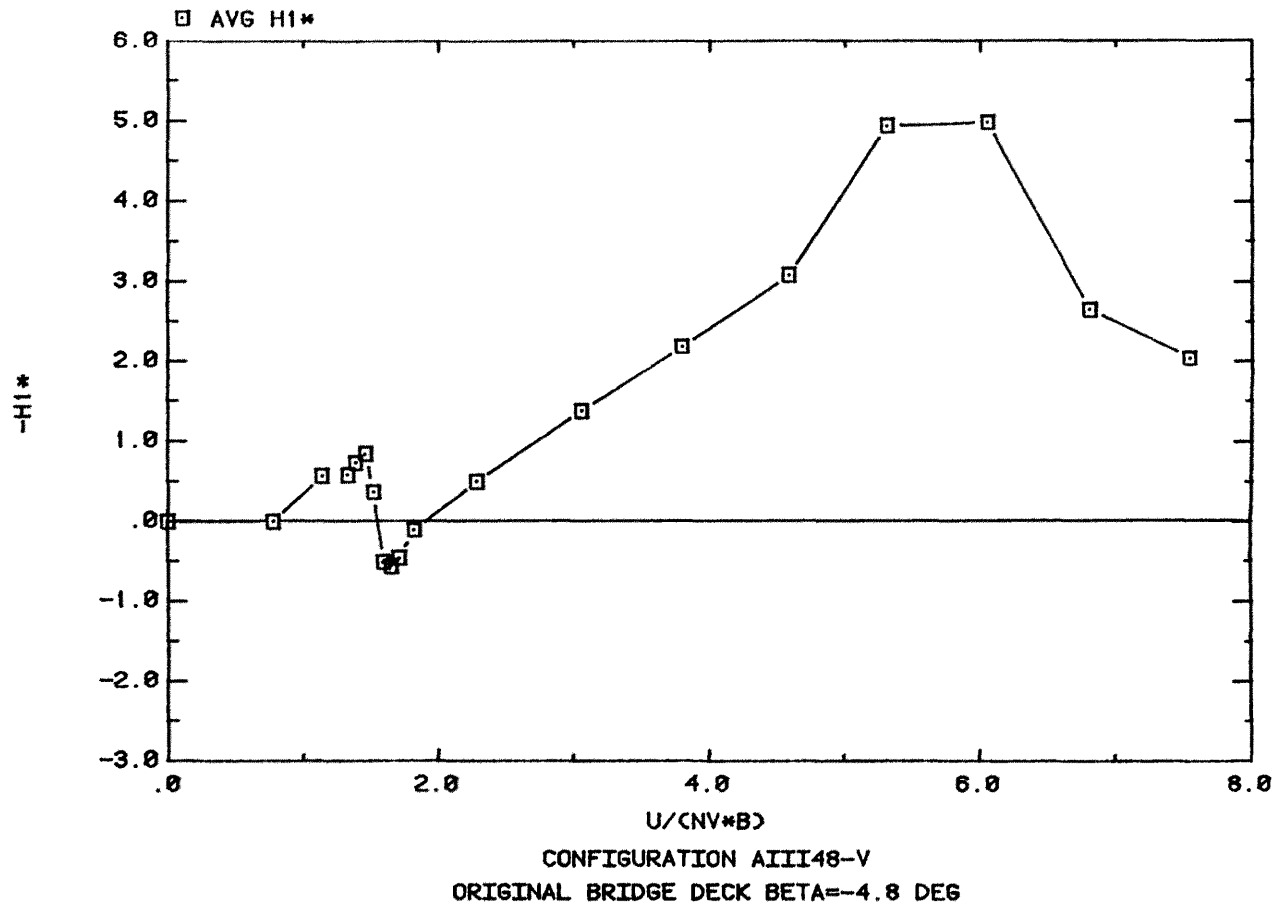
Figure 24. Aerodynamic Derivative $-H_1^*$, Angle of Attack $\beta = -4.8$
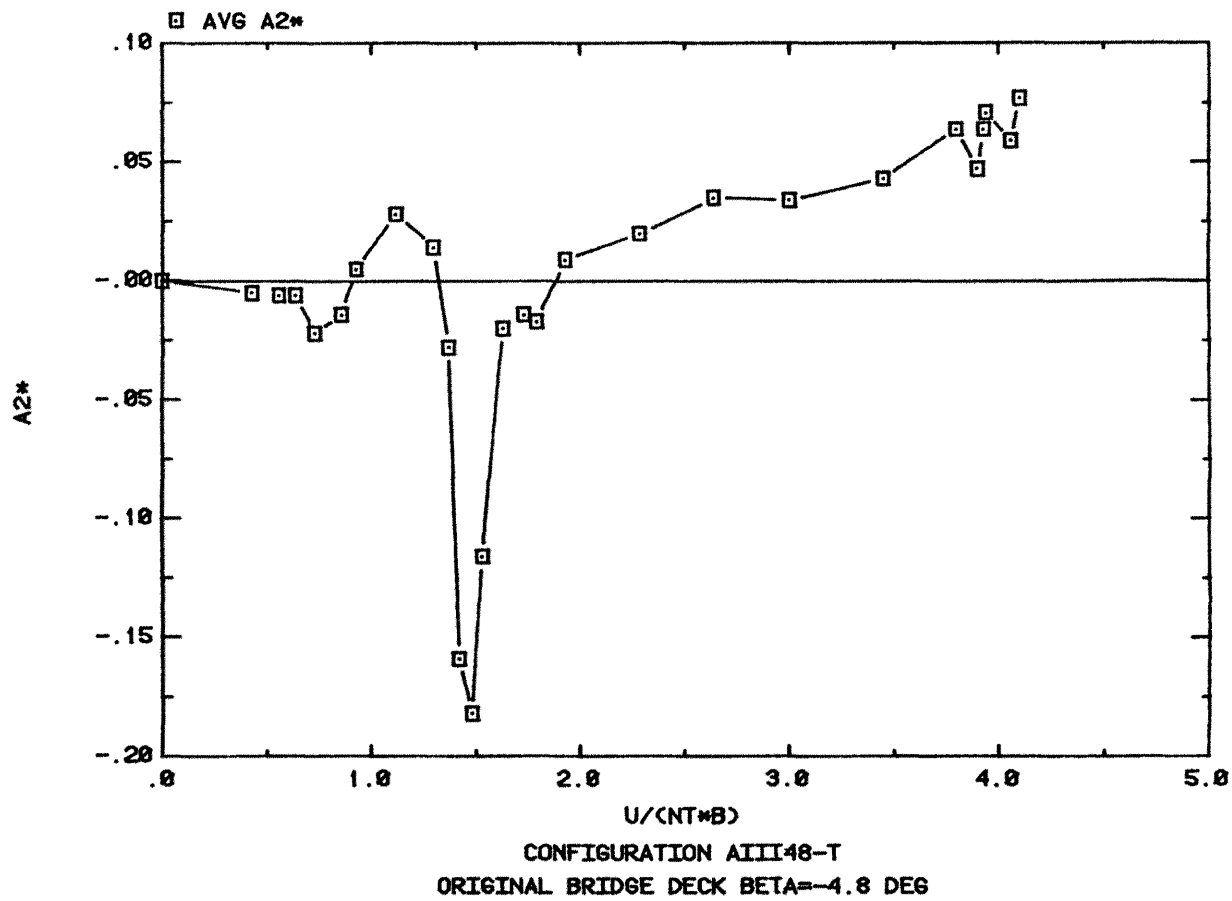
Figure 25. Aerodynamic Derivative A_2^*, Angle of Attack $\beta = -4.8°$
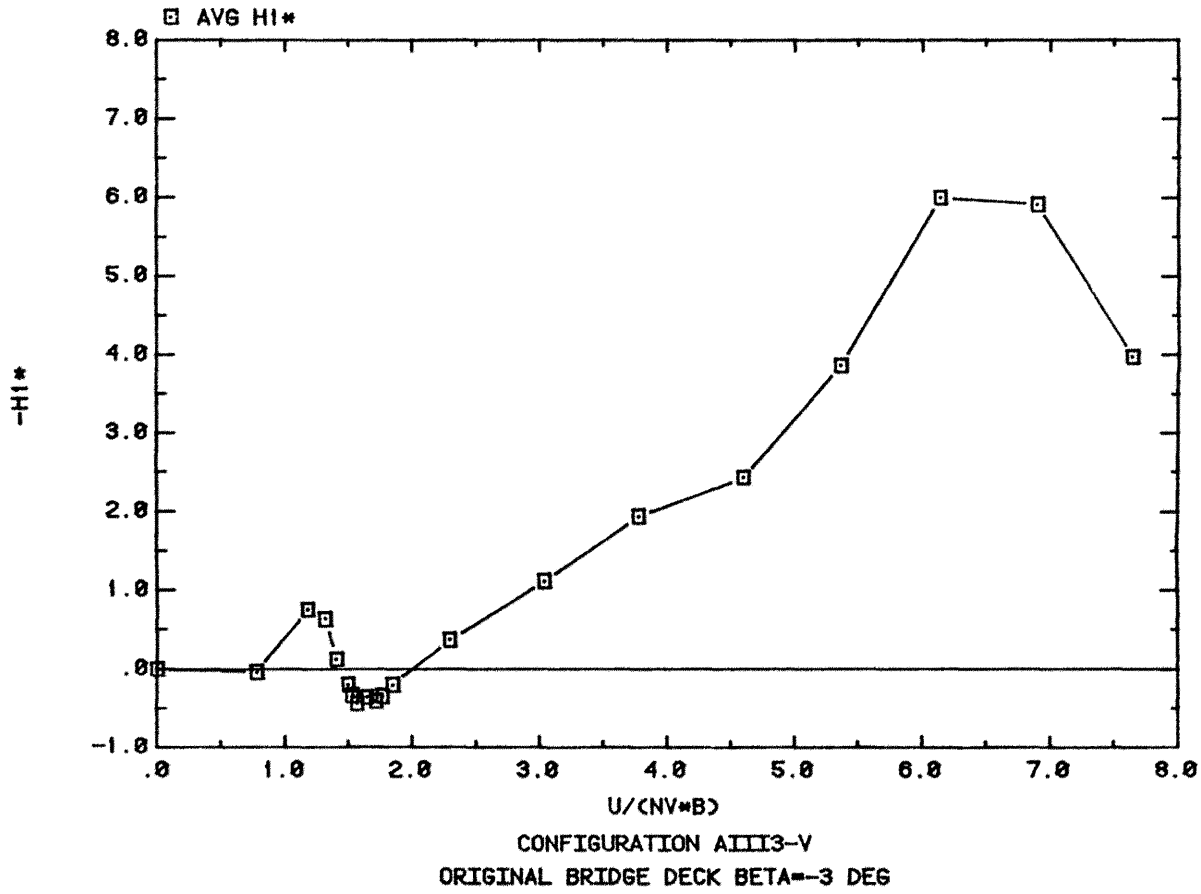
Figure 26. Aerodynamic Derivative $-H_1^*$, Angle of Attack $\beta = -3°$
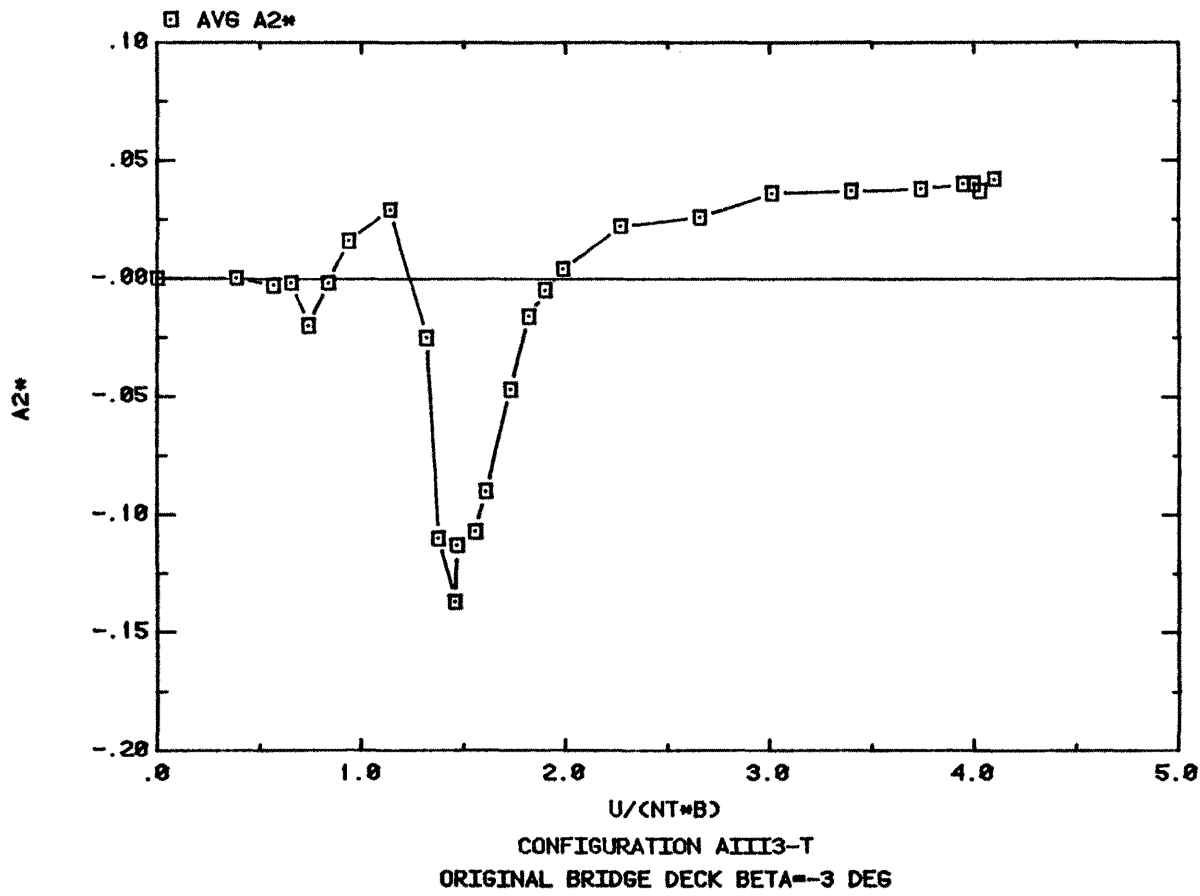
Figure 27. Aerodynamic Derivative A_2^*, Angle of Attack $\beta = -3°$
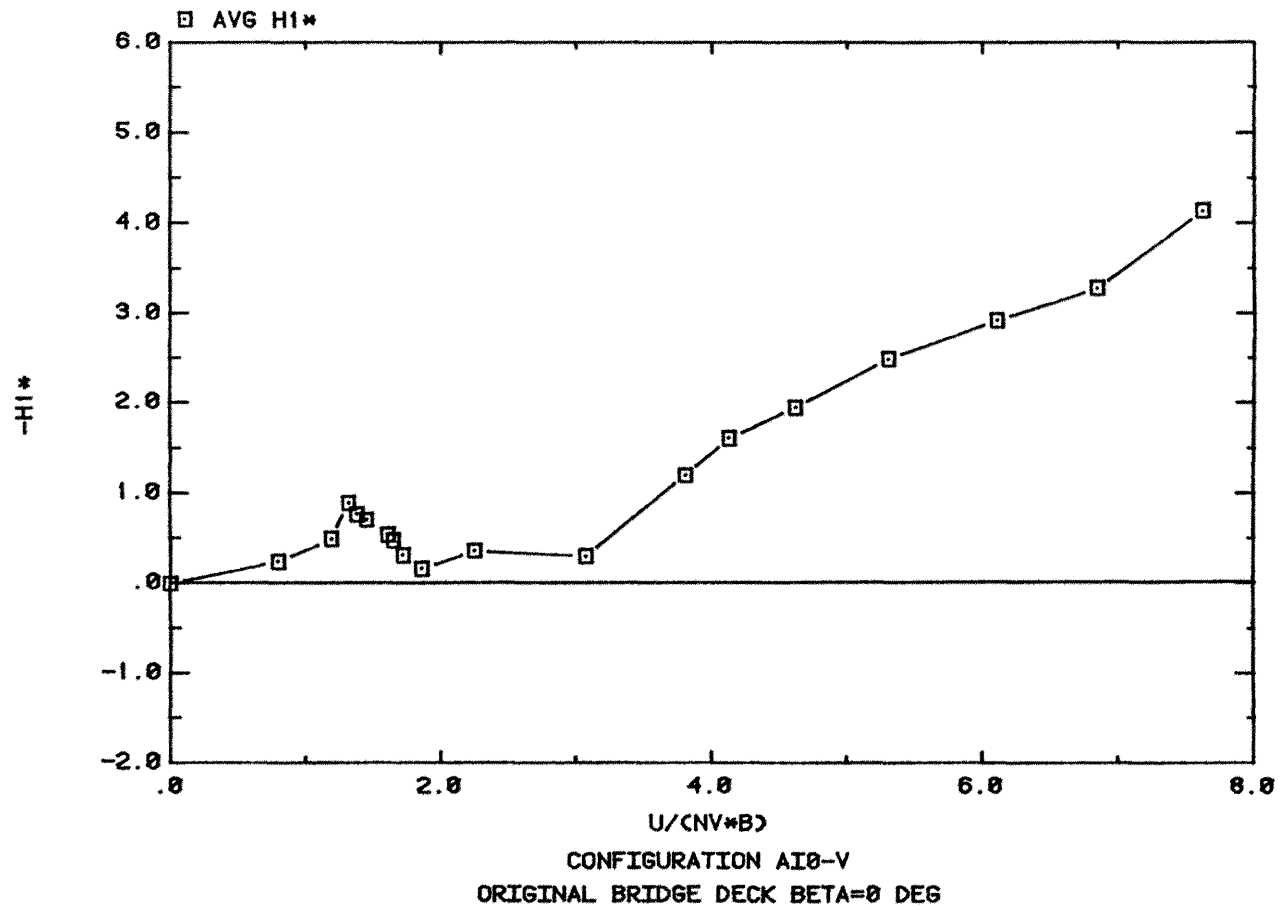
Figure 28. Aerodynamic Derivative $-H_1^*$, $\beta = 0°$
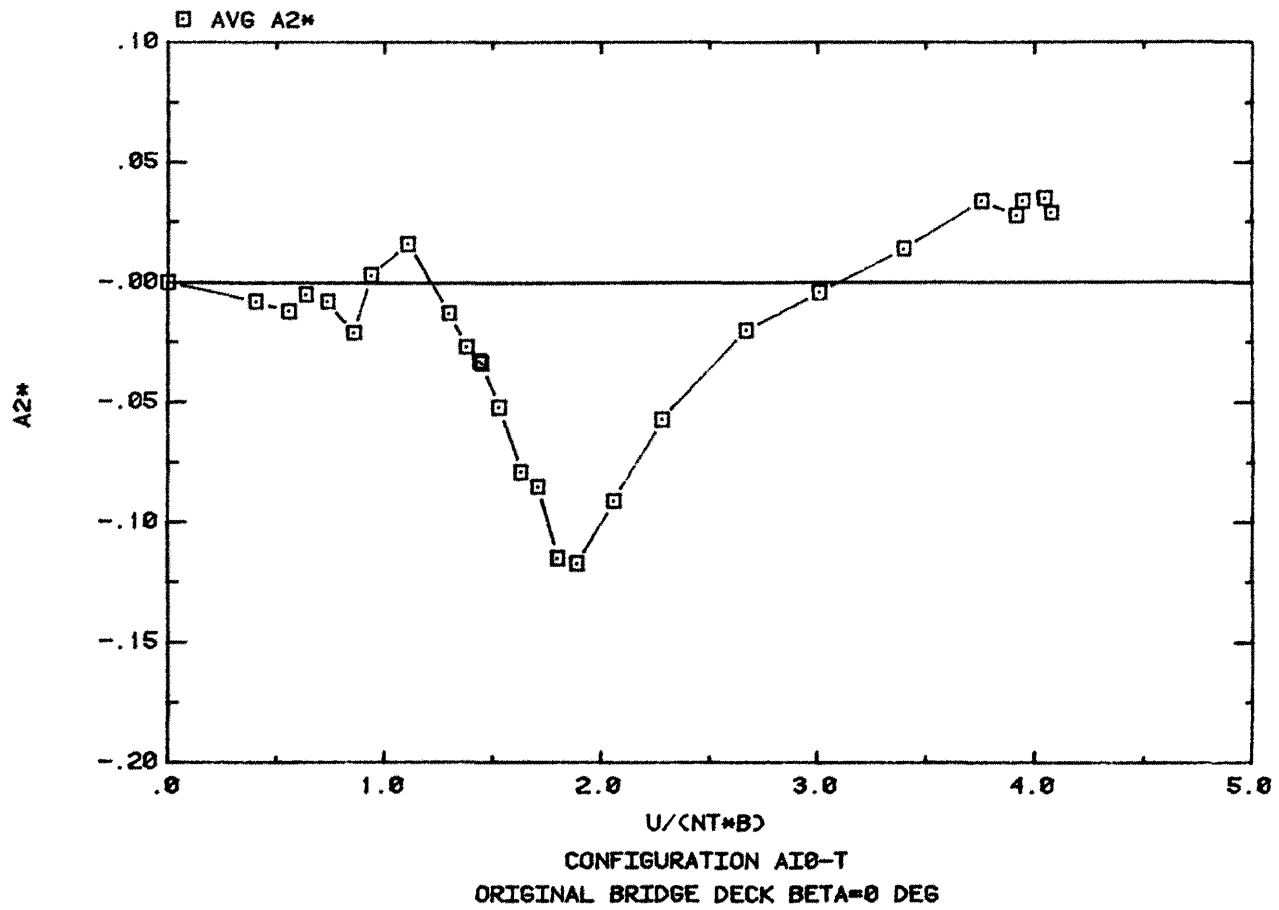
Figure 29. Aerodynamic Derivative A_2^*, $\beta = 0°$
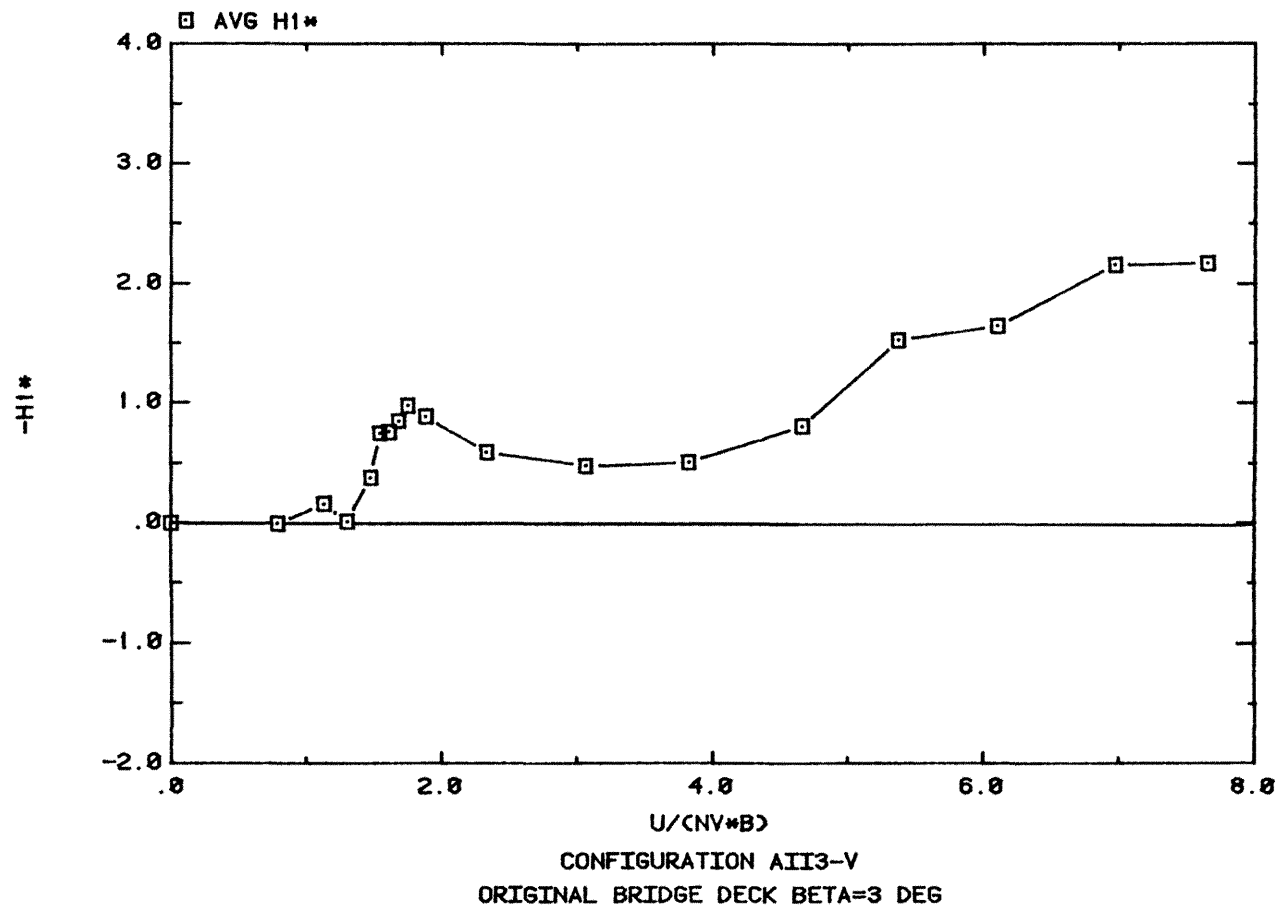
Figure 30. Aerodynamic Derivative $-H_1^*$, Angle of Attack $\beta = +3°$
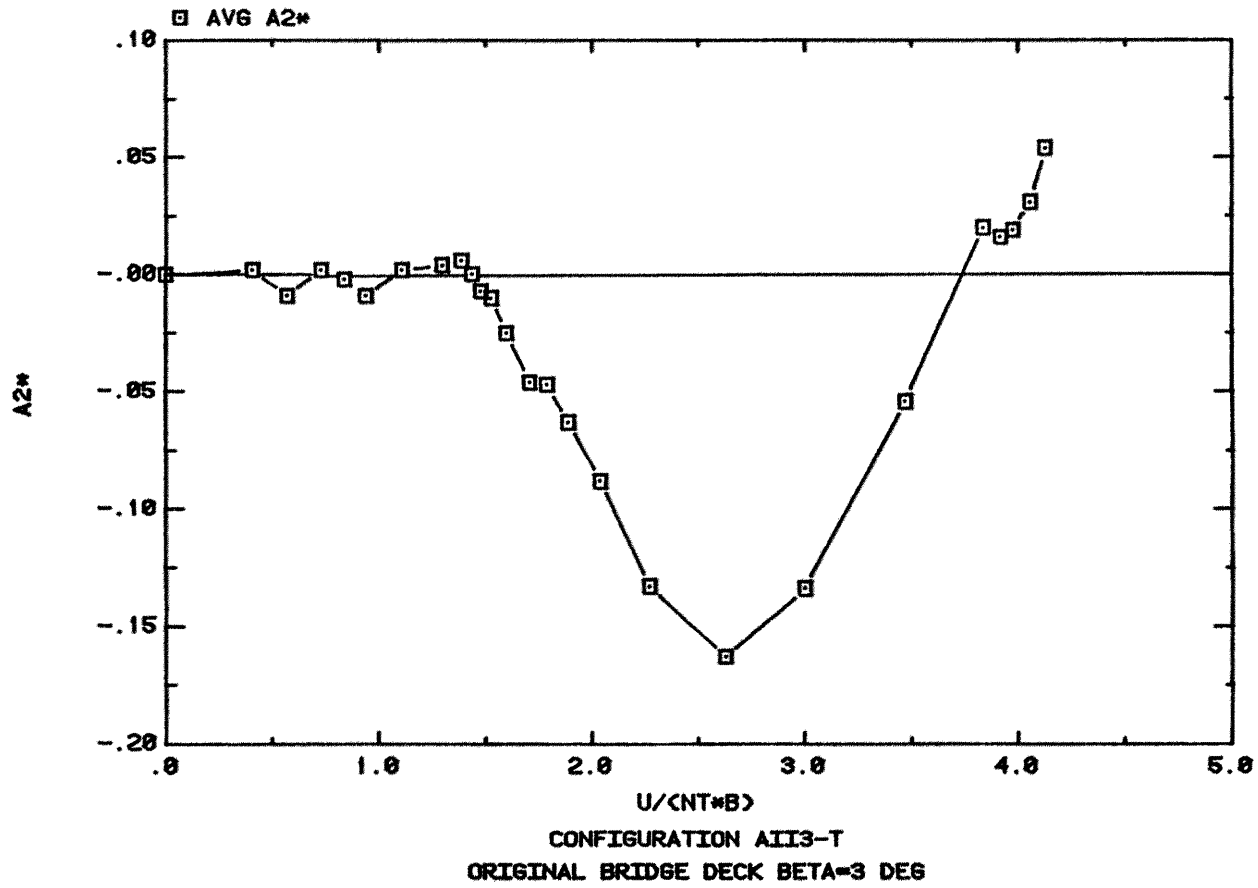
Figure 31. Aerodynamic Derivative A_2^*, Angle of Attack $\beta = +3°$
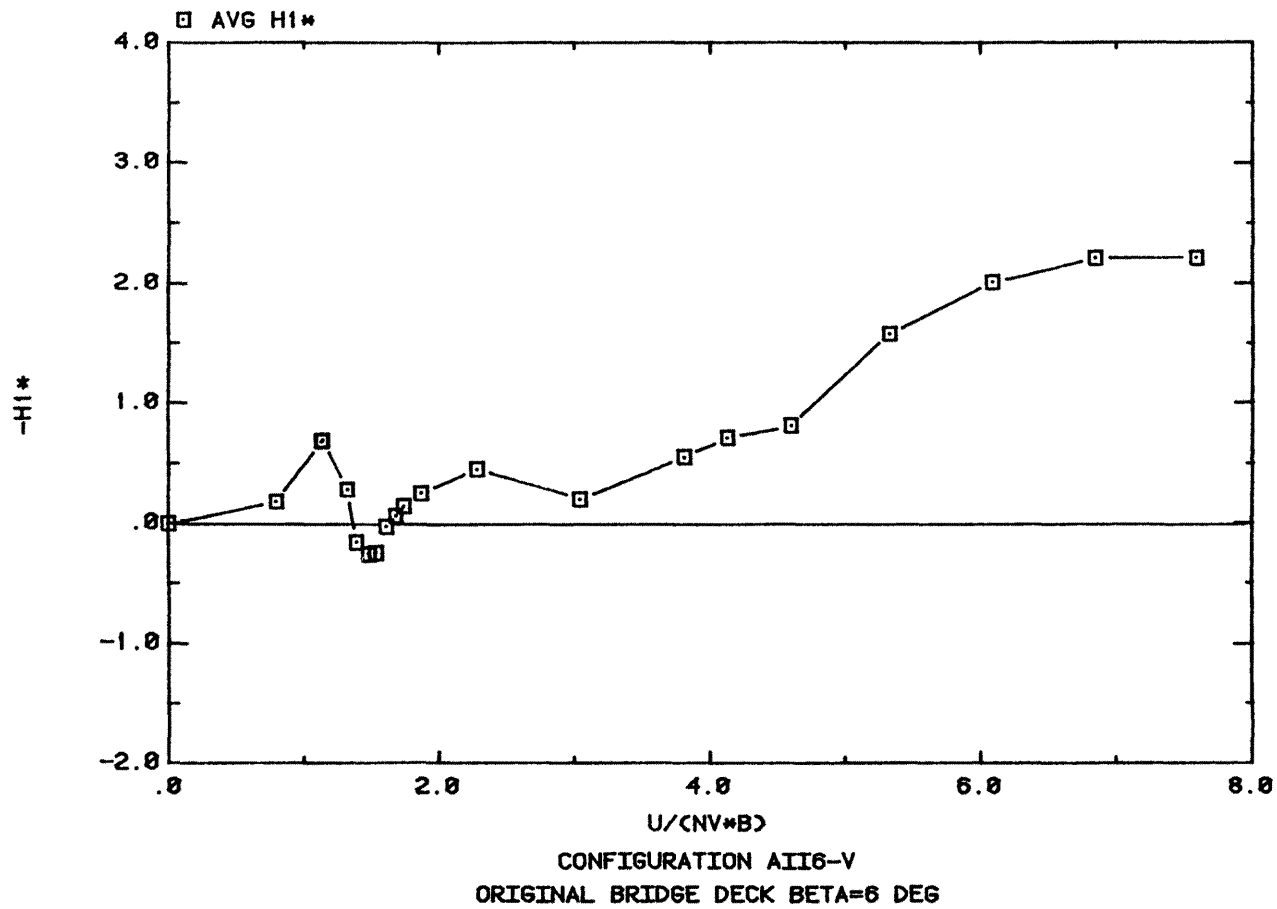
Figure 32. Aerodynamic Derivative $-H_1^*$, Angle of Attack $\beta = +6°$
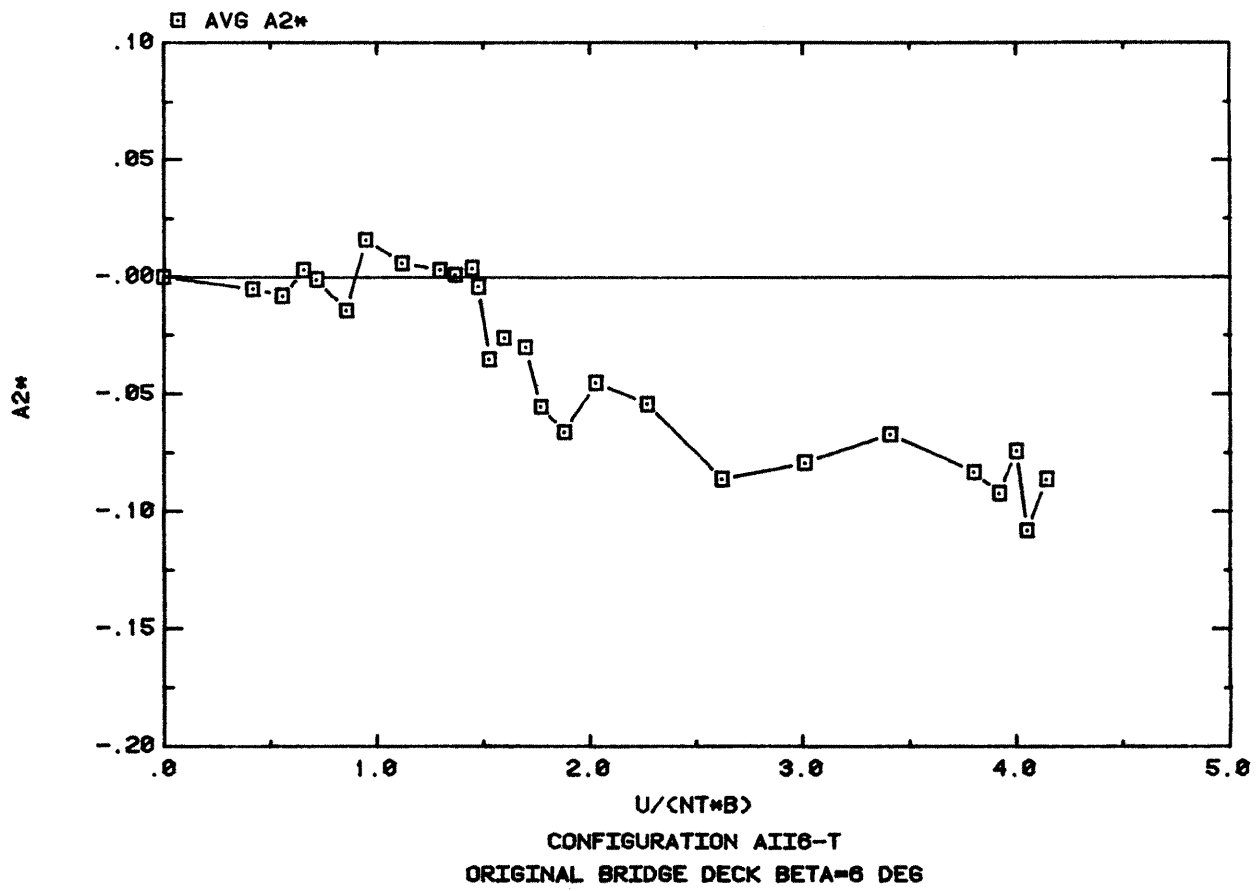
Figure 33. Aerodynamic Derivative A_2^*, Angle of Attack $\beta = +6°$
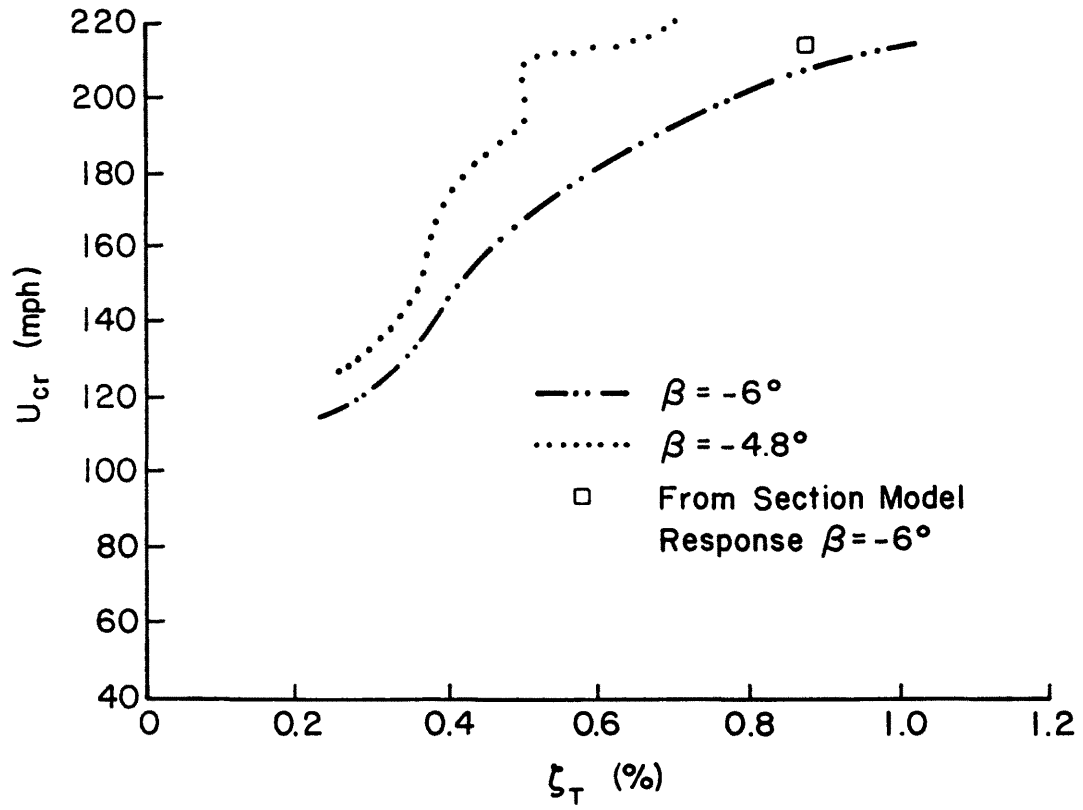
Figure 34. Prototype Critical Wind Speed
for Torsional Flutter
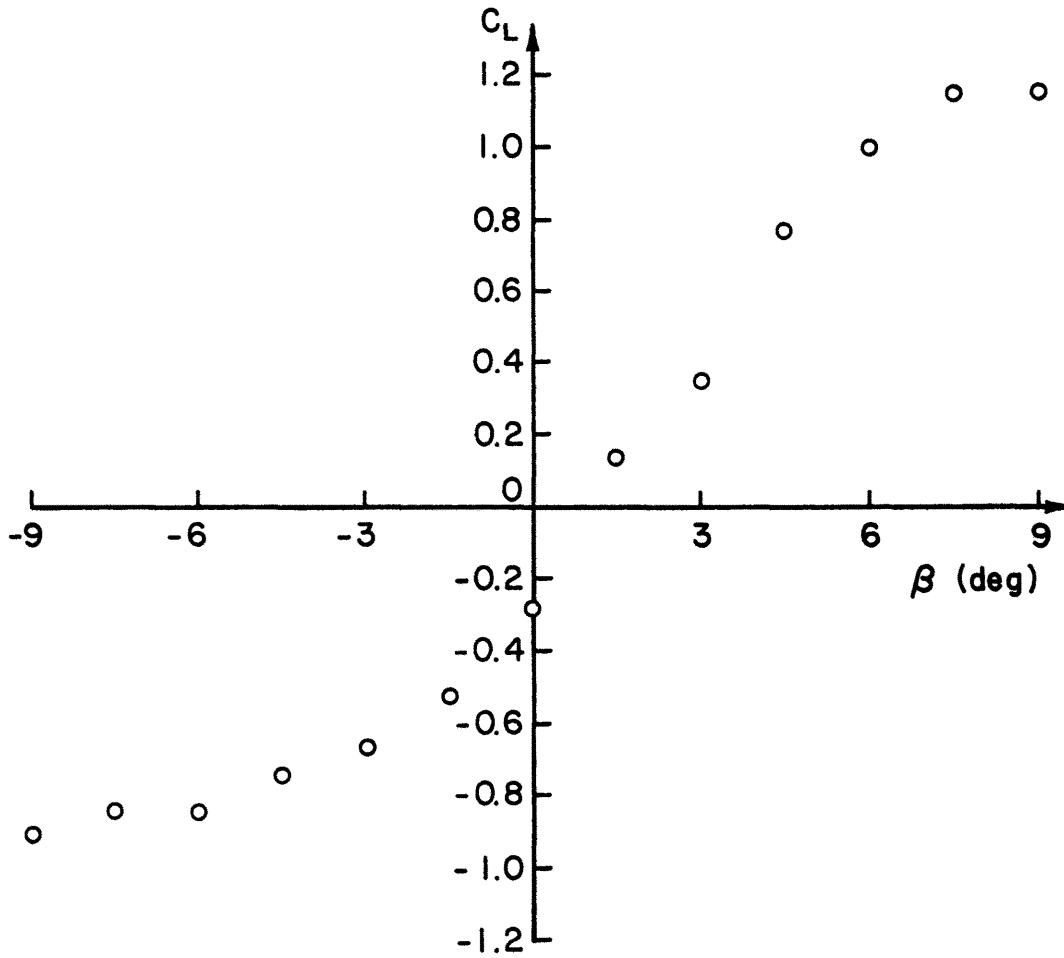
Figure 35. Mean Lift Force Coefficient
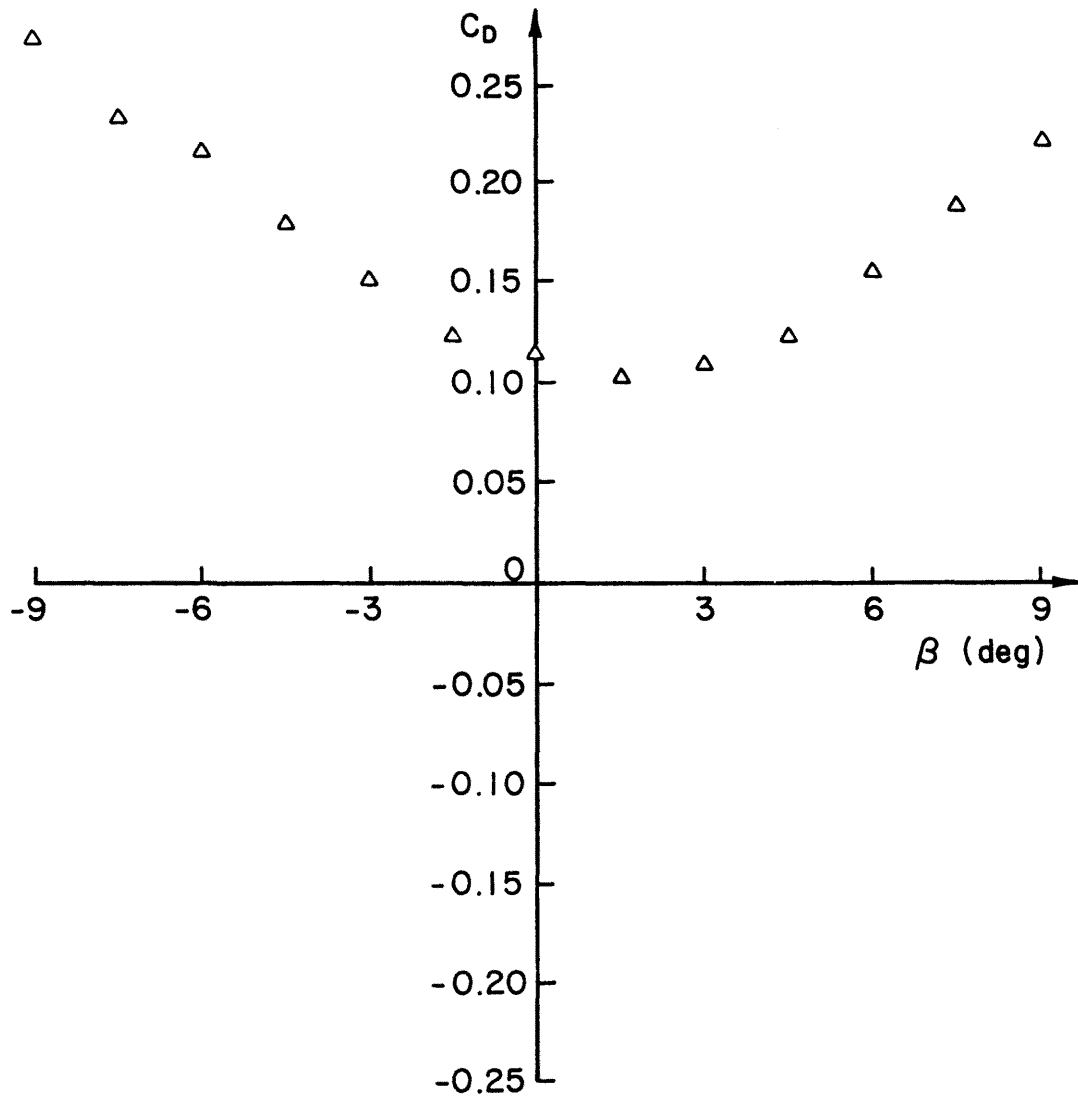
Figure 36. Mean Drag Force Coefficient
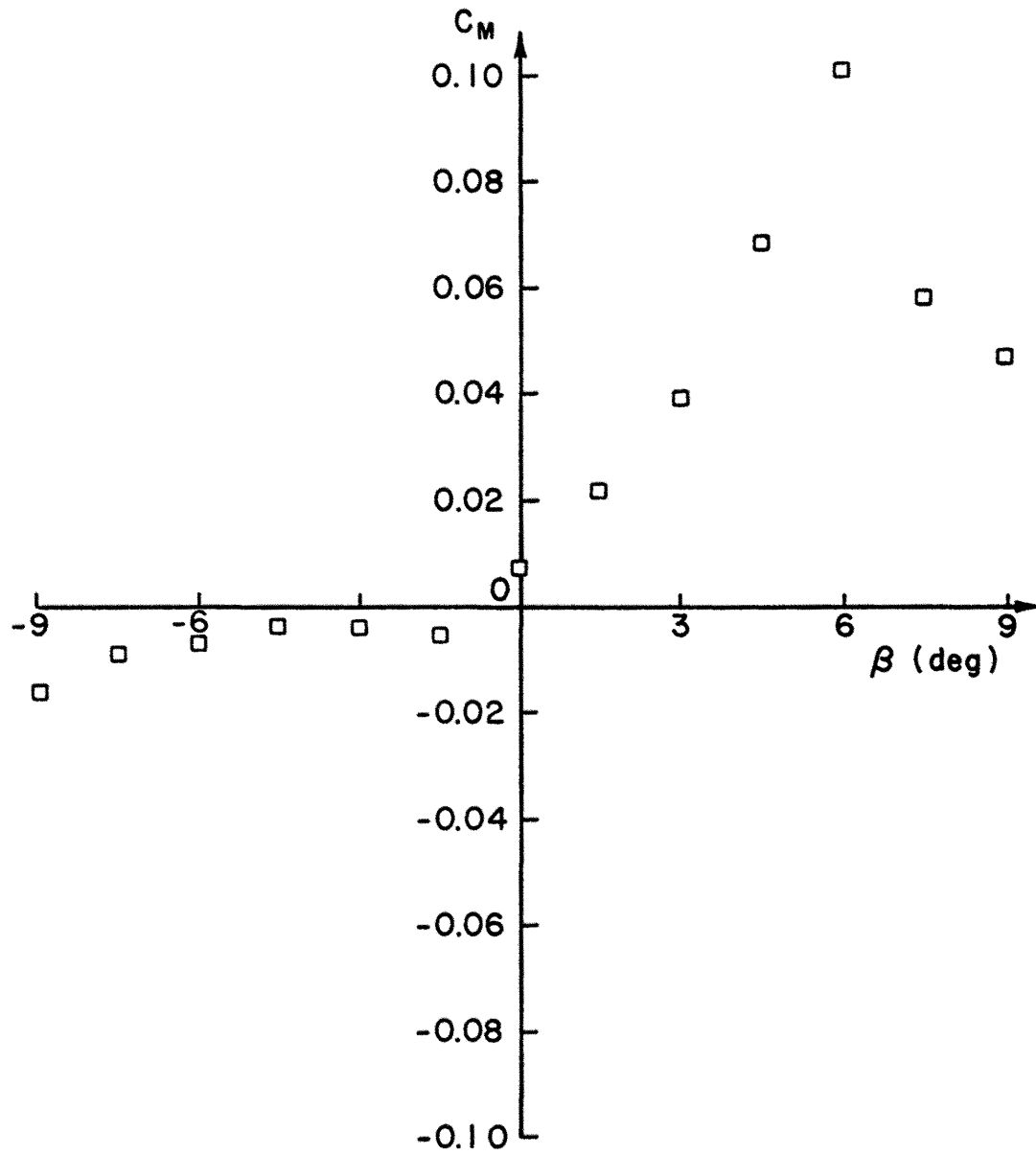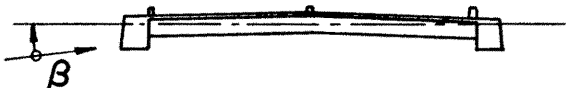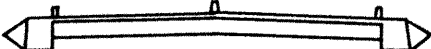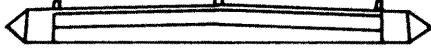
Figure 37. Mean Pitching Moment Coefficient

Bridge Deck	β		
	-6°	0°	6°
1	X	X	X
2	X	X	X
3	X	X	X
4	X	X	X

X Configurations Tested

Figure 38. Experimental Configurations: Original Bridge Deck (1) and Bridge Deck with Modifications (2-4)
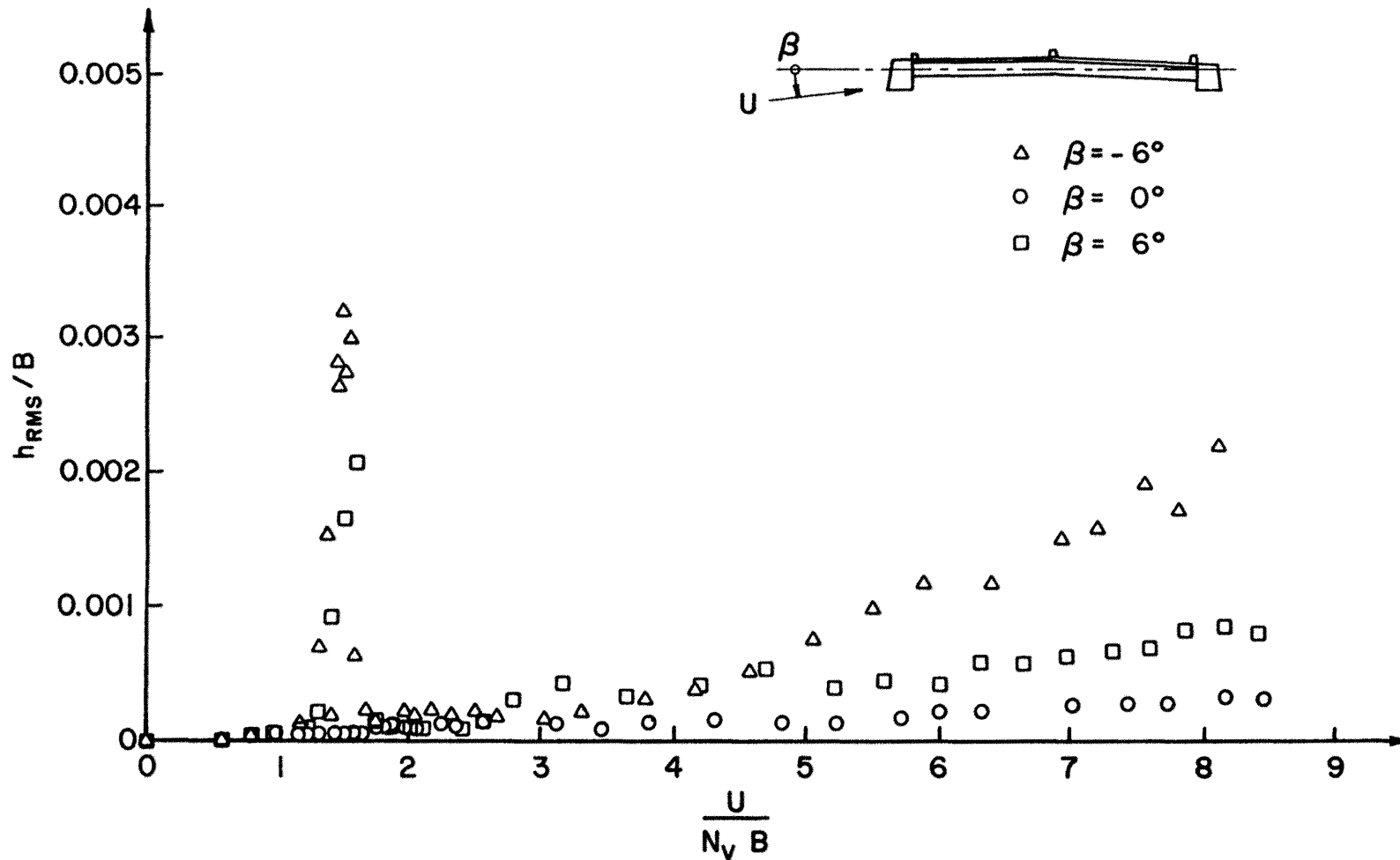
Figure 39.   Vertical Response of Original Deck 1 with Moderate Damping at Angle of Attack
β = -6°, 0°, +6°
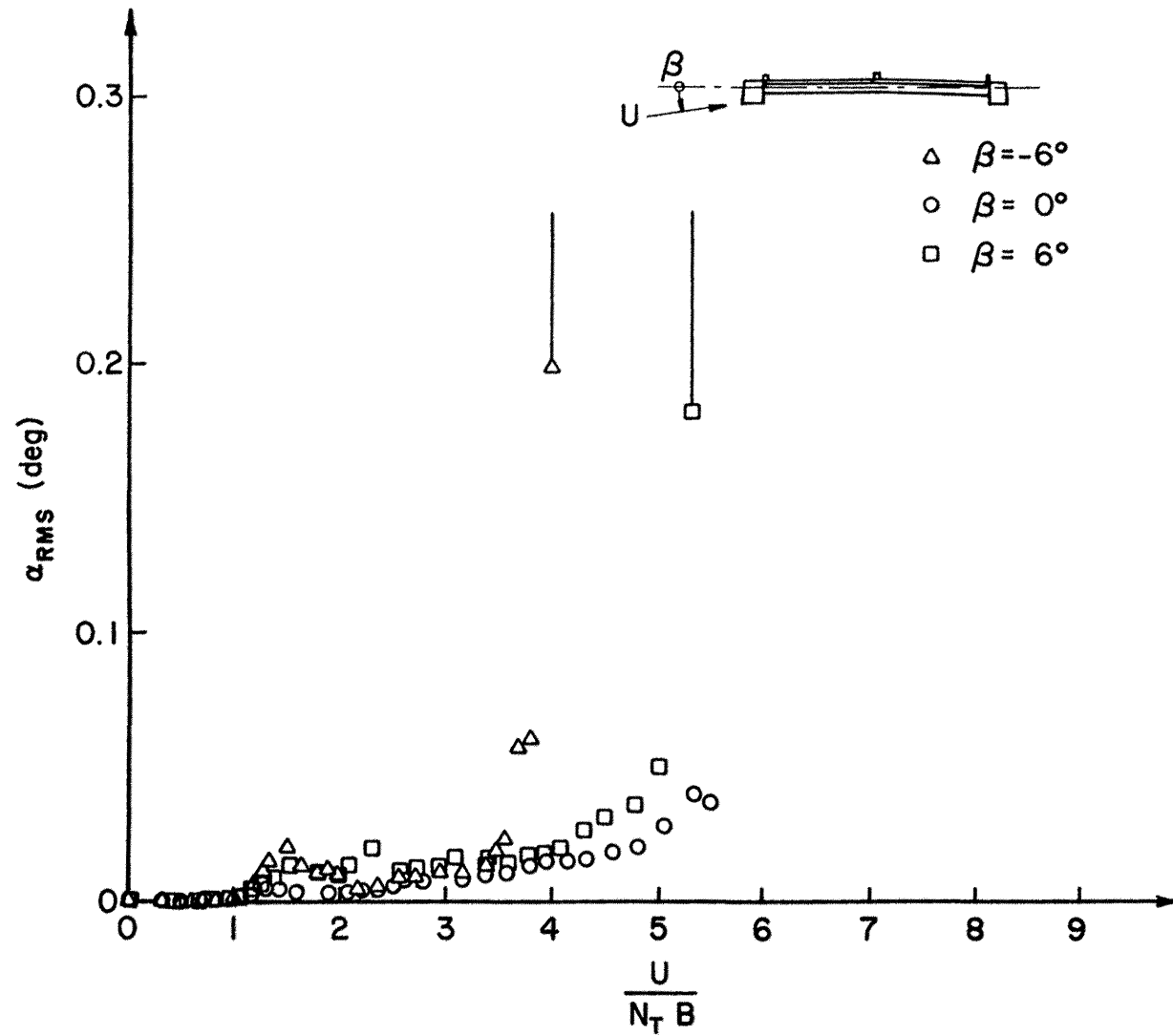
Figure 40. Torsional Response of Original Bridge Deck 1 with Moderate Damping at Angle of Attack $\beta = -6°$, $0°$, $+6°$
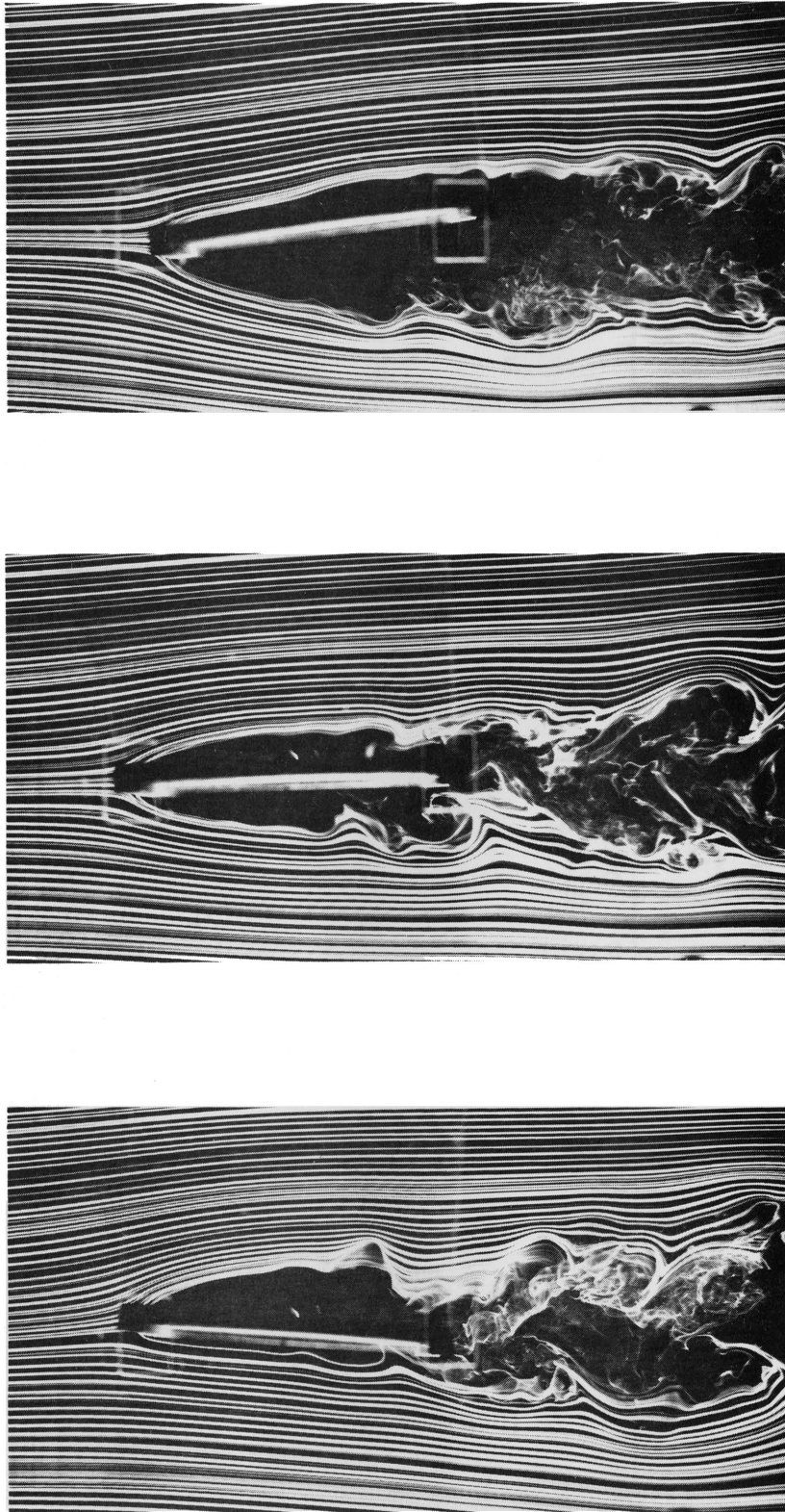
Figure 41. Flow Patterns Around Original Bridge Deck 1
at Angle of Attack β = -6°, 0°, +6°
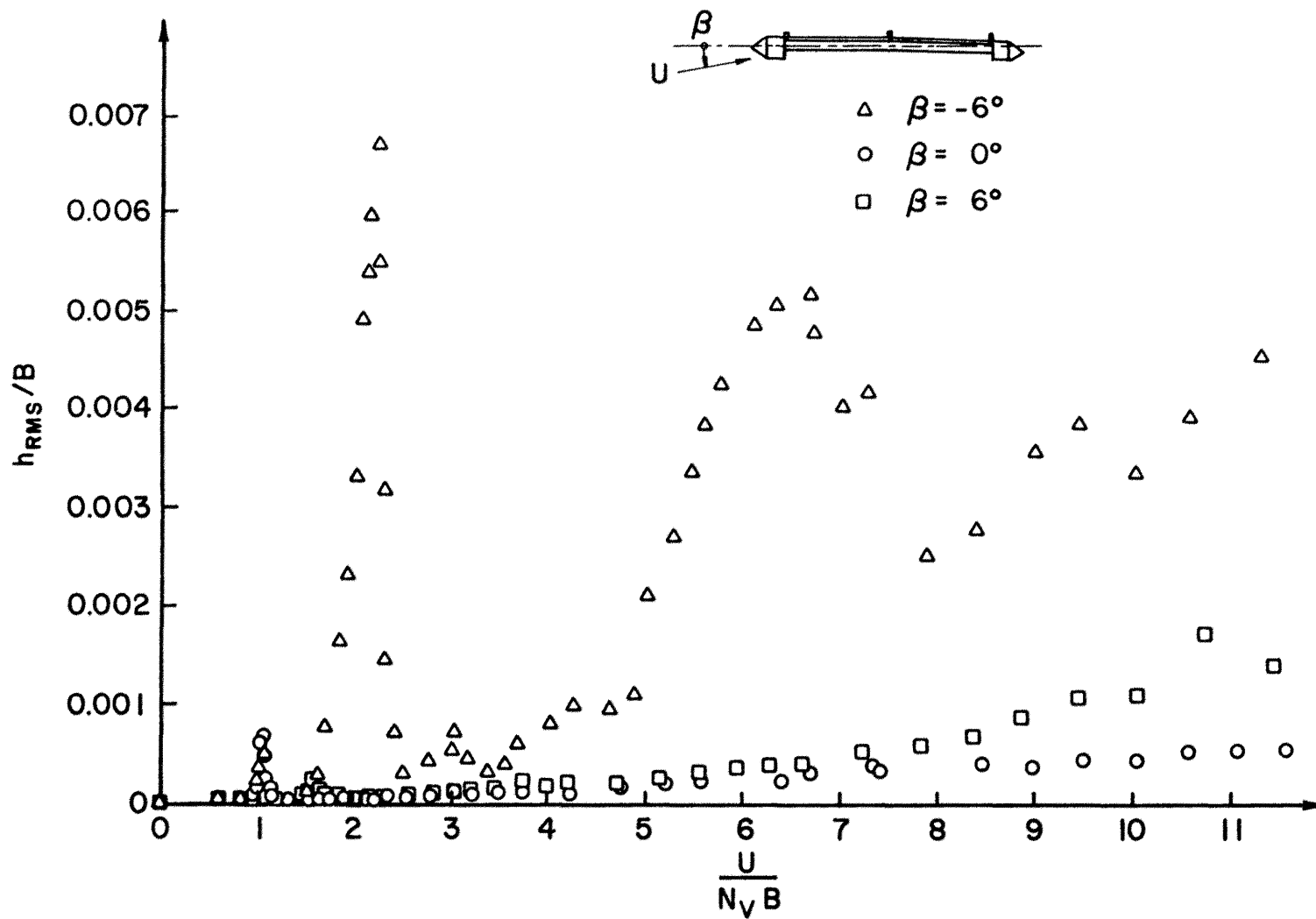
Figure 42. Vertical Response of Modified Bridge Deck 2 with Moderate Damping at
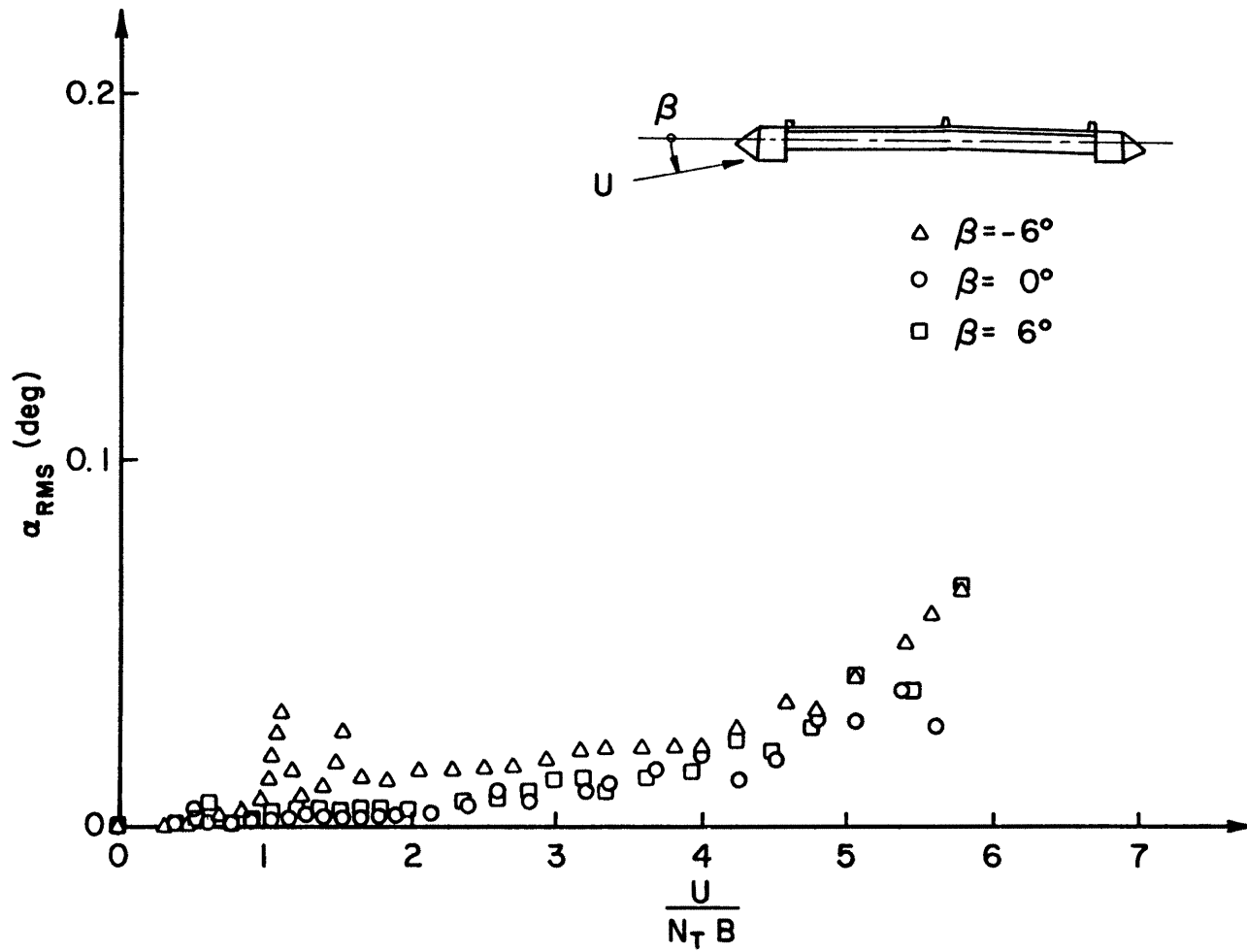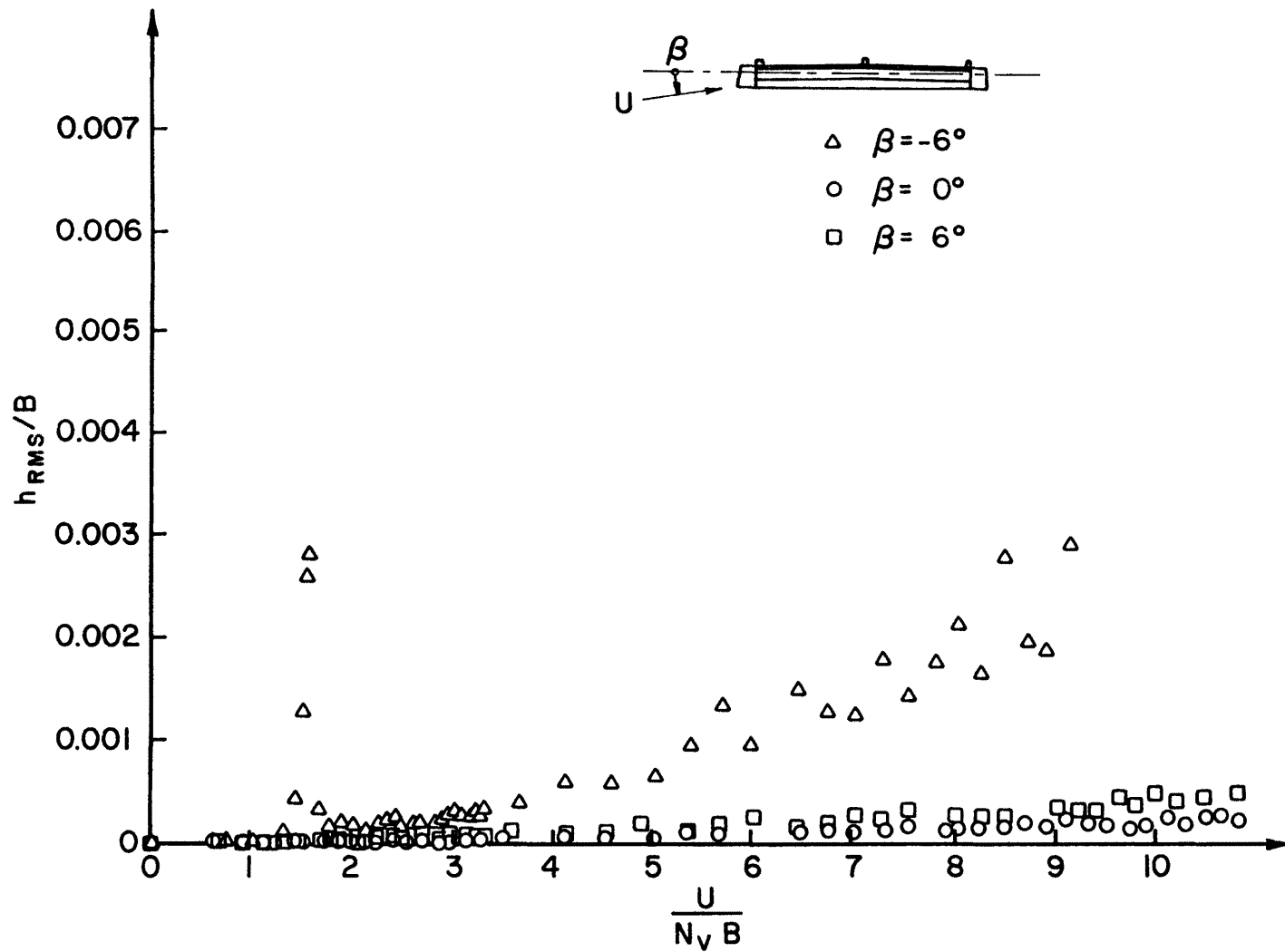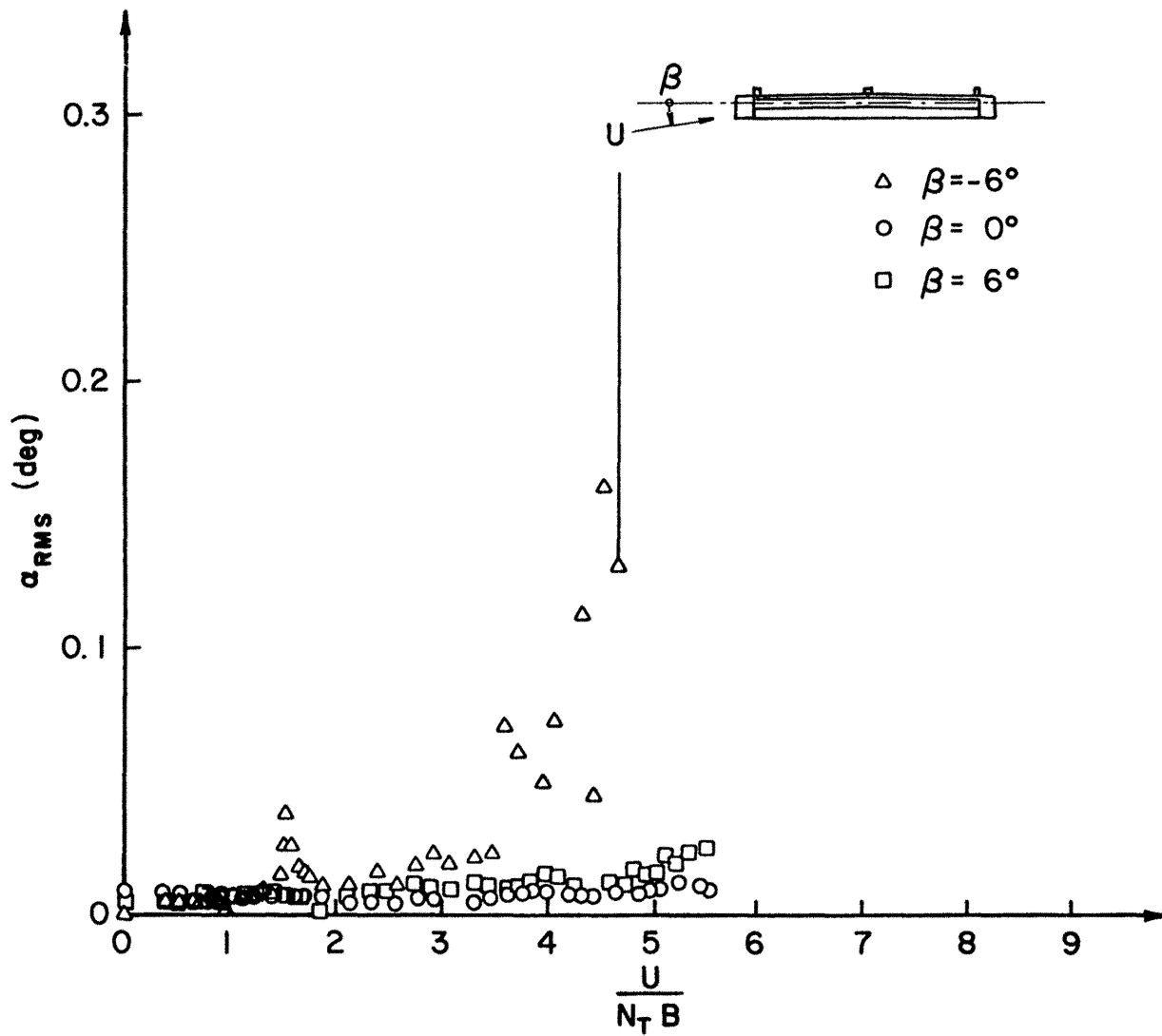Angle of Attack β = -6°, 0°, +6°

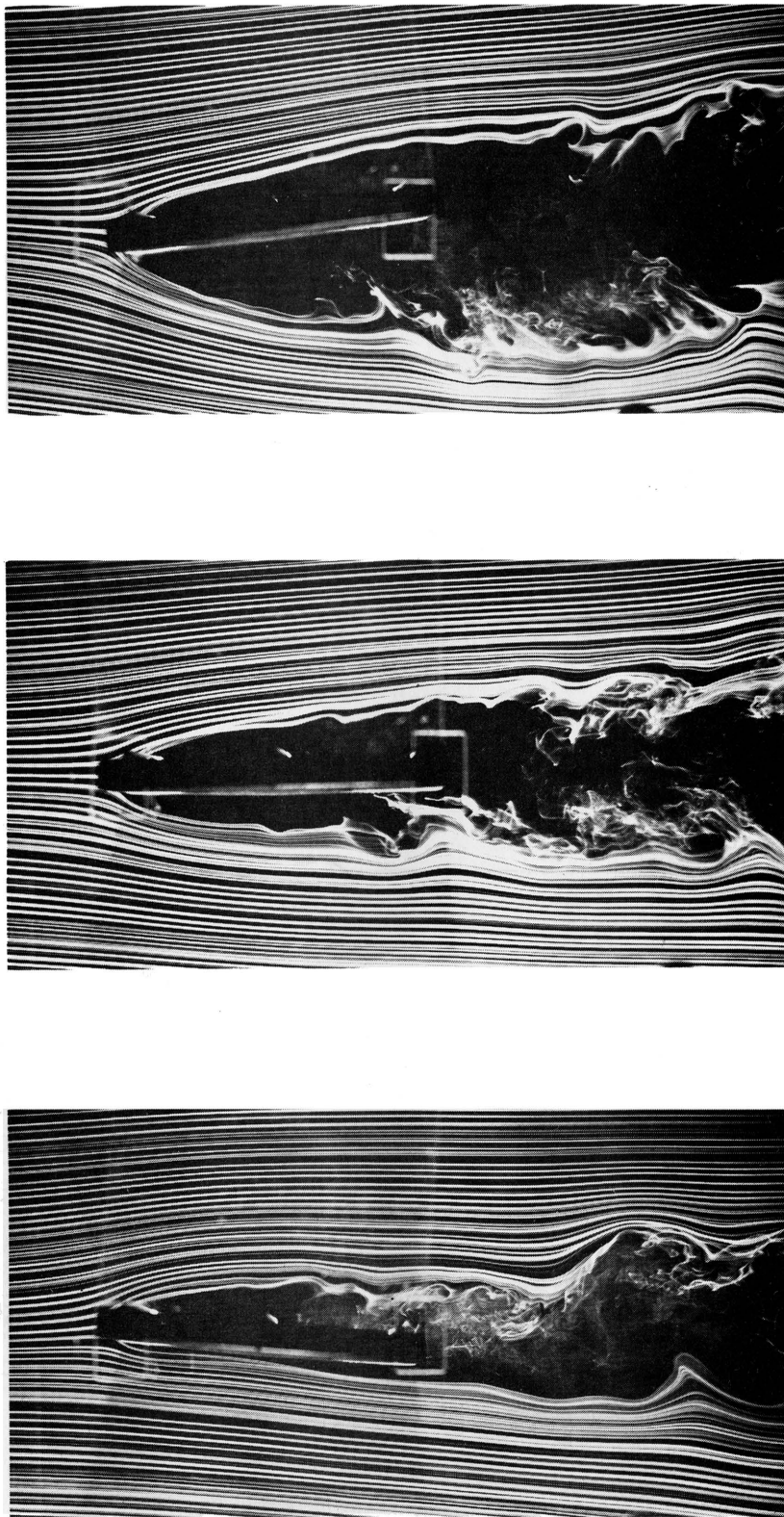Figure 43. Torsional Response of Modified Bridge Deck 2 with Moderate Damping at Angle of Attack β = -6°, 0°, +6°
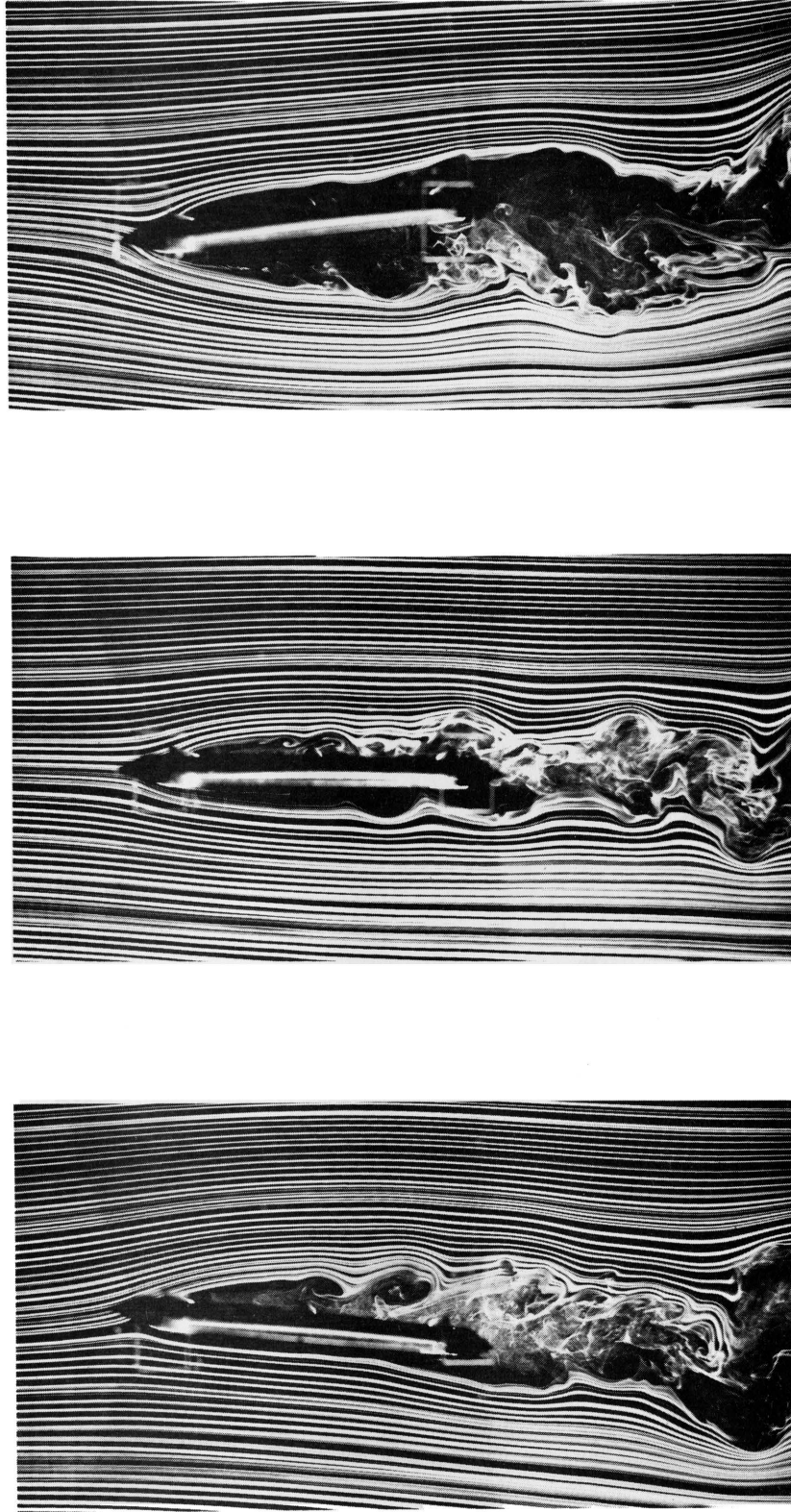
Figure 44. Flow Patterns around Modified Bridge Deck 2
at Angle of Attack β = -6°, 0°, +6°

Figure 45.   Vertical Response of Modified Bridge Deck 3 with Moderate Damping at
Angle of Attack β = -6°. 0°, +6°

Figure 46. Torsional Response of Modified Bridge Deck 3 with Moderate Damping at Angle of Attack β = -6°, 0°, +6°

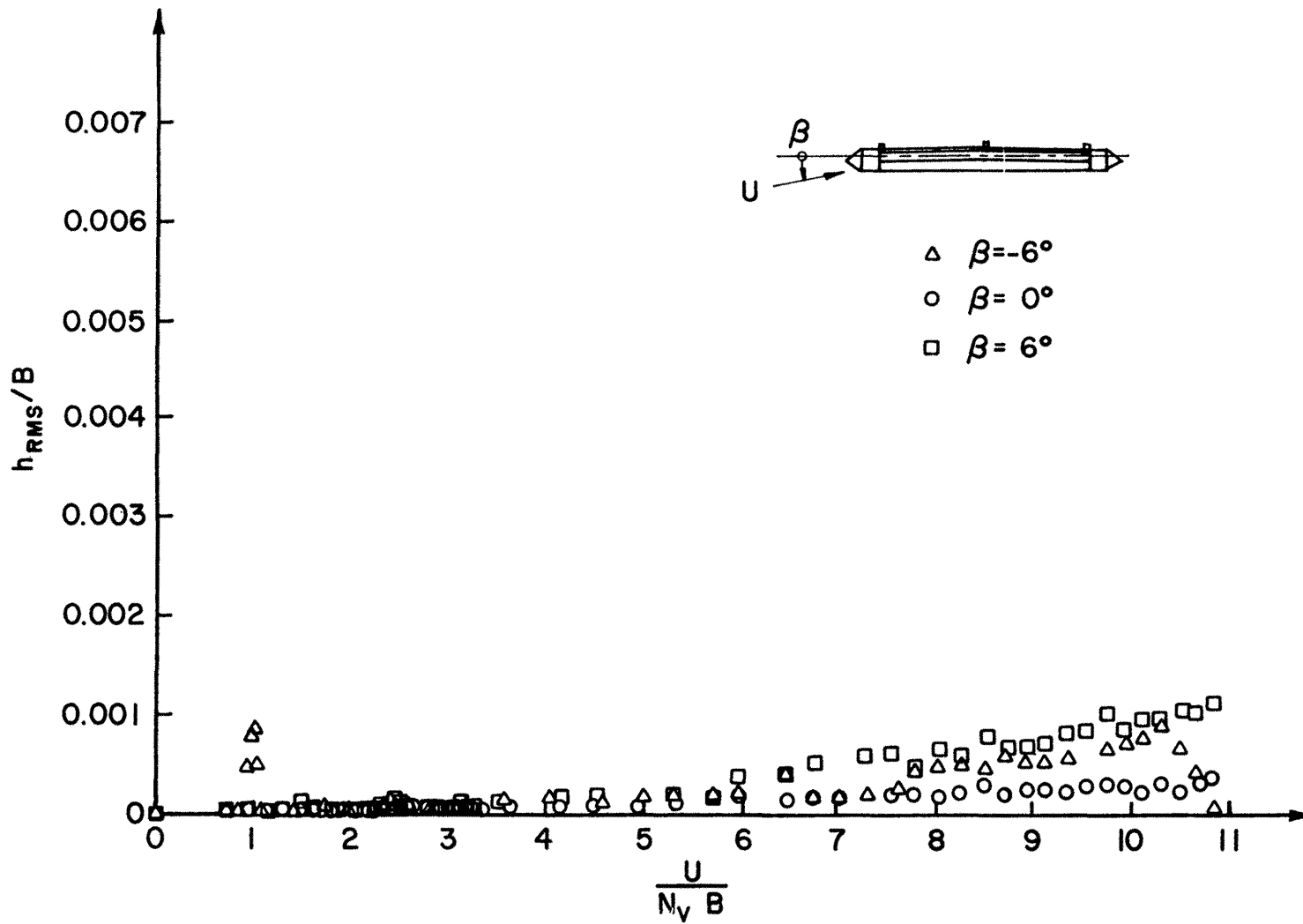Figure 47. Flow Patterns around Modified Bridge Deck 3
at Angle of Attack β = -6°, 0°, +6°

Figure 48.   Vertical Response of Modified Bridge Deck 4 with Moderate Damping at
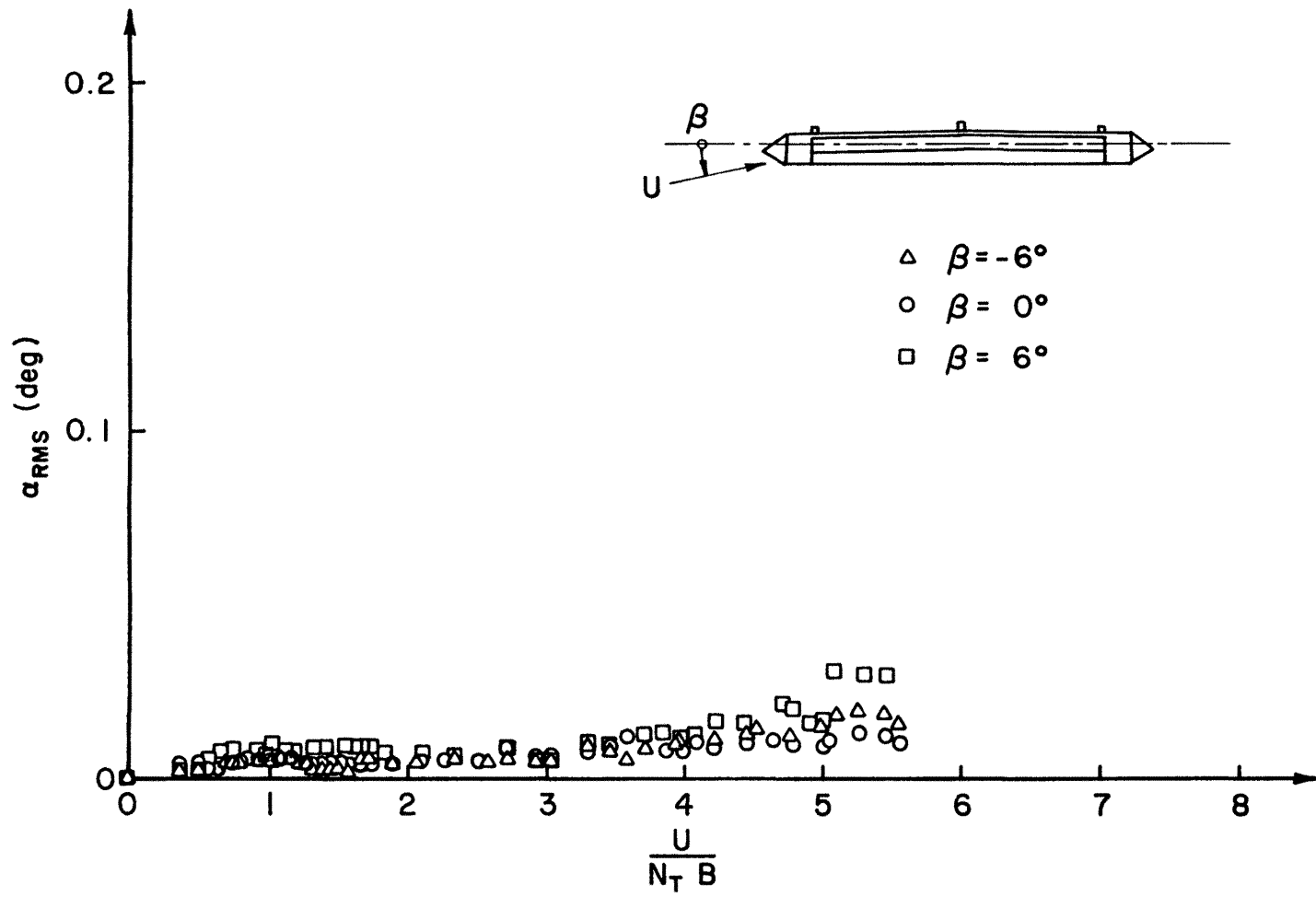Angle of Attack β = -6°, 0°, +6°

Figure 49.   Torsional Response of Modified Bridge Deck 4 with Moderate Damping at Angle of Attack β = -6°, 0°, +6°

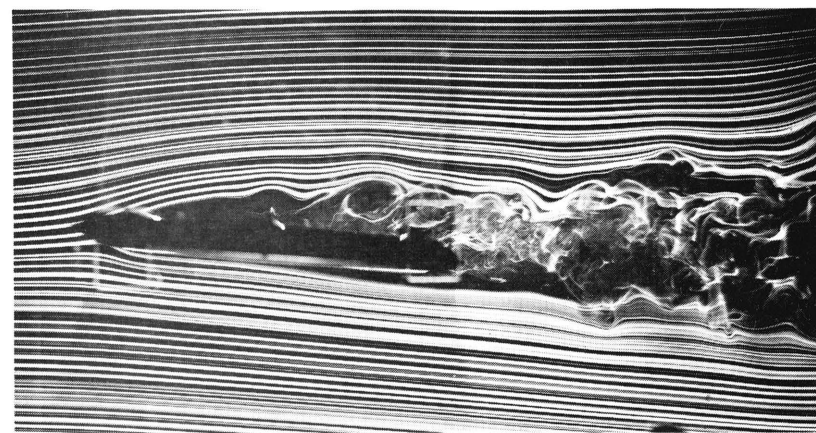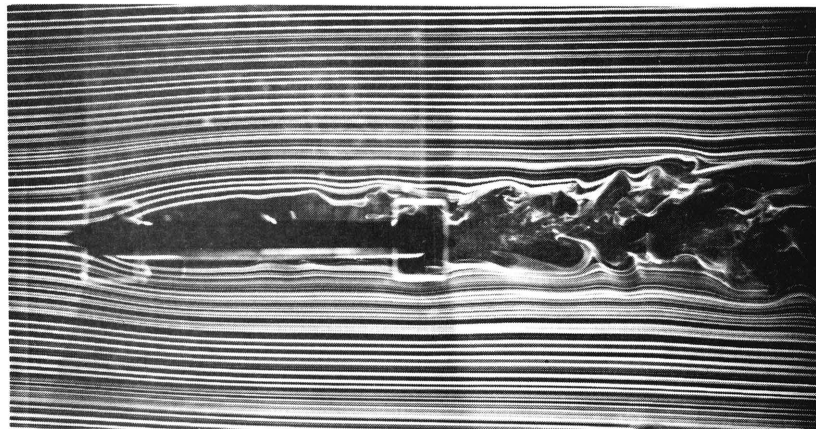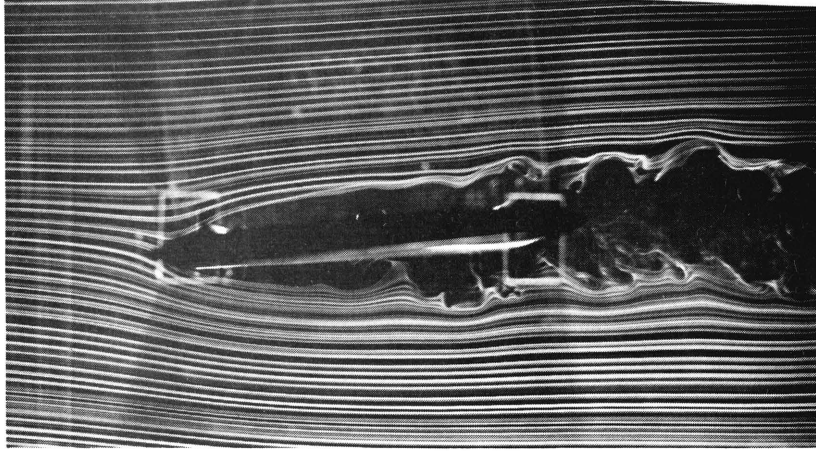Figure 50.   Flow Patterns around Modified Bridge Deck 4
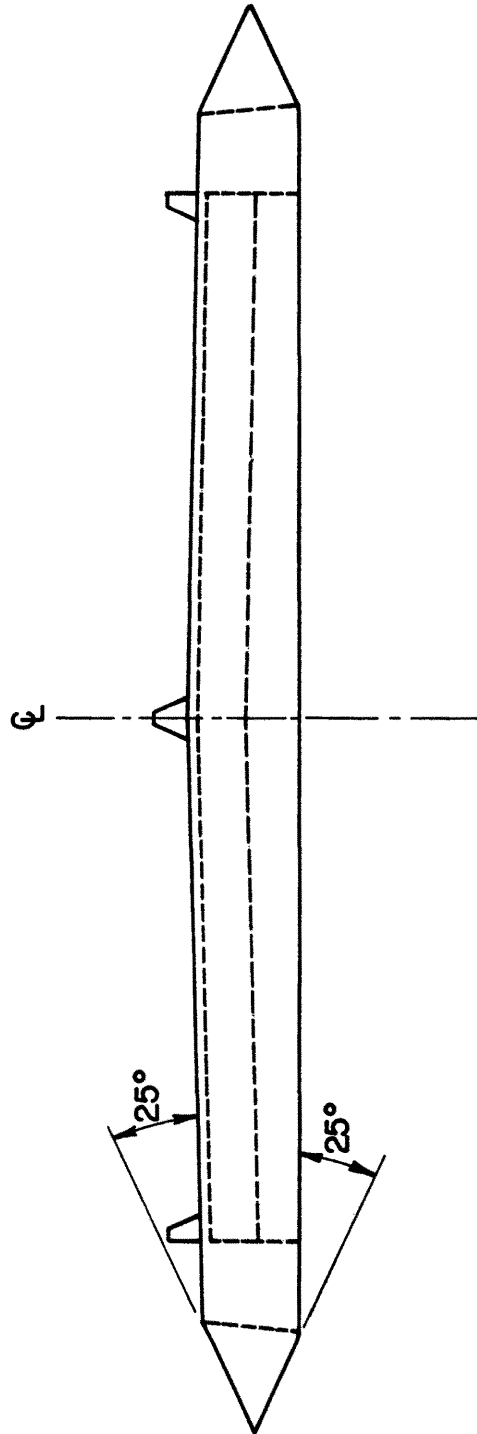at Angle of Attack β = -6°, 0°, +6°

Figure 51. Aerodynamically Stable Modified Bridge Deck

Figure 52. Aerodynamic Derivative $-H_1^*$, for Modified Bridge Deck, Angle of Attack $\beta = 0°$

Figure 53. Aerodynamic Derivative A_2^*, for Modified Bridge Deck,
Angle of Attack $\beta = 0°$

Figure 54. Aerodynamic Derivative $-H_1^*$, for Modified Bridge Deck, Angle of Attack $\beta = -6°$

Figure 55.   Aerodynamic Derivative A_2^*, for Modified Bridge Deck,
Angle of Attack $\beta = -6°$
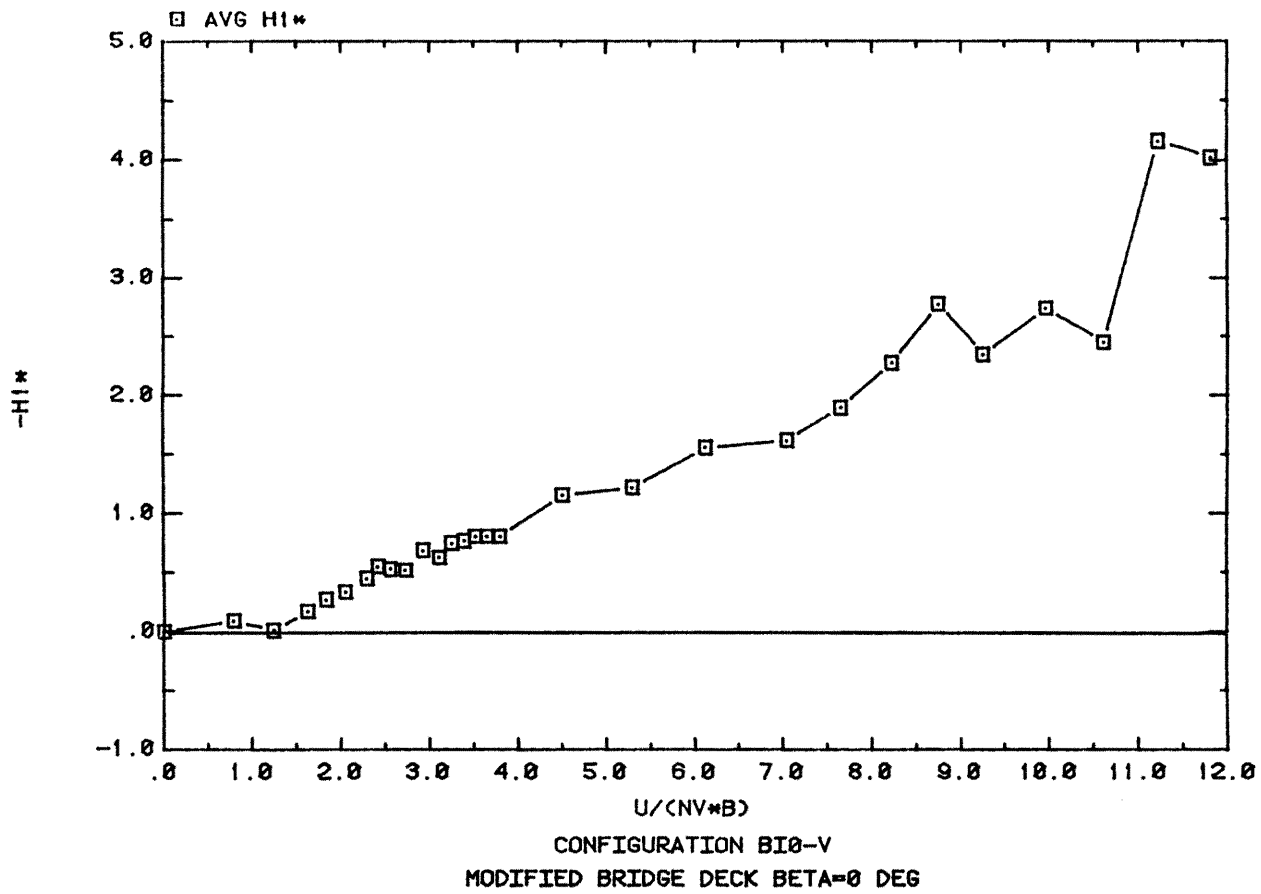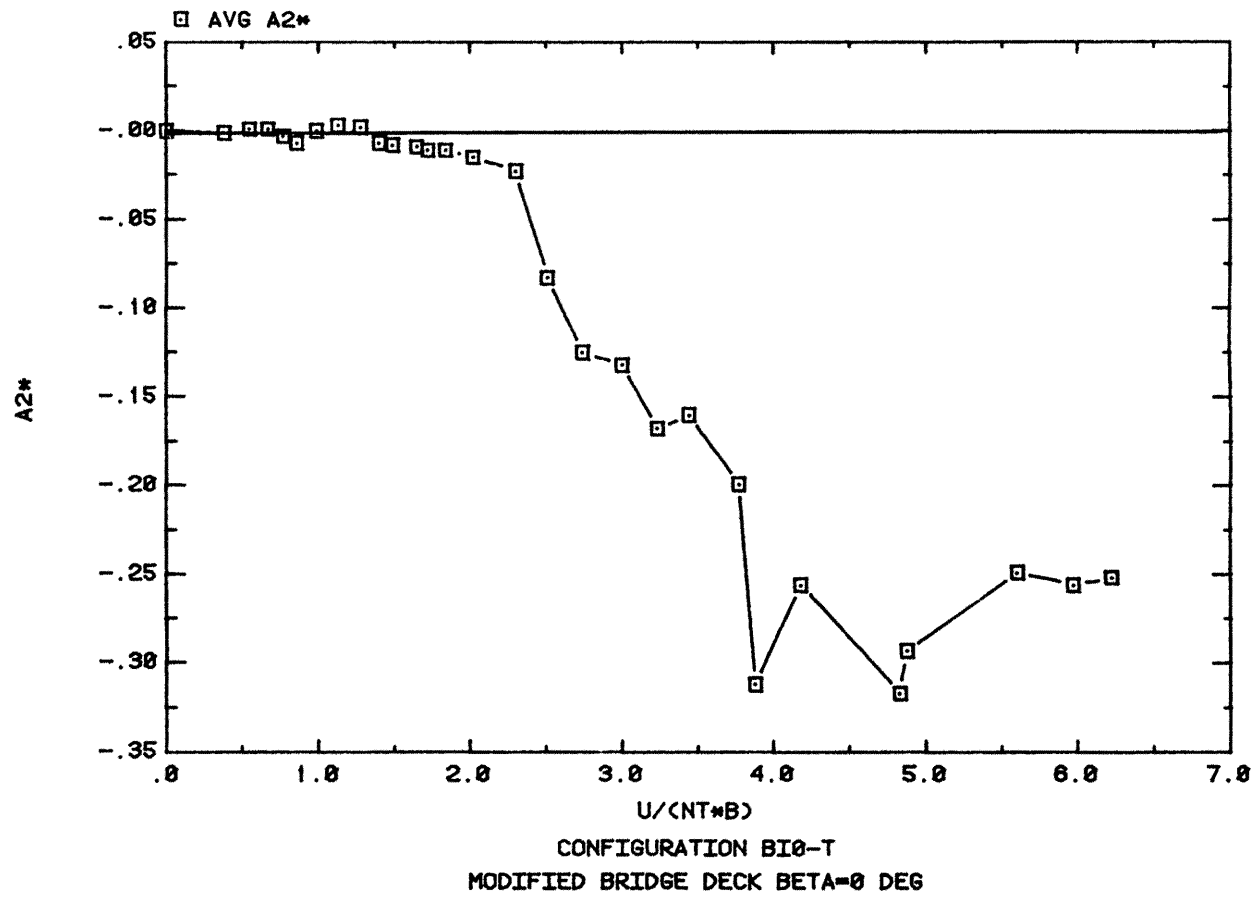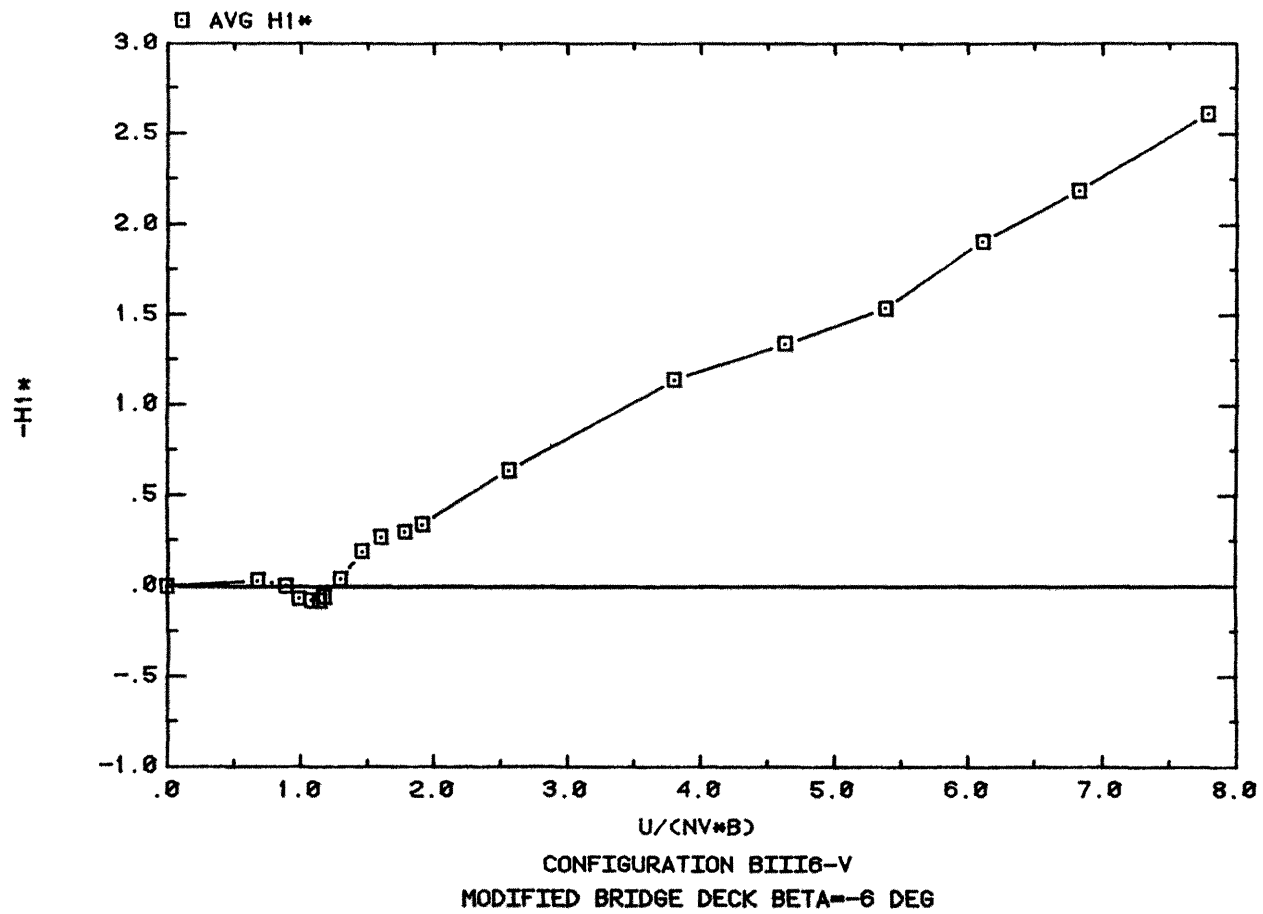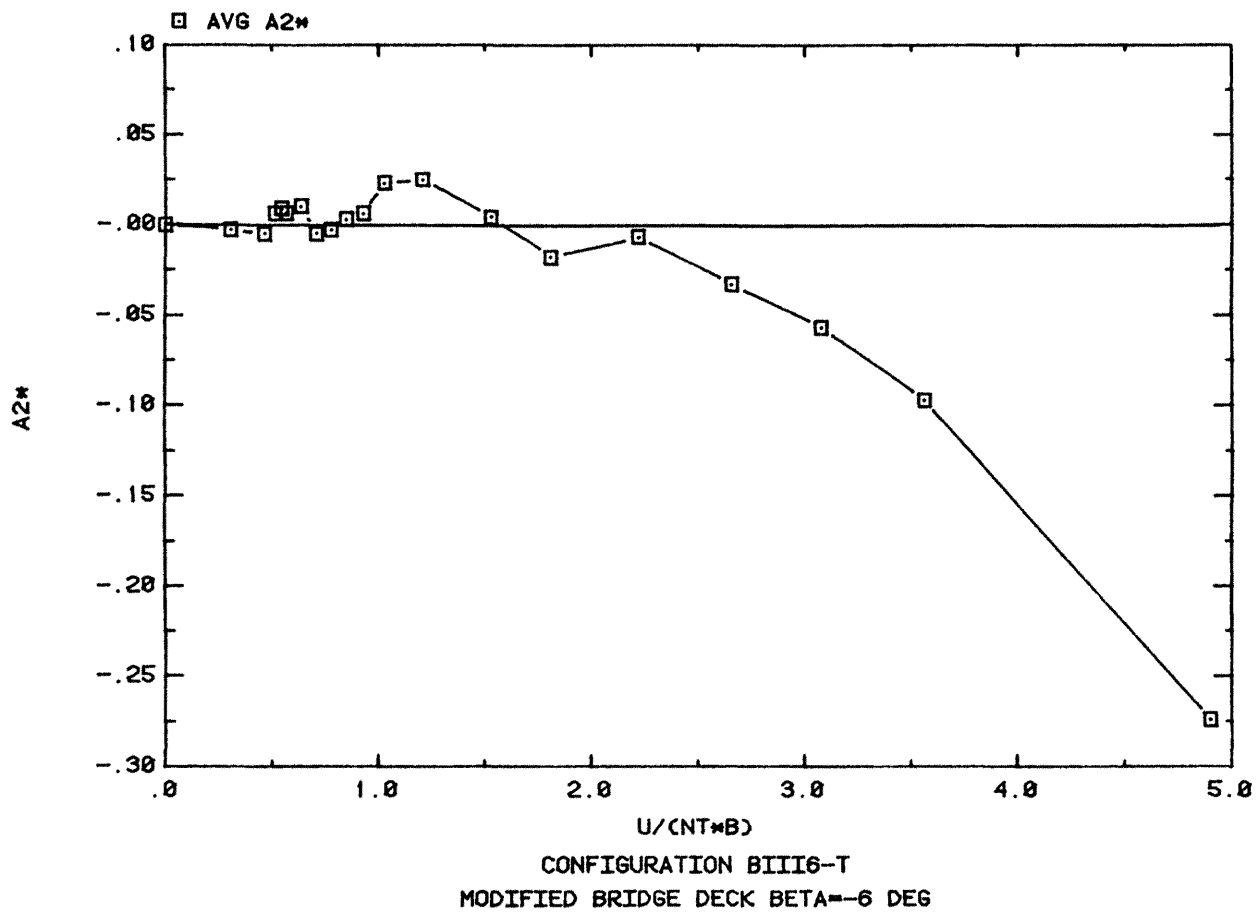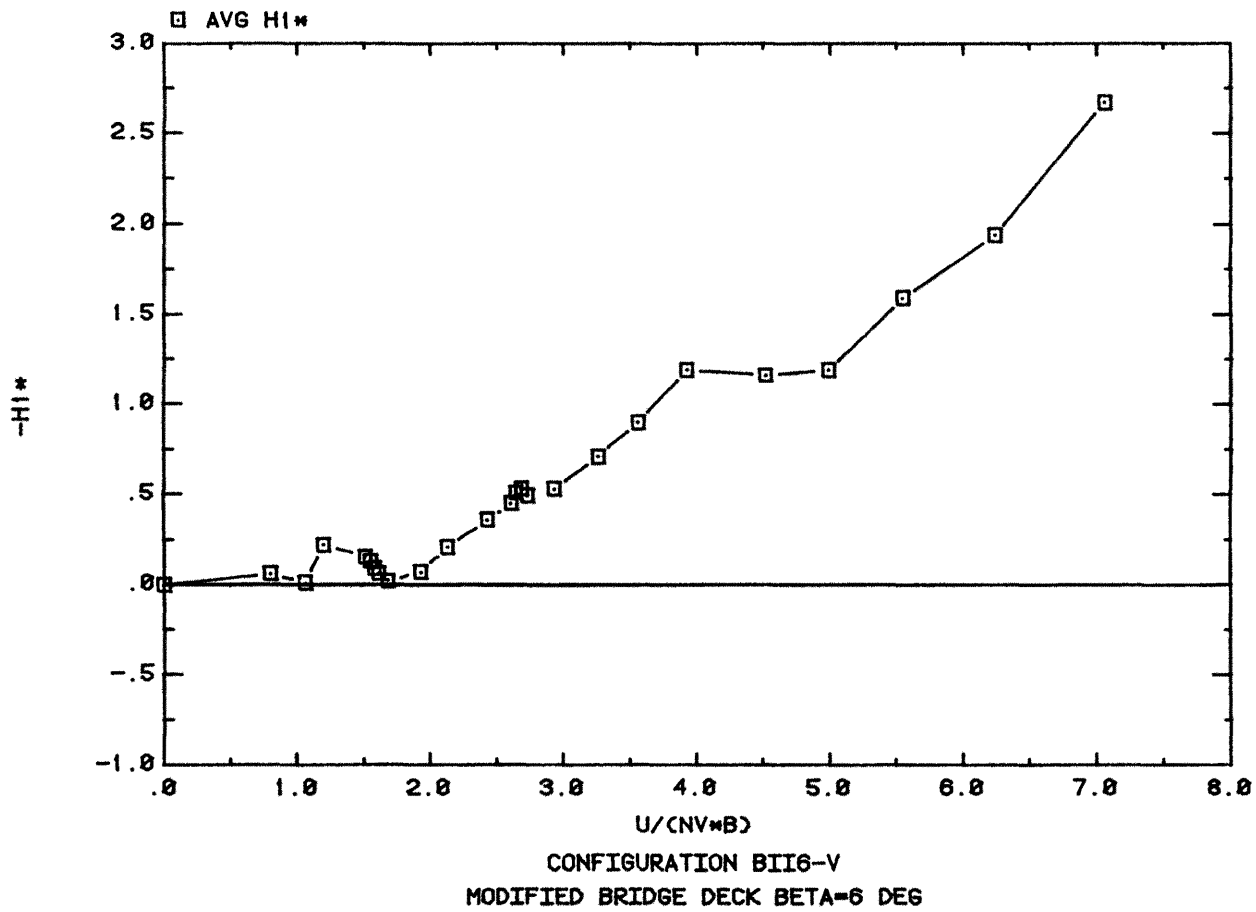
Figure 56.   Aerodynamic Derivative $-H_1^*$, for Modified Bridge Deck,
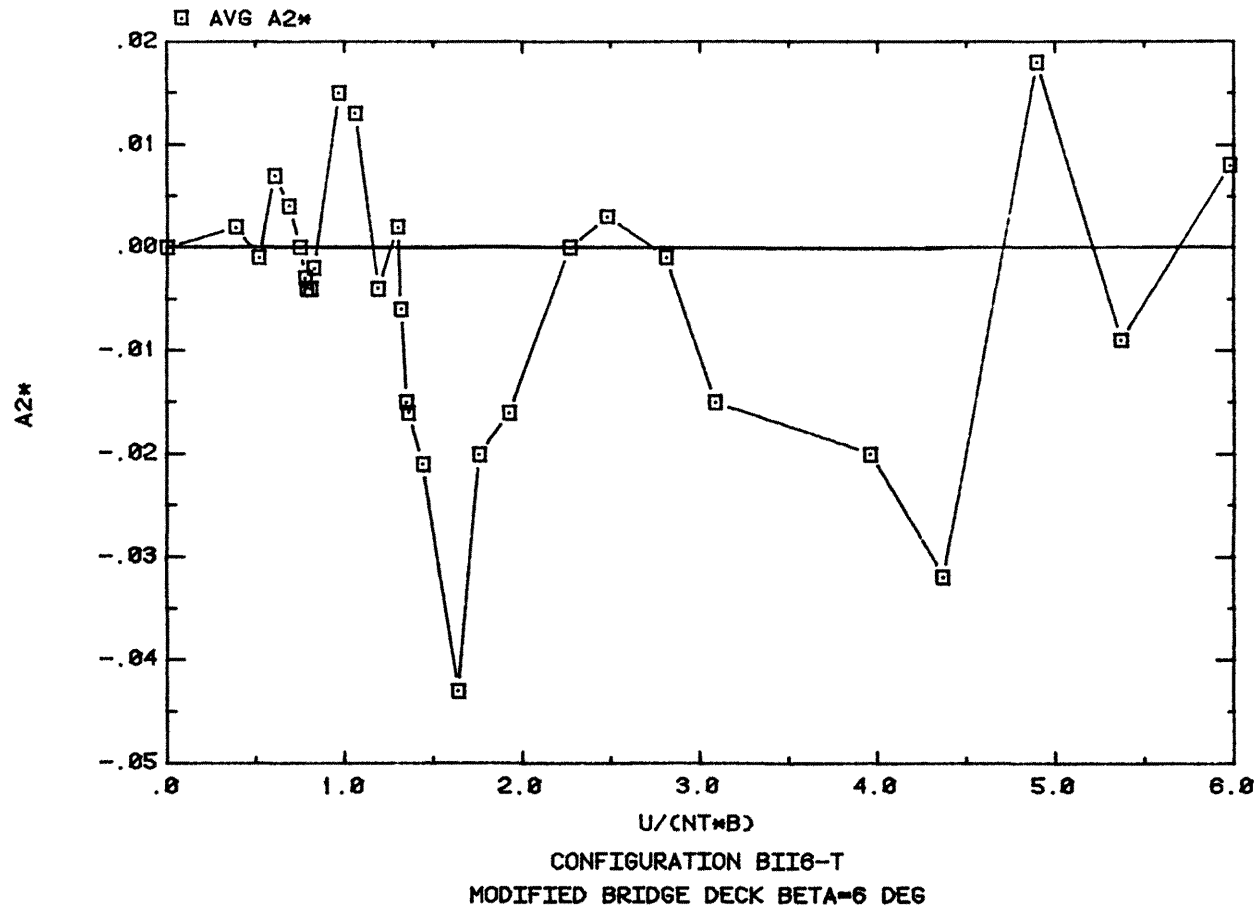Angle of Attack β = +6°

Figure 57. Aerodynamic Derivative A_2^*, for Modified Bridge Deck, Angle of Attack $\beta = +6°$

11. TABLES

Table 1. Parameters for Prototype and "Exact" Model
(Original Bridge Deck)

Property	Units	Prototype*	"Exact" Model 1:140
Deck Width (B)	ft	103.5	0.7393
Deck Depth (D)[A]	ft	8.5 [~11.2]	0.0607 [0.0800]
Mass per Unit Span (m)	slug-ft^{-1}	1050.	0.0536
Polar Mass Moment of Inertia per Unit Span (I)	slug-ft^{2}-ft^{-1}	1357000.	0.003532
Inertia Ratio (I/mB^{2})	--	0.12	0.12
Vertical Bending Frequency (N$_v$)	Hz	0.30	3.55
Torsional Frequency (N$_T$)	Hz	0.76	8.99
Torsional-to-Vertical Frequency Ratio (N$_T$/N$_v$)	--	2.53	2.53
Assumed Damping Ratio for Vertical Motion (ζ_v)	%	1.	1.
Assumed Damping Ratio for Torsional Motion (ζ_T)	%	1.	1.

*Based on data attached to letter of October 10, 1980 from Dr. John M. Kulicki, Modejski and Masters, Consulting Engineers, to Dr. Jack E. Cermak, Colorado State University

Table 2. Parameters of Actual Model (Original Bridge Deck)

Property	Units	Model with Low Damping Value	Error*	Model with Moderate Damping Value	Error*
B	ft	0.7393	0	0.7393	0
D [A]	ft	0.0607 [0.0800]	0	0.0607 [0.0800]	0
m	$slug\text{-}ft^{-1}$	0.0520	-3.	0.0520	-3.
I	$slug\text{-}ft^{2}\text{-}ft^{-1}$	0.003663	4.	0.004418	20.
I/mB^2	---	0.13	8.	0.16	22.
N_V	Hz	3.50	-1.	3.50	-1.
N_T	Hz	7.83	-15.	7.13	-26.
N_T/N_V	---	2.24	-13.	2.04	-24.
ζ_V	%	0.06	-	0.81	-
ζ_T	%	0.13	-	0.84	-

* Error = $\dfrac{(\ )\ actual\ -\ (\ )exact}{(\ )\ actual}$ [%]

87

Table 3. Vortex-Induced Vertical Oscillation for Prototype Bridge Deck

(Damping Ratio $\zeta_v \cong 0.81\%$)

Angle of Attack β[deg]	Deflection Amplitude h_o[ft]	Acceleration Amplitude $\frac{a_o}{g}$ [%]
-6	0.47	5.2
-4.8	0.27	3.0
-3	0.05	0.6
0	~0	~0
+3	~0	~0
+6	0.29	3.2

12. APPENDIX

Full-Span Torsional Flutter of the Prototype Bridge

The equation for torsional motion of a typical section of the bridge deck considered in Section 2.3 is given by Equation (12)

$$I[\ddot{\alpha} + 2\zeta_\alpha \omega_\alpha \dot{\alpha} + \omega_\alpha^2 \alpha] = \rho B^4 \omega_\alpha A_2^* \dot{\alpha} \quad . \tag{A1}$$

It is necessary to consider the spanwise modes of torsion that are expected to take part in full-span torsional flutter. It is usually sufficient to consider the mode of the lowest frequency (the fundamental mode) since the lowest flutter speed is sought. Therefore, the torsional displacement $\alpha(x,t)$ where x is a spanwise coordinate and t is time can be expressed in terms of the torsion fundamental spanwise mode $\Phi_1(x)$ and the generalized coordinate $\alpha_1(t)$ as follows:

$$\alpha(x,t) = \Phi_1(x) \cdot \alpha_1(t) \quad . \tag{A2}$$

Substituting (A2) in Equation (A1), multiplying by $\Phi_1(x)$, and integrating over the span gives the following equation:

$$I_1 \ddot{\alpha}_1 + (I_1 2\zeta_\alpha \omega_\alpha - C_1 \rho B^4 \omega_\alpha A_2^*)\dot{\alpha}_1 + I_1 \omega_\alpha^2 \alpha_1 = 0 \tag{A3}$$

where

$$I_1 = \int_0^L I(x)\Phi_1^2(x)dx$$

and

$$C_1 = \int_0^L \Phi_1^2(x)dx \quad .$$

From this equation the flutter condition has the following form:

$$A_2^* = \frac{2I_1}{\rho B^4 C_1} \zeta_\alpha \quad . \tag{A4}$$

If the bridge deck is uniform along the span and

$$I(x) = I = const$$

then

$$I_1 = I * C_1 \quad .$$

The flutter condition (A4) for the full span of the prototype bridge becomes identical with the same requirement for the bridge section model (16) --

$$A_2^* \left(\frac{U_c}{NB} \right) = \frac{2I}{\rho B^4} \zeta_\alpha \quad . \tag{A5}$$